Implementation of Refractory Foam Technology for Silencing Small IC Engines

By

Josh Sesler

Thesis submitted to the Faculty of the
Virginia Polytechnic Institute and State University
in partial fulfillment of the requirements for the degree of

Master of Science
in
Mechanical Engineering

Ricardo A. Burdisso, Chair
William R. Saunders
Jon Fleming

September 9, 2005
Blacksburg, Virginia

Keywords: Silencer, Dissipative muffler, Refractory foam, Sound absorption, Absorptive material

Implementation of Refractory Foam Technology for Silencing Small IC Engines

Josh Sesler

(ABSTRACT)

With the need for stealth in defense applications steadily increasing, noise reduction continues to play an important role in the world of aeronautics. With the ever increasing number of small UAV flight vehicle designs and their stringent weight requirements, acoustic solutions become progressively more complex. This thesis investigates the use of refractory foam, a new class of porous material, for designing effective silencers for small IC engines. The solution must be lightweight, compact, conformable, and capable of handling the rigors of flight. Throughout the course of this research, many silencer designs were fabricated to take advantage of refractory foam technology. These silencer designs were then tested against existing designs using both anechoic and outdoor testing techniques. These results proved refractory foam to be a superior broadband noise absorber that can survive harsh flight environment. Silencer designs using this material showed overall improvements in the areas of noise reduction, weight, size, and backpressure, compared to commercial designs. The final silencer design boasted an A-weighted overall sound pressure level that was 12.1 dBA lower than the reference case. This result was accomplished using nearly half the volume required by other designs to attain similar results.

Acknowledgments

I would first like to thank Dr. Ricardo Burdisso for providing me with the opportunity to work on such an exciting project. Your experience in the field of acoustic was a great asset in developing effective silencer solutions. Jon Fleming and Mathew McCarty deserve thanks as well for being there through the countless hours of silencer testing. In addition, I'd like to thank Dr. Will Saunders for agreeing to be on my committee. I am also grateful for the assistance of Cathy Hill, who was amazing at keeping me on track with deadlines and paperwork.

Thanks to all my friends who followed me up to Blacksburg from Tennessee Tech for their advanced degrees. It's immeasurable how impactful it is to have the support of great friends. Special thanks to Jono Aggett who not only shared a basement with me through the hours of revisions done on this thesis, but was a voice of wisdom in many facets of my life.

I would also like to thank my family. Without their love and guidance, I would not be anywhere near where I am today. Thanks to my father and grandfather who were nice enough to pass down the engineering genes without which my interest in solving problems would not be what they are. Also, thanks to my fiancé Lori for being such an amazing supporter, especially in recent days of final thesis revisions in the midst of wedding planning.

Finally, I most importantly thank the Lord Jesus Christ whose love is better than life. Glorifying Him is my sole purpose in living.

Table of Contents

List of Figures

List of Tables

Chapter 1 Introduction

Unmanned air vehicles (UAVs) are defined by the Department of Defense (DOD) as powered, aerial vehicles that do not carry a human operator, use aerodynamic forces to provide vehicle lift, can fly autonomously or be piloted remotely, can be expendable or recoverable, and can carry a lethal or nonlethal payload [1]. Current UAVs greatly vary in size, weight, payload capabilities, operation altitudes, and flight range, but their primary design is geared toward intelligence gathering.

Two typical UAV designs currently available are the Gnat 750 pictured in Figure 1.1 and the Exdrone pictured in Figure 1.2. The Gnat 750 [2] weighs 1142 lbs. and has a max speed of 161 mph. It can fly for up to 48 hours and has a payload capacity of 140 lbs. The Exdrone [2] is a smaller and lighter vehicle weighing 89 lbs. and having a max speed of 115 mph. It can fly for up to 2.5 hours and carries a payload up to 25 lbs.

This project investigates the engine acoustic properties of a UAV design by Allied Aerospace [3]. A picture of this 19" diameter vehicle is shown in Figure 1.3. The power plant is a 2-stroke internal combustion (IC) engine, and is capable of vertical takeoff and landing, hover, and high-speed horizontal flight. Its purpose is to provide small infantry units with easily carried and deployed surveillance vehicles. They have the capability to fly to a target area, perch and gather intelligence, and then move on to the next area [4]. Since it is still in the design phase, its weight and speed statistics are not yet known. It is designed to operate in the 100'-500' altitude range, therefore engine noise is a significant consideration.

Figure 1.1: Gnat 750 UAV.

Figure 1.2: Exdrone UAV.

Figure 1.3: The prototype Allied Aerospace VTOL UAV vehicle.

Stealth is of utmost importance in UAVs for mission success and survivability. Noise is a significant factor in the stealth of these vehicles, so reducing the acoustic energy radiated from the UAV is a high priority. Many noise sources are present in flight vehicles. This research will focus on noise reduction of two small IC 2-stroke engines,

one of which will power the vehicle. Noise reduction of the UAV poses a unique problem because of size and weight constraints. Exhaust noise was found to be the dominant noise source of the UAV, so its reduction became essential in increasing the stealth of the vehicle. When dealing with exhaust noise reduction, backpressure is an important consideration. High backpressure can cause a reduction in engine efficiency [5]. The decrease in engine power caused by high backpressure also leads to a decrease in engine fuel efficiency. In the search for a UAV silencer solution, conventional silencers attaining the desired acoustic reduction did not fit the size and weight constraints required for the vehicle. Conventional designs also lacked the ability to be physically integrated to the vehicle for aerodynamic reasons. To solve this unique acoustic problem, a silencer design was required that could provide a lightweight, small, and effective silencer that was conformable and able to handle harsh flight environment. Research led to the design of a silencer utilizing a refractory foam absorbent [6] inside a lightweight shell. Refractory foam is lightweight, temperature resistant, and easily machined. By taking advantage of refractory foam an effective silencer capable of completing the goals of this research was developed.

In this chapter, a description of engine noise sources is first explained. Next, a review of conventional silencer designs is performed. Following an overview of reactive and dissipative silencers, a literature review on dissipative silencers and their absorptive materials is discussed. Then, the refractory foam absorptive material used to fabricate the silencer designs tested during the course of this research is explained in detail. Finally, the objectives and approach are outlined, followed by the thesis organization.

1.1 – Engine Noise Sources

Two-stroke internal combustion engines have many noise sources. The most well recognized of these noise sources are those caused by the presence of gas pressure waves in the intake and exhaust systems. In the case of exhaust flow, the cylinder pressure falls with the rapid opening of the exhaust port, causing unsteady gas flow behavior. Unsteady gas flow yields an exhaust pipe pressure that changes with engine rpm [7]. This means that the tones present in exhaust noise are dependent on the rpm of the engine. These tones occur at multiples of the engine base frequency. The engine base frequency is simply the frequency of the engine, i.e. revolutions per second.

Inlet noise is dominated by engine base frequency tones much like exhaust noise. It is a change in intake pipe pressure caused by piston motion affecting the cylinder pressure. This causes a volumetric change within that space. Another noise source is present in intake systems containing a reed valve. As flow passes the reed valve, its vibration causes high frequency noise components over a narrow frequency band.

There is also structurally radiated noise from the engine body. Pressure signals caused by combustion pressure rises can be transmitted through the cylinder walls to the atmosphere. This causes the fins of air-cooled engines to become potential noise sources. Another noise source is made by vibration transmission through the piston, bearings, and crankcase walls to the connecting rod. Piston slap is also a common engine noise source. Piston slap occurs when the piston rocks on the gudgeon pin within the cylinder walls around the top dead center and bottom dead center positions [8]. Of the many noise sources present on 2-stroke engines, experts agree that exhaust noise is by far the most significant component of engine noise [8, 9].

1.2 Review of Conventional Silencers

To reduce the exhaust noise present in IC engines, a silencer (muffler) can be used. Depending on the frequency range that requires reduction and constraints that may be present, many silencer options are available. In most cases, the silencer is placed inline with the exhaust pipe. Noise is reduced in conventional silencer designs by using either successive reflections of sound by means of impedance mismatching, or dissipating incident sound energy as heat. According to the technique employed for noise reduction, silencers are divided into two types; reactive silencers and dissipative silencers.

1.2.1 Reactive Silencers

A reactive silencer uses an impedance mismatch to reduce the acoustic energy in the exhaust duct. An expansion chamber is an example of a reactive silencer. Expansion chambers often require large volumes, but they are capable of attaining absorption over a wide frequency band [10]. Many existing silencer configurations, including some fabricated for this research, use variations of an expansion chamber to reduce noise emissions. Therefore, it is important to understand the physics of an expansion chamber. Figure 1.5 is an illustration of the pressure wave reflections present in an expansion chamber. Here p^{in} is the incident pressure wave, p^{r} is the wave reflected at each area discontinuity, and p^{tr} is the transmitted wave. The cross sectional area of each silencer section is S_i.

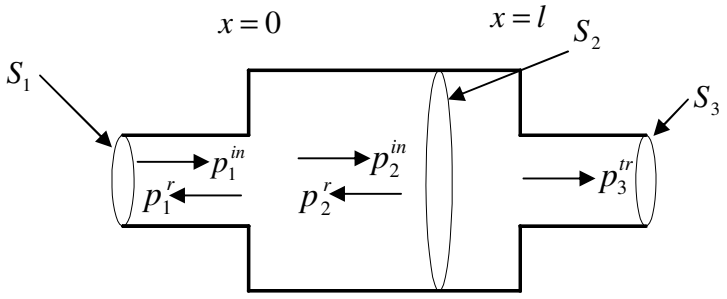

Figure 1.4: Pressure wave reflections in an expansion chamber.

The derivation of how sound propagates in an expansion chamber is reviewed in Appendix A. This derivation results in the following transmission loss equation

$$TL = 10\log_{10}\left[1+\frac{1}{4}\left(\frac{S_2}{S_1}-\frac{S_1}{S_2}\right)^2 \sin^2(kl)\right] \qquad (1.1)$$

This equation is valid for $S_1 = S_3$ and assumes no reflections at the tail pipe. It must also be noted that this derivation is valid for low frequencies where a plane-wave assumption can be used. In this case, the theory is only valid for wavelengths $\geq 0.82D$, where D is the diameter of the chamber [10]. This theory is an approximation, but it predicts the general attenuation behavior of plain-wave sound in an expansion chamber for low to mid frequencies.

It can be readily seen from these equations, that no net power loss results from the use of an expansion chamber. This is because there is no absorption present in a reactive silencer. Area discontinuities simply reflect a substantial amount of power back toward the source. Hence, these designs are often referred to as reflective silencers. These reflections can cause a power robbing load on the engine called backpressure [9]. Backpressure is due to a loss in stagnation pressure that occurs in silencer elements and their junctions [5]. Figures 1.6 and 1.7 provide a graphical representation of Equation 1.1 as the cross-sectional areas and chamber lengths change. These figures show the frequencies of effective absorption as well as the pass-band or resonant frequencies present in an expansion chamber.

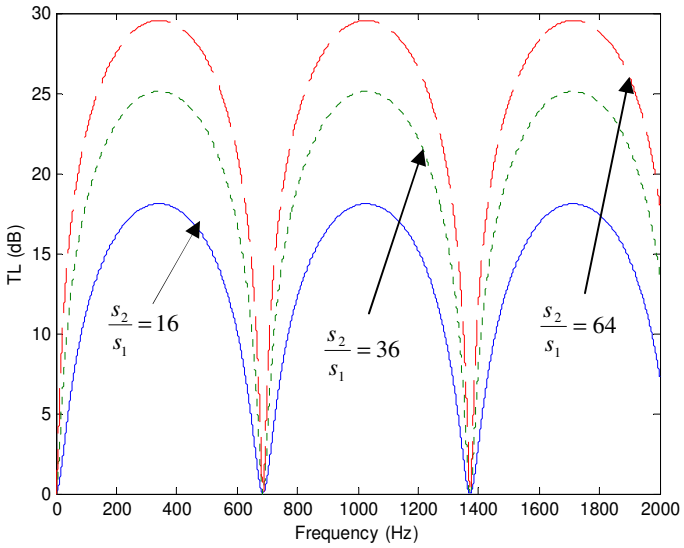

Figure 1.5: Effect of expansion ratio (s_2/s_1) on the TL of a 10" expansion chamber.

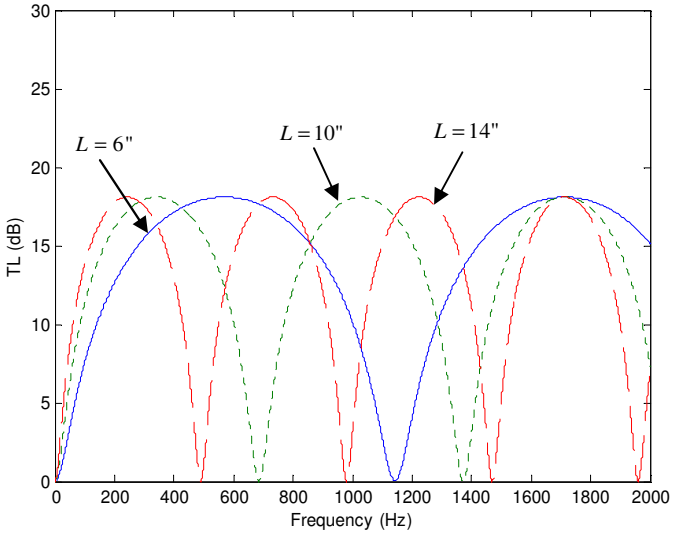

Figure 1.6: Effect of chamber length on the TL of an expansion chamber.

Resonant frequencies in an expansion chamber occur when the length of the chamber is equal to integer amounts of half the wavelength [7]. Resonances in a silencer are identified by a sharp drop in the TL curve that results in a frequency pass-band where minimal sound reduction is achieved. The resonances can be seen in Figure 1.6 as sharp drops in TL at 686 Hz and 1372 Hz. Expansion ratio is defined as the ratio between the cross-sectional areas S_2 and S_1. Figure 1.6 shows the effect of the expansion ratio on

the TL. As the expansion ratio increases, an increase in overall TL is seen. Inspection of Figure 1.7 reveals that the effect of chamber length does impact the chamber resonances. This is because length is present in the $\sin^2$ term of Equation 1.1. Theoretically, the length of an expansion chamber does not impact the amount of TL, but simply shifts the resonance. These resonate frequencies can make the design of a simple expansion chamber difficult when the source produces a varying noise spectrum like an engine changing rpm.

Another type of reactive silencer is the side branch resonator. This design presents a useful way of suppressing pure tones of constant frequency. The side branch resonator works by placing a low impedance element in parallel with the impedance of the remaining flow at its point of insertion [11]. Impedance is a ratio of pressure to velocity, therefore a side branch resonator essentially makes a path of little resistance for a narrow range of frequencies. One advantage of a side branch resonator is that it is generally smaller than an expansion chamber. A side branch resonator may take the form of a Helmholtz resonator similar to the one shown in Figure 1.8, or a quarter wave resonator like the one illustrated in Figure 1.9.

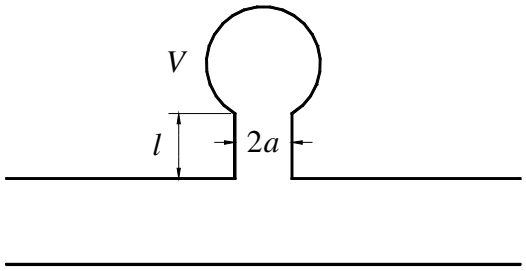

Figure 1.7: Helmholtz resonator.

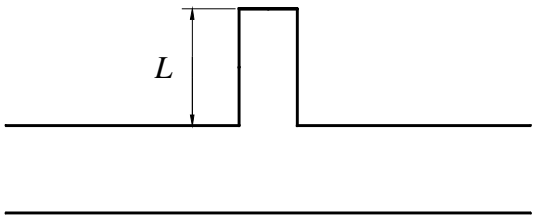

Figure 1.8: Quarter wave resonator.

The Helmholtz resonator consists of a neck with a connected chamber. In a Helmholtz resonator, the fluid in the chamber acts like a spring and the neck acts like a mass. Therefore, the system behaves like a simple oscillator [12]. The system reduces noise across a small frequency band centered about the natural frequency of the resonator. The natural frequency of a Helmholtz resonator is

$$f_0 = \frac{c_0}{2\pi}\sqrt{\frac{S}{l'V}} \tag{1.2}$$

where c_0 is the velocity at which sound travels through the media, S is the cross-sectional area of the neck, l' is the effective length of the neck

$$l' = l + \Delta l \tag{1.3}$$

and V is the volume of the chamber. Equation 1.3 requires an end correction factor, Δl, given by

$$\Delta l = 1.7\,a \quad \text{(outer end flanged)} \tag{1.4a}$$

$$\Delta l = 1.4\,a \quad \text{(outer end unflanged)} \tag{1.4b}$$

A quarter wave resonator is simply a stub off the main flow path whose length is designed to be approximately a quarter wavelength of the frequency of interest. Therefore, the equation for the resonant frequency of a quarter wave stub is

$$f_0 = \frac{c_0}{4L} \tag{1.5}$$

where c_0 is the speed of sound and L is the length of the neck. The TL of a quarter wave resonator is defined as

$$TL = 10\log_{10}\left[1+\left(\frac{S_b}{S}\right)^2 \tan^2\left(\frac{\pi f}{2 f_0}\right)\right]$$

where f is the excitation frequency, S is the cross-sectional area of the main duct, and S_b is the cross-sectional area of the side branch.

To show the acoustic reduction trends present in a side branch resonator as the dimensions change, the TL graphs for some quarter wave resonators are shown in Figures 1.10 and 1.11. In Figure 1.10, the TL curves for quarter wave resonators of different lengths are plotted. It can be seen in this plot that as the length of the tube increases, its resonant frequency decreases. It is also important to note that the 0.15 m tube has two resonances in the 0-2000 Hz range. This is because odd harmonics of the quarter wavelength are also resonant frequencies in a quarter wave resonator. Figure 1.11 graphically depicts the TL of a quarter wave resonator as it varies for different cross-sectional areas. It can be seen that the resonant peaks start to spread as the cross-sectional area of the resonator is increased. Therefore, as cross-sectional area increases, the frequencies in the vicinity of a resonance are more effectively attenuated.

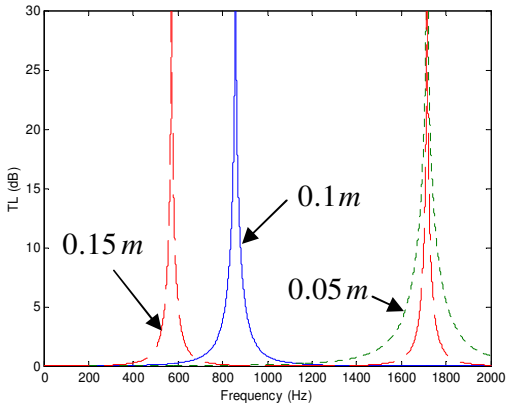

Figure 1.9: TL plots for a quarter wave resonator of different lengths.

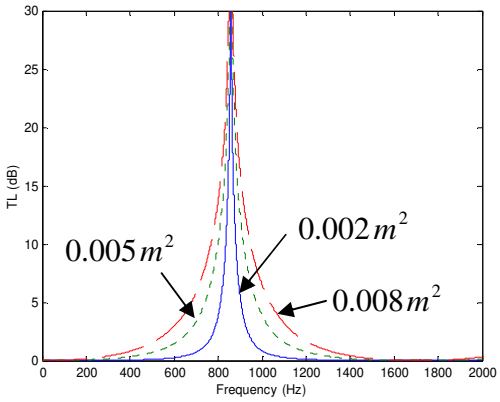

Figure 1.10: TL plots for a quarter wave resonator with different cross-sectional areas.

1.2.2 Dissipative Silencers

Dissipative silencers reduce noise by placing an absorptive material inside the silencer cavity. Using this technique, sound waves are reduced in strength by converting sound energy to heat by means of viscosity [13, 14]. This method is very effective at reducing high frequencies [13]. Dissipative silencer designs often take the form of reactive silencers with added absorptive material. If done correctly, a silencer design using this technique can benefit from the advantages of both silencer types.

Many articles have reported on the effectiveness of dissipative silencers and how they can be improved. Studies by Selamet [14] and Venkanna [8] have shown that lined expansion chambers are preferred over standard expansion chambers with regard to both acoustic attenuation and performance. Clark [13] notes in his paper on fiber metal lined ducts, that the down side to traditional absorptive materials is their tendency to soak up liquids and deteriorate with heat and time. Clark also states that absorptive silencers are the best selection when high flow rates are present in the duct. Porosity of the absorptive material is also mentioned by Paun [15] as an important consideration in a dissipative silencer design. Paun [15] states that in general, higher porosity gives more surface area for flow to contact the material, yielding higher absorption. Unfortunately, many of the best acoustic absorbers can not withstand the heat, vibration, and overall abusive conditions present in aeronautical environments.

One common problem with the design of dissipative silencers is the current difficulty in accurately predicting acoustic results. Without accurate predictions, experiments must be performed to ascertain acoustic performance. Lack of accurate prediction methods presents both a cost and design efficiency problem. The literature presents many different prediction theories for varying silencer configurations, but accurate acoustics predictions of flow through a porous media has not yet been documented in the literature. Cummings and Chang [16] have shown that internal mean flow in porous media can have a dramatic effect on acoustic properties, even for flow velocities as low as 0.5-2 m/s. They go on to say that any method of predicting the transmission loss of bulk-reacting absorbents should account for internal mean flow. In their paper outlining many of the theories used for muffler analysis (most of which do not account for mean flow), Sharkawy and Chazly [10] concluded by commenting that more studies are required to accurately predict the performance of dissipative silencer designs. When discussing acoustic predictions concerning the effects of sound-absorbing material in silencers, Ishikawa [17] states that there are numerous effects which are not yet clear. Based on these observations, Ishikawa has centered his future work on real experimental results. Similarly, Rittmueller [18] chose an iterative approach driven by experimental data to design an effective dissipative silencer rather than using theoretical analysis.

Many absorptive materials have been explored in the literature. The most common temperature resistant absorbents are low stiffness fibrous materials like steel wool, which require the use of a perforated through-pipe inside an expansion chamber. Absorptive material is packed between the perforated pipe and the outer expansion chamber to keep the absorbent in place. This results in a relatively effective design that yields good noise reduction and low backpressure. Selamet [14] revealed that as the perforated pipe porosity is increased, the attenuation is also increased. This presents a problem, because as porosity increases, so do the chances of loosing absorptive material through the perforates. These simple designs usually take advantage of glass wool, steel wool, or mineral wool as the absorptive material. Shenoda [9] tested these different materials and found that glass wool is not preferable for high temperature silencer use, due to the strong variation in acoustic performance as a function of gas temperature and velocity effects.

Shenoda also discovered that mineral wool increased noise reduction by 5-10 dBA compared to using steel wool in the same orientation.

Another method of building an absorptive silencer is to engineer a porous fiber metal sheet that is mounted with a fixed spacing from the wall of an expansion chamber, as explored by Clark [13]. This method of absorption is common among aircraft applications because of its lightweight and lack of liquid absorption. Texturized fiber glass roving is explained by Selamet [14] as another effective acoustic absorbent. The texturization process separates 4000 filament roving strands of fiber glass into individual filaments using turbulent air flow. Fibrous materials are also used for sound absorption. These metallic fiber materials are characterized by their very high porosity and large frequency spectrum of absorption [15]. Compared to fibrous materials, cellular materials are similar, but have a lower degree of porosity. Cellular materials also have a narrower spectrum of acoustic absorption, but they can withstand compressive loads better than fibrous materials [15]. A new temperature resistant shell material is currently being tested as a substitute for sheet metal in muffler systems. This polyamide material held its rigidity to temperatures above 100˚C and yielded good results when tested in adverse automobile conditions [19].

In the search for an absorptive material to achieve project objectives, conventional materials failed to deliver the properties needed to solve the UAV acoustic problem. Absorbents like Glass wool, steel wool, mineral wool, and texturized fiber glass roving can not provide the stiffness required to design effective silencers without the use of a perforated pipe. This leads to bulky silencers that are difficult to conform to the UAV. Use of fiber metal yields a lightweight design, but this technique does not provide broadband absorption. Fibrous materials can absorb sound over a large frequency, but it is unable to resist mechanical loads. Cellular materials can withstand mechanical loads, but its spectrum of acoustic absorption is narrow. Further searching led to the discovery of a material with the all the properties desired for the UAV silencer solution. Refractory foam is a new class of open cell low density material developed to produce lightweight refractory structures for a variety of aerospace and industrial applications [6]. Refractory

foam is currently used for thermal insulation, lightweight precision mirrors, impact absorption, catalyst support, and metal and gas filtration. The only previous effort using this material for noise reduction was performed by Ultramet [20,21]. Their testing incorporated refractory foam in conventional expansion chamber silencers for reduction of exhaust noise on Continental and Lycoming airplane engines. From their experimental work, two important conclusions were obtained. First, the combined dissipative/reactive muffler design developed in this effort was capable of meeting noise reduction, weight, and size requirements for general-aviation aircraft. Second, tuning of the combined dissipative/reactive muffler system is a highly complex and difficult task. In fact, the required analytical tools do not exist for this type of design.

Fabrication of this material begins with pyrolyzing a polymer foam to make a reticulated vitreous carbon (RVC) foam. RVC foam has substantial mechanical and thermal properties. By further chemical vapor infiltration (CVI) processing, ceramic (e.g. silicon carbide [SiC]) and/or metal or mixed material foams can be fabricated [22]. Using CVI to form a SiC foam results in greatly improved structural characteristics. Figure 1.12 is a picture of what refractory foam cells look like under magnification. Table 1.1 shows the available porosities and bulk densities of refractory foam, and the maximum temperatures the material can withstand. The availability of different porosities provides the ability to optimize the material to the application. A porosity of 80 ppi was used in the silencers designed for this project. Figure 1.13 contains strength and modulus graphs for SiC foam, both of which increase with increased bulk density as expected.

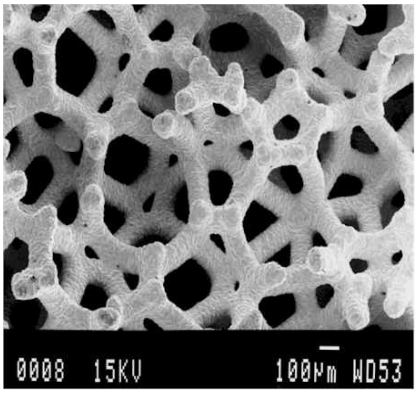

Figure 1.11: Refractory foam under magnification [6].

Table 1.1: Mechanical Properties of SiC Foam.

Porosities available (ppi)	**10, 20, 45, 65, 80, 100**
Bulk densities available (g/cm³)	**0.10-1.45**
Maximum use temperature (°C)	**(in air) ---------- 1700** **(inert) ---------- 2500**

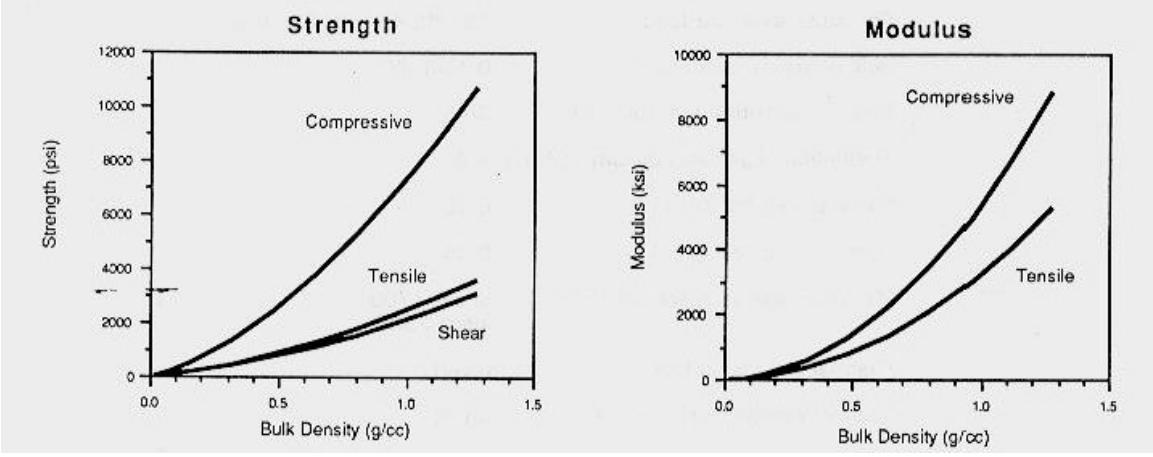

Figure 1.12: Mechanical Property graphs for SiC Foam.

The refractory foam benefits explored in here will focus on its ability to absorb sound energy while surviving the temperature and vibration environments common to exhaust silencers. Another notable advantage of refractory foam is its ability to be easily machined into complex shapes. An example of the type of complex configurations possible is shown in Figure 1.14. Machining capability will allow complex flow patterns in a silencer system which would be very difficult to achieve with conventional material. Cost is one downside to refractory foam. The carbon foam used in the majority of these silencers is $1.50 per cubic inch. The SiC foam is presently $13.00 per cubic inch because it is not a production item. However, if a design implementing this material was mass produced, it could drive the price down.

Using refractory foam technology, it is possible to make an effective dissipative silencer with broadband absorption characteristics that can survive the abusive environments seen in many silencer applications. Refractory foam silencers can also be designed to provide compact and lightweight designs that can be easily conformed to the UAV.

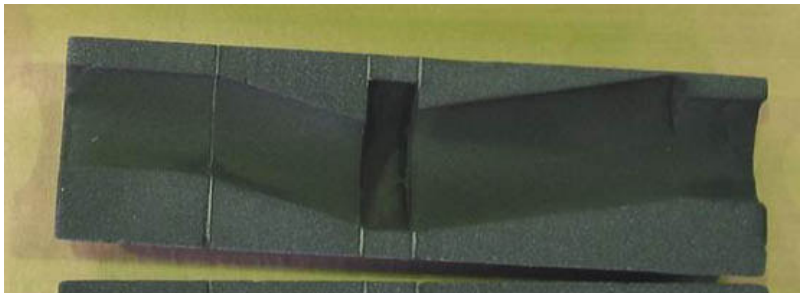

Figure 1.13: Cross section of refractory foam used in previous testing performed by Ultramet.

1.3 Research Objective and Approach

The main objective of this work is to fabricate a small IC engine silencer for use on the UAV that is lightweight, small, acoustically effective, durable, and conformable. It must do all this without placing excessive backpressure on the engine. This objective will be reached by fabricating and testing silencers incorporating refractory foam. For the purpose of comparison, a number of silencers were also collected from commercially available designs. Based on the complexity and lack of accuracy in predicting noise attenuation in porous media, an experimental approach was chosen as the primary design tool for this research. In the first phase of testing, the silencers were tested in an anechoic chamber using a speaker to provide a consistent noise source. Since the goal of these experiments was for preliminary evaluation of the silencer designs, only noise measurements were carried out. In the second phase, the silencers were tested on two IC engines to evaluate their performance under realistic environmental conditions, i.e. temperature, flow, vibrations, and so forth. Upon analysis of the results, silencers were modified and new designs were fabricated. Testing was then repeated and the silencer designs were optimized in an iterative fashion. Engine testing involved the measurement of noise, engine speed, temperature, and backpressure. During the course of research, all objectives were achieved with silencers incorporating refractory foam technology.

1.4 Thesis Organization

The remainder of this thesis is presented in 5 additional chapters. The experimental setup and data processing are explained in Chapter 2. The experimental setup and data acquisition for testing in the anechoic chamber is outlined. Setup and data acquisition for engine testing is reported. The post processing performed to allow easy assessment of the data is summarized. In Chapter 3, pictures, drawings, and a short description of each silencer design fabricated for testing is provided. Chapter 4 starts by graphically presenting trends in inlet and exit tube geometries in the form of insertion loss plots. Then, insertion loss plots and the conclusions drawn from these plots are provided for each silencer design tested. The results for the engine tests are shown in Chapter 5. These results are shown graphically in the form of frequency response curves and directivity plots. The trends that can be drawn from these results are then summarized. For easy comparison, each silencer plot is compared to the results found for the baseline case. Finally, the conclusions of the research along with recommendations for future work are outlined in Chapter 6.

Chapter 2 – Experimental Setup & Data Processing

This chapter presents the experimental setup, procedure, and data processing for the tests performed during the course of this research. First, the preliminary speaker input tests are described. The speaker test setup is summarized, followed by explanations of the data acquisition process and the testing procedure. Next, the engine input tests are outlined. A description of the engine test setup is followed by an explanation of the data acquisition process. The testing procedure is then outlined. This chapter ends with details of the data post processing.

2.1 Preliminary speaker tests

The main objective of speaker input testing was to investigate possible silencer designs using a consistent noise source that encompassed the frequencies of interest. These tests were performed in an anechoic environment. In acoustic testing, insertion loss (IL) measurements are often used to determine the potential of a silencer for reducing noise across a frequency band. Insertion loss is defined as the sound pressure level reduction at a particular point in space with and without a noise control device. Though similar, transmission loss (TL) is also used as a metric to evaluate the performance of noise control devices. Transmission loss is the reduction in sound power level due to a noise control device. However, under some conditions the insertion loss is the same as transmission loss. In silencers, TL is the difference between the incident sound power recorded at the silencer entrance and the sound power transmitted by the silencer [11]. Because of the reflections present at the silencer inlet, reactive silencers can yield very different IL and TL results. In most cases, IL and TL are the same when dealing with dissipative silencer devices [11]. IL results were used here as the metric to gain understanding of the acoustic characteristics of different silencer design concepts. These tests provide accurate acoustic data without the added complications inherent in the engine input testing like noise reflections, propeller noise, and engine noise sources.

Preliminary speaker test setup:

To perform speaker input tests, the signal generator in a Hewlett Packard (HP) analyzer was used to feed a white noise signal through a two channel Proton power amplifier to a Universal Sound compression driver(s). This driver(s) was then connected to the silencer inlet(s). Since silencers were tested on both single and twin cylinder engines during later engine testing, both engine configurations were simulated in the speaker tests. Therefore, depending on the silencer design being tested, a single or two speaker input configuration was required. Silencers fabricated for the single cylinder engine use a single speaker as shown in Figure 2.1. Silencers fabricated for the twin cylinder engine require two drivers to simulate the two engine exhaust exits, as seen in Figure 2.2. Due to the size of the compression drivers and the distance between exhaust exits on the dual exhaust engine, a pair of bent inlet pipes was required for installation. In the dual speaker configuration, it was important to run the two drivers in phase because the cylinders of the twin cylinder engine fire simultaneously.

To monitor the sound pressure output from the system, a Brüel & Kjear (B&K) microphone was used. This microphone was mounted two feet directly above the silencer exit to measure the sound pressure level with the silencer installed and two feet above the speaker exit to find the sound pressure level of the source, i.e. without a silencer. A single microphone was used because both the compression driver input and the tested silencers behave as monopole sources. The signal recorded by the microphone was sent through a B&K pre-amp and then to the HP analyzer for viewing and recording. All speaker tests were performed in an anechoic chamber.

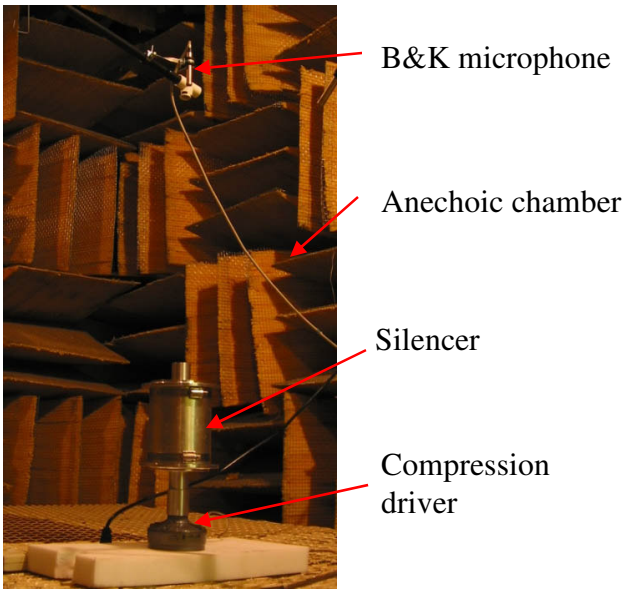

Figure 2.1: Speaker test using a single driver to model the single cylinder engine.

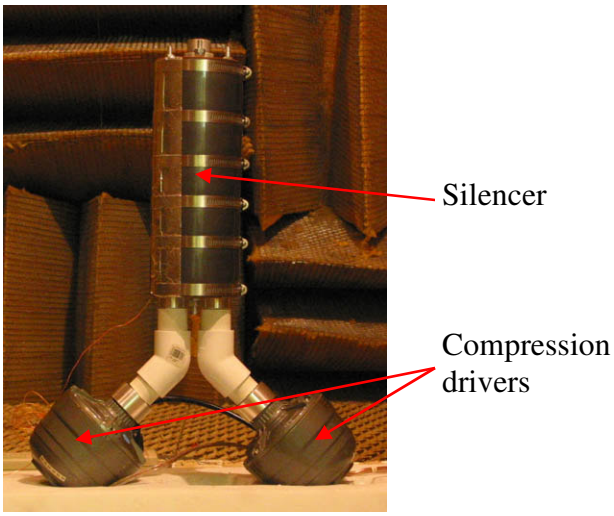

Figure 2.2: Speaker test using two drivers to model the twin cylinder engine.

Data acquisition for speaker tests:

Data acquisition of speaker test results was accomplished using a HP analyzer. Sound pressure level measurements from the microphone were recorded using 20 averages over a 0-6 kHz frequency range. Preliminary engine measurements yielded a 0-3 kHz range of target reduction, but knowledge out to 6 kHz helped to better characterize the silencers and the refractory foam. In this frequency range, 800 lines of resolution were recorded. This resulted in a frequency resolution of 7.5 Hz.

Procedure for speaker testing:

Throughout the course of speaker testing, the following procedure was followed. A 5Watt/8Ω white noise signal was sent to the compression driver(s). First, the sound pressure level spectrum was measured two feet above the speaker exit. Then, the silencer was installed on the compression driver(s) and the microphone was moved to a location two feet above the silencer exit. When testing the dual compression driver configuration, a 5Watt/8Ω white noise signal was sent to each driver in phase to simulate the twin cylinder engine. After the silencer and microphone were in place, the same 5Watt/8Ω white noise signal was sent to the source and the sound pressure level with the silencer in place was recorded and saved. This procedure was performed for each silencer design tested.

2.2 Engine performance tests

Engine tests were done to determine how the silencers would perform in a more realistic flight environment. Accurate acoustic behavior can be predicted by speaker testing, but factors such as backpressure, temperature, and vibration effects remain unknown without performing engine tests.

Engine test setup:

During the course of this project, testing was performed using two different engines. One engine tested was the ZDZ 40-RE 2-stroke single cylinder engine [23] seen in Figure 2.3. The other engine was the 3W-150iB2 2-stroke twin cylinder engine [24] shown in Figure 2.4. The ZDZ 40-RE 40 single cylinder engine has a power rating of 4.8 HP and a weight of 3.4 lbs. Its RPM range is 1200-7800 RPM, and it has a 2.4 cu.in displacement. The 3W-150iB2 twin cylinder engine has a power rating of 13.5 HP and a weight of 8.58 lbs. It covers the 1100-8500 RPM range and has a displacement of 9.2 cu.in.

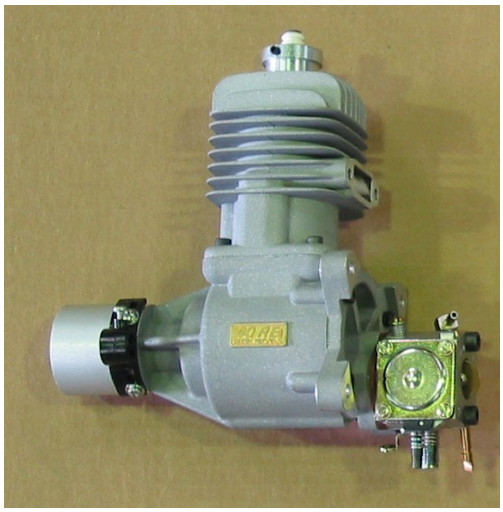

Figure 2.3: ZDZ 40-RE 40 engine.

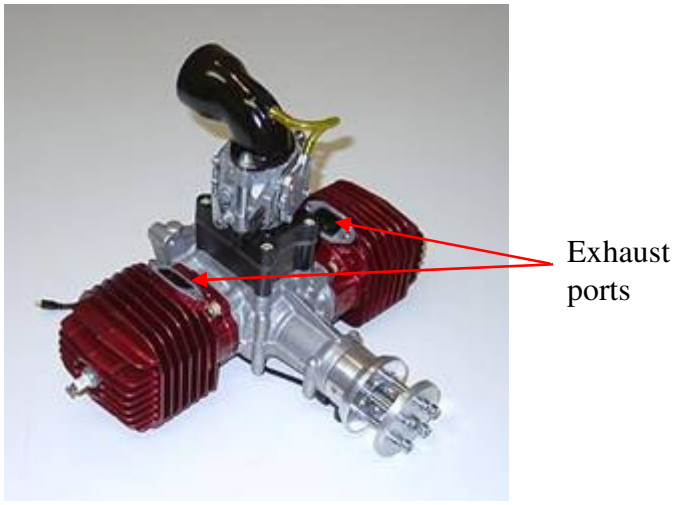

Figure 2.4: 3W-150iB2 engine.

For testing these engines, a test stand was fabricated. The main structure of this test stand was built from extruded aluminum bars which were bolted to the surface of a heavy duty wheeled cart, as seen in Figure 2.5. This cart was used to mount either the ZDZ 40-RE 40 or the 3W-150iB2 engine. Foam was also added to the main frame to help damp any structural vibration during testing.

To attain the correct noise signature, the engine must be run under load. For these tests, a propeller was used to provide engine loading. Both two and three-bladed propellers were used during the course of engine testing. A 2-bladed propeller was used for all single

cylinder engine testing. For measurements on the twin cylinder engine, a 3-bladed Fuchs propeller [24] was used. To learn what contribution the propeller had to the noise spectrum, some twin cylinder engine tests were performed using a 2-bladed Fuchs propeller [24]. Propeller noise occurs at multiples of the engine harmonics corresponding to the number of blades on the propeller. For example, if a 2-bladed propeller is used, it will contribute to the noise spectrum at even multiples of the engine harmonics. For a 3-bladed propeller, noise will be increased at every third engine harmonic, and so on. Therefore, propeller noise can be compensated for after testing propellers with different blade numbers to learn their contribution to the frequency spectrum.

To represent the size of the Allied Aerospace UAV with respect to the silencer designs, an aluminum pod the same size as the center body of the Allied Aerospace UAV [3] vehicle was added to the test stand. A 3d model representing this pod in relation to the UAV vehicle is shown in Figure 2.6. The addition of this pod to the experimental setup assists in visualizing how integration of the muffler into the final vehicle might be accomplished.

Figure 2.5: Test cart with the 2 cylinder engine mounted.

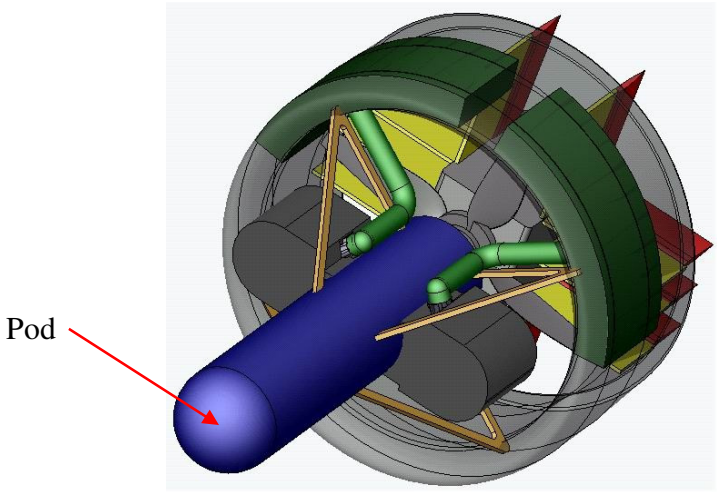

Figure 2.6: 3d model of the Allied Aerospace UAV.

This section outlines the sensors used during engine testing to record acoustic, engine speed, temperature, and backpressure measurements for the tested silencers. For recording acoustic data, a 180˚ microphone arc, consisting of 7 PCB Piezotronics (PCB) microphones, was laid in a 12' radius around the engine. An illustration of this microphone arc is shown in Figure 2.7. Each microphone in this arc was taped to an 8" x 8" sheet of aluminum, as seen in Figure 2.8, to provide consistent ground reflections. A ground-mounted array was used because it is less susceptible to wind noise and easier to implement than an arc placed at engine height. One factor that must be considered when using a ground mounted array is that ground reflections cause an increase in sound pressure level of up to 3 dB. To compensate for this increase in noise levels an 8th microphone was placed on a stand at engine height in the 90˚ position. An Extech Instruments sound level meter was also placed at engine height in the 90˚ location to record average A-weighted SPL data over the whole frequency spectrum [0-20 kHz]. A picture of the microphones placed in the 90˚ location is shown in Figure 2.9. The data from this sound level meter was used for recording overall acoustic values and for comparison with the data recorded by the 8th microphone. Since the 8th microphone is only recording data up to 6 kHz, the difference between the values recorded by the sound level meter and the 8th microphone indicate the presence of high frequency noise content. All microphones, including the sound level meter, were calibrated with a 1000 Hz signal at 93.8 dB using a B&K calibrator. To prevent any direct reflections from a near

building, a large piece of absorbing foam was placed in the area where direct reflection could occur as shown in Figure 2.10.

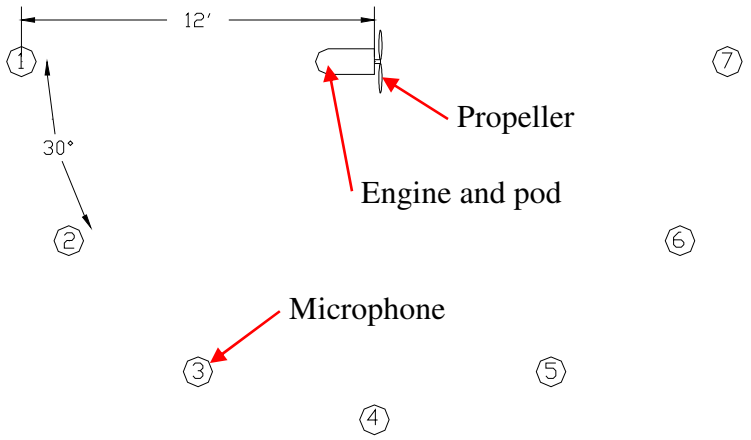

Figure 2.7: Microphone arc in relation to engine.

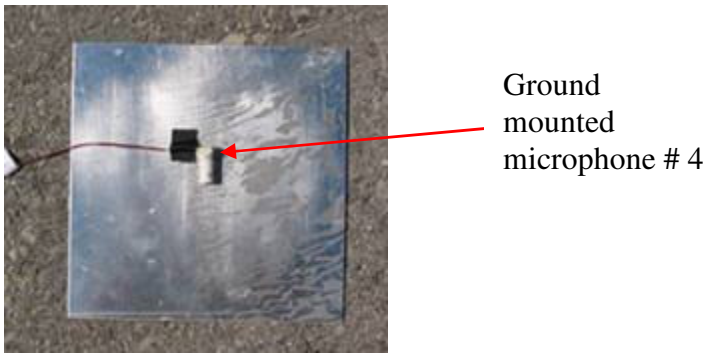

Figure 2.8: PCB microphone mounted in the ground-mounted arc.

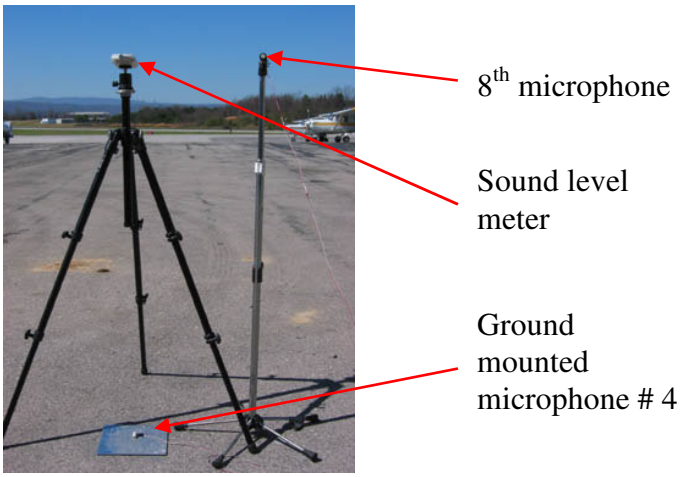

Figure 2.9: 90° arc location in the microphone arc.

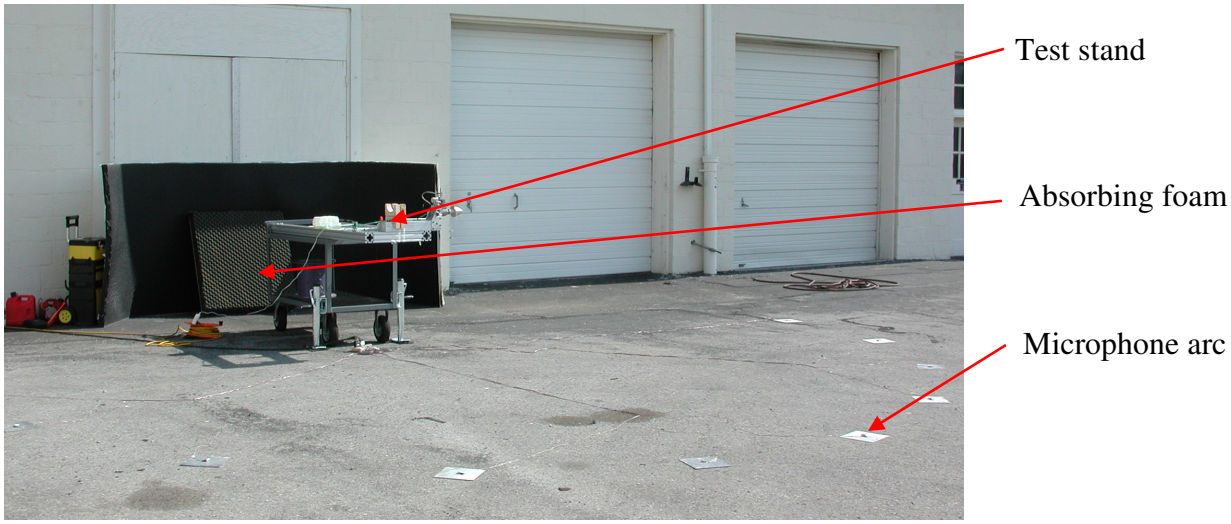

Figure 2.10: Engine test area.

For temperature measurements, an Omega 36 gauge thermocouple(s) was used to record silencer inlet temperature in the configuration pictured in Figure 2.11. Temperature gives an indication of the amount of load present on the engine, and it also provides a design point for the use of nonmetallic materials used in the silencer designs.

An Extech digital tachometer was used to measure the propeller speed. Engine speed measurements were important because accurate data comparisons hinge on the ability to test silencers at approximately the same speed.

To perform mean backpressure measurements, a Dwyer digital manometer was set to record readings from the pressure tap pictured in Figure 2.11. The higher the engine exhaust port pressure, the higher the load induced on the engine. This has negative effects on engine performance and fuel efficiency. This measurement provides a quantitative means to compare designs based on the backpressure they place on the engine.

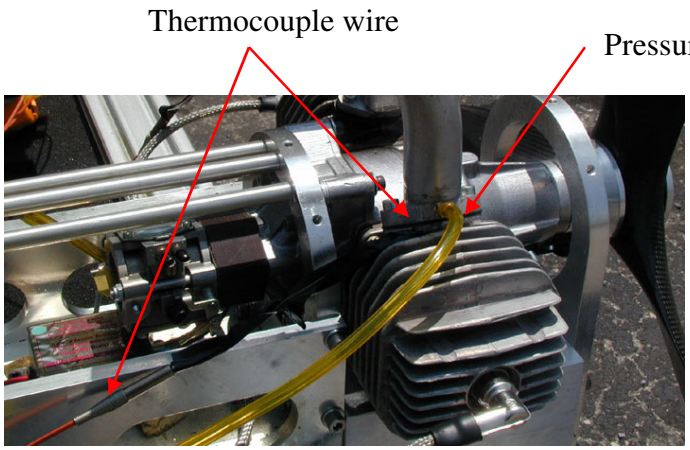

Figure 2.11: Thermocouple and pressure tab installation on the twin cylinder engine.

Data acquisition for engine tests:

For capturing engine test data, a National Instruments data acquisition (DAQ) system was used to send the measurements from the microphones to Labview software. The low pass filter in the data acquisition system was set at 5000 Hz, but the results are only plotted to 3000 Hz because of a roll off in engine noise seen after 3000 Hz. The sampling frequency was set at 16000 Hz. A voltage range of +/-5V was used for each microphone channel. All acoustic data was saved by Labview in the form of a frequency spectrum with 8192 spectral lines of resolution recorded over the 0-5 kHz frequency range.

Procedure for engine testing:

The following procedure outlines the steps that were taken during engine testing. First, the engine was started and the throttle was adjusted until the digital tachometer reached the target engine speed. The target engine speed for testing the single cylinder engine was 6500 rpm. For the twin cylinder engine, the target engine speed was 5000 rpm. After the engine was warmed up, acoustic data from the microphone arc was taken simultaneously over 20 averages. This data was then saved in Matlab format for later analysis. After the microphone data was taken, the sound level meter data was recorded. For the twin cylinder engine tests, the mean backpressure was recorded. Backpressure was not recorded for single cylinder engine because that engine was only used for preliminary acoustic engine testing. Finally, temperature measurements were recorded at the engine exhaust port(s). When all measurements had been taken, the engine was

turned off. After the engine was allowed to cool, this procedure was repeated with another silencer.

2.3 Data post processing

Post processing of speaker test data:

The microphone signals from the speaker tests were recorded by the HP analyzer in the form of A-weighted SPL frequency spectrums. Once these frequency spectrums were recorded, IL spectrums were generated simply as

$$IL = SPL_{source} - SPL_{silencer\ exit} \qquad (2.1)$$

where SPL_{source} serves as the baseline and is defined as the sound pressure level recorded two feet above the speaker(s) and $SPL_{silencer\ exit}$ is the sound pressure level recorded two feet above silencer exit.

Post processing of engine test data:

This section outlines how the engine test results were processed. First, all the frequency spectrums were calibrated and converted to decibel (dB) values and A-weighted (dBA). To correct for ground reflections caused by the ground-mounted microphone arc, an average difference was taken between the ground-mounted 90˚ microphone and engine height 90˚ microphone. Based on these results, a 2.8 dB correction factor was subtracted from the acoustic data recorded with the ground-mounted arc. Since the main focus was to determine silencer noise reduction, correcting the data for ground reflections is not of great importance. However, this correction provides more accurate noise level values.

Engine noise test results are graphically displayed in three ways: (i) average SPL spectrum, (ii) envelope spectrum, and (iii) radiation directivity plots. For average and envelope plot calculations, microphone 1 was removed from the data because of excess wind noise. Microphone 1 was located on the ground directly behind the propeller, causing a significant increase in the low frequency noise content which masked the

engine signature. For directivity plots however, microphone 1 was still used because the low frequency wind noise caused by the propeller was not significant when averaging results over the recorded frequency span.

Average plots:

The data from microphones 2 through 7 in the arc were log averaged to yield a single frequency spectrum. Figure 2.12 plots the frequency spectrum of each separate microphone on the same graph for the twin cylinder engine baseline case. The corresponding average spectrum of the twin cylinder engine baseline case is shown in Figure 2.13. Comparing multiple acoustic tests without averaging the microphone locations would make the results hard to distinguish, and comparing the spectrums of single microphones would be impractical. This averaging method simplifies graphical comparisons between different silencer tests, while still providing results that reflect the data from the whole microphone arc.

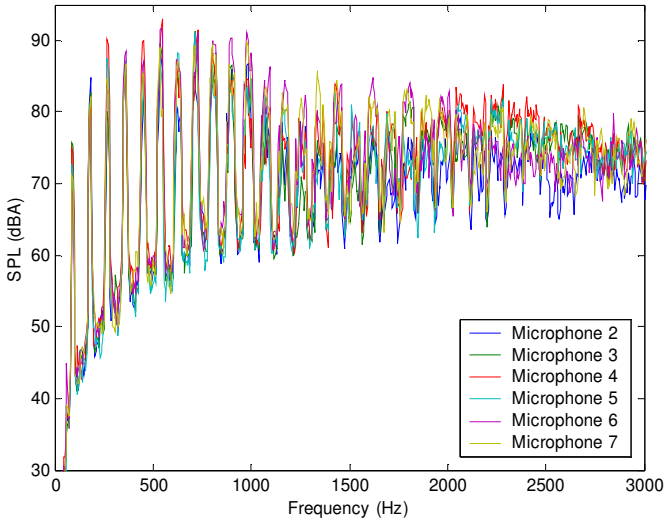

Figure 2.12: Acoustic data from each microphone in the array for the 3W150 twin cylinder engine baseline case.

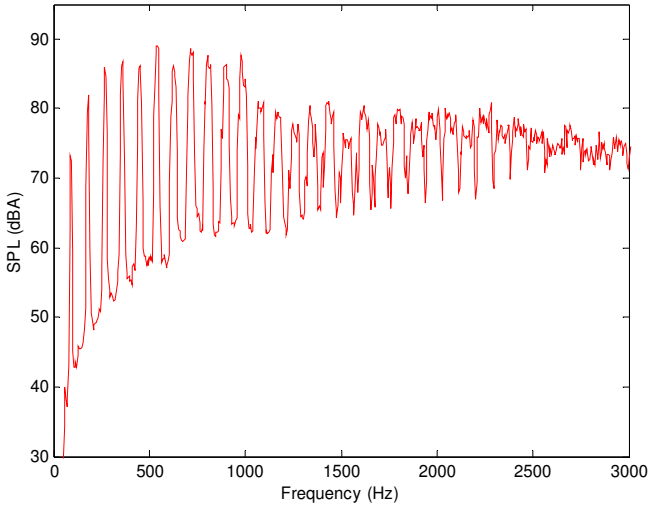

Figure 2.13: Averaged acoustic data across the microphone array for the 3W150 twin cylinder engine baseline case.

Envelope plots:

As you can see in Figure 2.13, engine noise is dominated by tones. The goal of envelope plots is to provide an easy graphical comparison between the acoustic levels of engine tones for different silencers. Envelope plots, as they are defined in this paper, simply plot the data points of each peak in the average acoustic spectrum. These peaks represent engine base frequency multiples. Exhaust noise occurs as the fundamental and higher harmonics of an engine base frequency. The engine base frequency is the frequency of the engine, i.e. revolutions per second. An envelope plot of the twin cylinder engine baseline case can be seen in Figure 2.14. When multiple frequency spectrums are being compared on the same plot, the differences between the engine base frequency peaks are often hard to distinguish because of overlapping data. Envelope plots were prepared so multiple tests could be easily compared on the same plot. Since engine tones are the most dominant engine noise, comparing them was the best approach to rate the effectiveness of a given silencer. Envelope plots easily illustrate how much a given silencer is reducing each particular engine tone. It should be noted that at frequencies above 3 kHz, it becomes difficult to distinguish the engine base frequency multiples. This is why frequency data only goes to 3 kHz. Reducing the engine tones is the most important factor in reducing engine noise, and after 3 kHz the tones become insignificant

compared to the tones found in the 0-3kHz range. This trend can be clearly seen in the twin cylinder engine baseline case shown in Figure 2.15. To make identification of the engine base frequencies easier in these plots, the frequency axis was normalized by the fundamental frequency as seen in Figure 2.16. The 35 engine tones in the 0-3000 Hz band correspond to the 35 data points used in Figure 2.16.

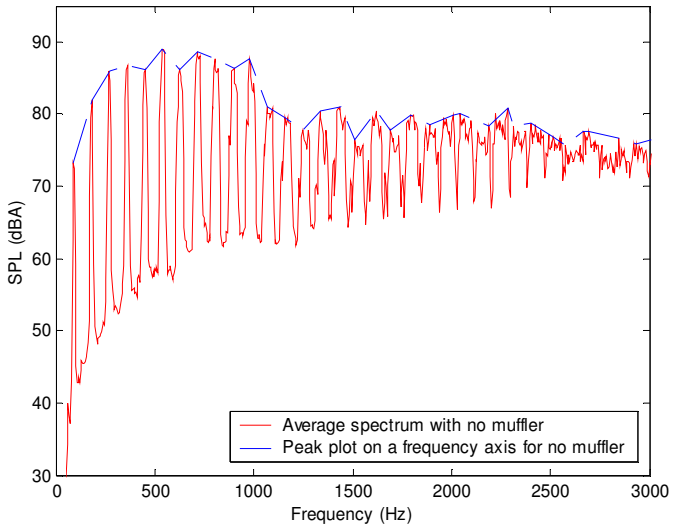

Figure 2.14: Average and envelope plots for the 3W150 twin cylinder engine baseline case.

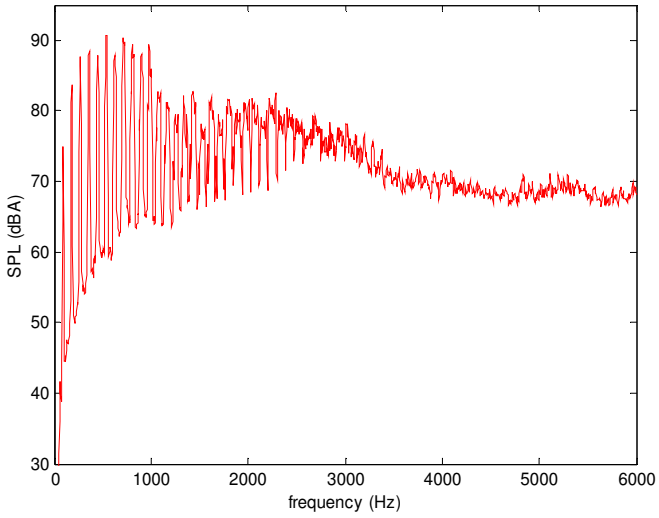

Figure 2.15: 0-6 kHz average plot for the 3W150 twin cylinder engine baseline case.

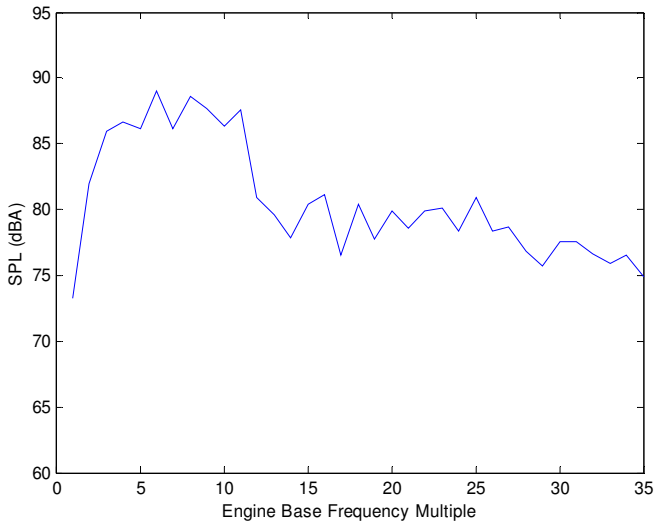

Figure 2.16: Envelope plot for the 3W150 twin cylinder engine baseline case using a normalized fundamental frequency axis.

Radiation Directivity Plots:

Radiation directivity plots are polar plots used to graphically represent the noise field radiated 12' from the engine on a horizontal plane. These plots were prepared using the overall A-weighted SPL (OASPL) of each microphone in the ground mounted arc to represent the radial noise field. The use of OASPL data was chosen over focusing on single harmonics because of the large amounts of data produced by inspection of single harmonics. It is assumed that the acoustic energy from these engines is symmetric in the horizontal plane about the engine axis. This is why 360˚ plots are able to be created from data that only accounts for 180˚. OASPL data provides a way to represent a lot of radial data in a single graph. The radiation directivity plot for the twin cylinder engine baseline case is shown in Figure 2.17. For the baseline case, the exhaust exits upward, perpendicular to the data represented in the graph. In this case, the acoustic energy spreads out to produce relatively consistent radial plot like the one shown in Figure 2.17.

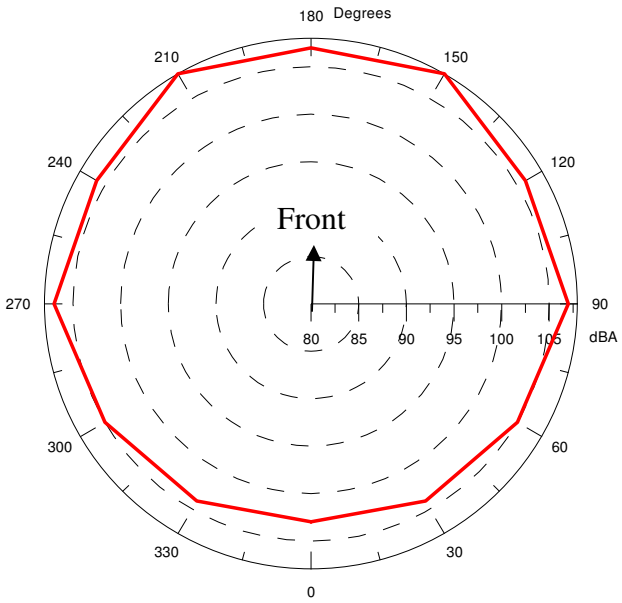

Figure 2.17: Overall sound pressure level directivity plot for the baseline twin cylinder engine case.

Chapter 3 – Silencer Designs

This chapter introduces the silencer designs tested during the course of this research. The chapter is separated into two main sections: silencers tested on the ZDZ 40-RE 40 and 3W-150iB2 engines, respectively. This separation is made because the ZDZ 40-RE engine has a single exhaust port, while the 3W-150iB2 engine has two exhaust ports. Some of the silencers tested were commercially available designs. The purpose of testing commercially available silencers was to provide a baseline so comparisons could be made to refractory foam silencers. However, most of the silencers were fabricated specifically to solve the acoustic problem presented by the UAV. The silencer descriptions include their internal volumes, weights, exit-to-inlet area ratios, and fabrication materials. The volume occupied by these silencers constitutes a key parameter in whether or not they can be effective in this UAV vehicle. Weight is also a large factor in designing a UAV silencer. Silencer exit-to-inlet area ratios provide a method of comparing the constriction imposed on the exhaust gas flow due to exit and inlet geometries. It is also an important parameter in noise attenuation. The materials used to fabricate a silencer have a large effect on the weight and effectiveness of the design. Standard materials such as aluminum and steel were used in many of the tested silencer designs, but more advanced materials were also explored. Pictures for each silencer and drawings showing the external and internal dimensions will be presented. The inside dimensions for the commercial designs are not known.

3.1 – Silencers designed for the single cylinder engine

Seven different silencers were tested on the ZDZ 40-RE 2-stroke single cylinder engine. Two of these were commercially available silencers and the remaining five silencers take advantage of refractory foam. Out of the five refractory foam silencers, one was previously tested for use on small passenger planes [20], and two were modifications of silencers previously tested on small passenger planes. The remaining two silencers were designed and fabricated in-house based on knowledge gained from testing previous designs.

Double exhaust exit:

The *double exhaust exit* silencer is commercially available as the ZDZ 40 RV-L and it was specifically designed for this engine [23]. Figure 3.1 shows the outer dimensions of the silencer, and a picture of the *double exhaust exit* design can be seen in Figure 3.2. It is made of aluminum and its inner volume is $6.9\,in^3$. It weighs 186.6g. The *double exhaust exit* has an exit-to-inlet area ratio of 0.79, which causes a small constriction in the exhaust gas flow.

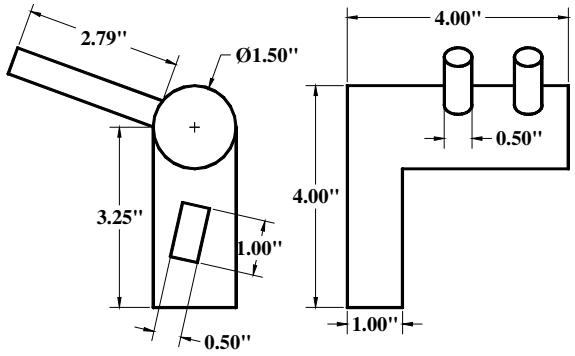

Figure 3.1: *Double exhaust exit* drawing.

Figure 3.2: *Double exhaust exit* picture.

Black single exit:

The *black single exit* is a silencer commercially available as the SMQ-M [25]. Figure 3.3 is a drawing showing its outer dimensions, and a picture of this silencer is shown in Figure 3.4. The exit-to-inlet area ratio is 0.39, which makes this the most constrictive silencer tested. The inner volume of the *black single exit* silencer is $15.5\,in^3$, and its weight is 218.3g.

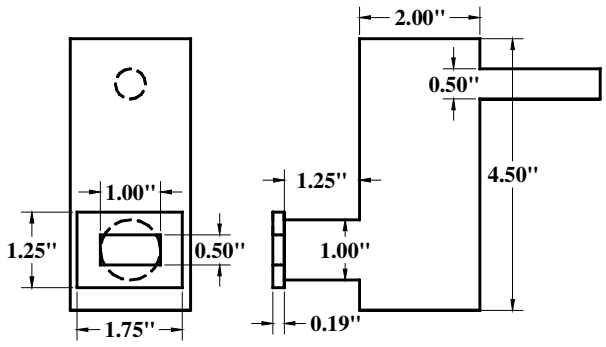

Figure 3.3: B*lack single exit* drawing.

Figure 3.4: B*lack single exit* picture.

Airplane silencer:

The *airplane silencer* incorporates SiC refractory foam material and it was previously tested as a small passenger plane silencer [20]. Therefore, it is larger than many of the acoustic solutions explored in this research, but knowledge of its acoustic performance will still be valuable. This design is very similar to the common dissipative design, i.e. an inner perforated tube and a mineral wool/steel wool filled chamber. The *airplane silencer* improves on this basic dissipative design by maximizing contact with the absorptive material. This improvement is accomplished by replacing the perforated pipe and mineral wool/steel wool combination with the refractory foam cylinder. By relying on the inherent stiffness of refractory foam, the perforated pipe can be removed. The design of the *airplane silencer* is shown in Figure 3.5. It incorporates a 1" thick cylindrical refractory foam absorbing liner housed inside a welded steel shell. The volume of the *airplane silencer* is $165.2\,in^3$, and its weight is 1969.0g. This silencer was originally designed for a larger engine, so it has an exit-to-inlet area ratio of 9.82, which is the largest of the silencers tested. The exhaust port area of the single cylinder engine is only 0.5in^2, so an adapter had to be made to match up to the 2.5" diameter silencer inlet used for the larger airplane exhaust it was originally designed for. According to Selamet [13], removing the inner perforate tube can greatly increases the effectiveness of a dissipative silencer. The stiffness of refractory foam provides a significant advantage over similar designs that require a perforated tube to keep the absorbent in place. A picture of the *airplane silencer* design can be seen in Figure 3.6.

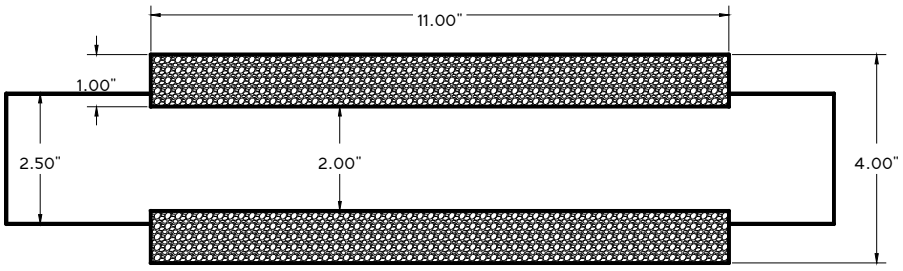

Figure 3.5: *Airplane silencer* drawing.

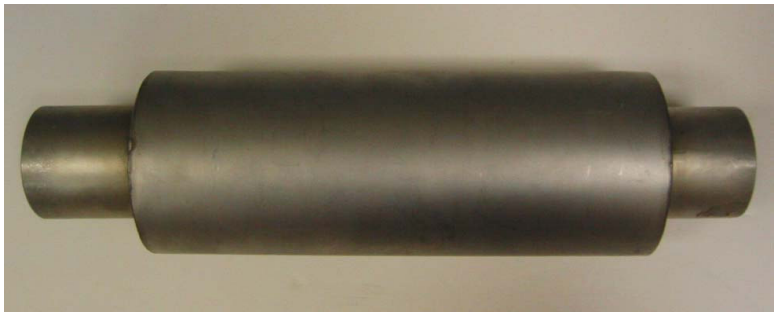

Figure 3.6: *Airplane silencer* picture.

Airplane silencer w/ plug:

Since the *airplane silencer* was originally designed for a much larger engine, improvement in noise attenuation can be achieved by reducing the silencers exit-to-inlet area ratio. This is achieved by reducing the exit area, which causes an increase in acoustic reflections inside the silencer. This increase in reflections will provide more contact time with the absorbent. To achieve this in the *airplane silencer*, a two layer perforated plug of refractory foam material and pine was added to the exit pipe of the *airplane silencer* as shown in Figure 3.7. The plug in the *airplane silencer w/ plug* design was perforated with 3 quarter inch holes, thus reducing the exit-to-inlet area ratio to 0.30. The added plug increased the weight to 2020.0g.

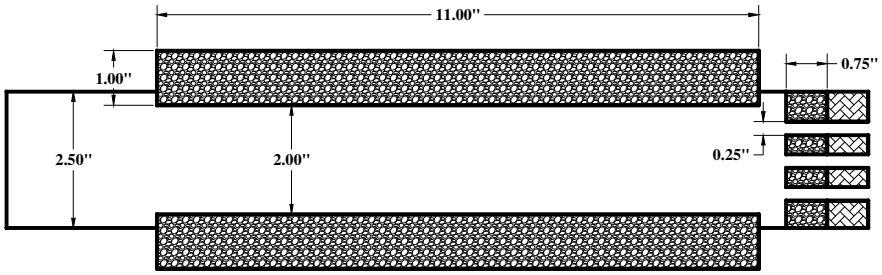

Figure 3.7: *Airplane silencer w/ plug* drawing.

Chevron liner:

The *chevron liner* silencer implements a more complicated flow pattern than the constant cross-section seen in the *airplane silencer*. It was named for the basic chevron shape of its refractory foam liner. A drawing of the *chevron liner* can be seen in Figure 3.8. It's $178.3\,in^3$ volume makes it the largest silencer tested. This refractory foam liner was also designed for silencing small passenger airplane noise in the same project that the *airplane silencer* was used [20]. The shell is made of aluminum sheet metal wrapped around machined aluminum end caps. A picture of the *chevron liner* silencer is shown in Figure 3.9. The purpose of this flow path was to break up pressure pulses by eliminating line-of-sight flow, and to provide a decrease in flow velocity by incorporating a small expansion in the middle of the liner. The exit-to-inlet area ratio for the *chevron liner* is 1.57, and its weight is 2356.0g. This means the exit area is larger than the entrance area, which allows for a more restrictive internal refractory foam flow path without greatly increasing the backpressure. This design is a good example of the kind of imaginative flow paths that can be formed using refractory foam.

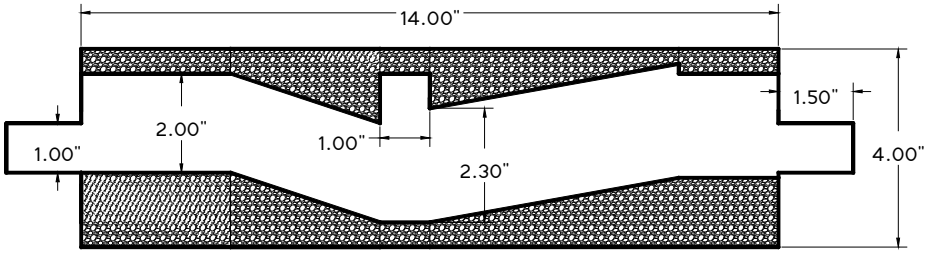

Figure 3.8: *Chevron liner* drawing.

Figure 3.9: *Chevron liner* picture.

Bend flow:

This design again takes advantage of the complex shapes that can be machined out of refractory foam. The *bend flow* silencer uses circular 1" thick cross sections of refractory foam glued together in alternating orientations. The internal dimensions that result from these cross sections can be seen in Figure 3.10. This method increases the effective length of the silencer by "bending" the path of least resistance through three half-inch diameter holes in each of the five walls. It is important to note that the path of least resistance is not the only path available to the flow. The porosity of the refractory foam causes absorption of exhaust noise as it flows though the walls. This design technique maximizes the exhaust flow contact with the refractory foam. A picture of the *bend flow* design can be seen in figure 3.11. For its $165.7\,in^3$ internal volume, this design provides more refractory foam area than the simple *airplane silencer*. The *bend flow* silencer has the same 1.57 exit-to-inlet area ratio as the *chevron liner* because they use the same aluminum end caps. The weight of this silencer is 2238.7g.

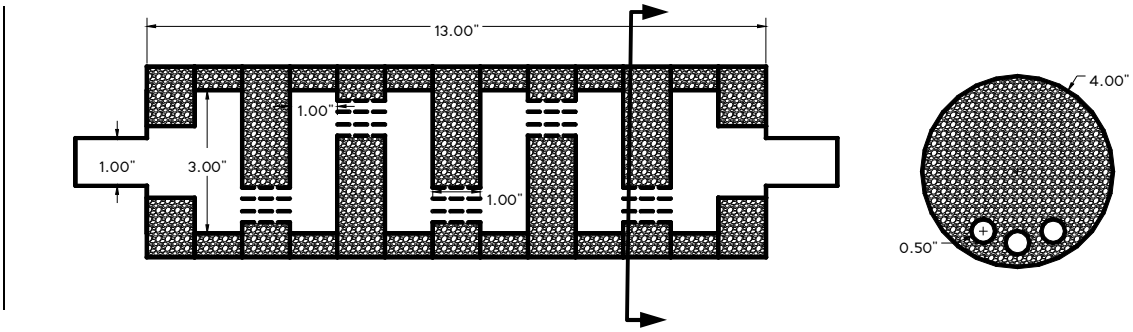

Figure 3.10: *Bend flow* drawing.

Figure 3.11: *Bend flow* picture.

Bend flow half:

This design uses the same concept as the previous *bend flow* silencer, but at $77.8\,in^3$, the *bend flow half* incorporates less than half the volume of the *bend flow* design. The dimensions of the *bend flow half* are shown in Figure 3.12, and a picture of this design can be seen in Figure 3.13. The *bend flow half* was designed to take what was learned from the *bend flow* silencer, and apply it to develop a more compact version. The exit-to-inlet area ratio of the *bend flow half* is the same as the *bend flow* silencer because it shares the same shell design as the two previous silencers. The reduced length of this design brought the weight to 1942.4g. This weight reduction is minimal because the aluminum end caps used on the last 3 designs account for 1510g. The *bend flow half* is a very promising silencer design for the UAV application, because it utilizes a small and lightweight package that still provides adequate flow contact with the absorptive material.

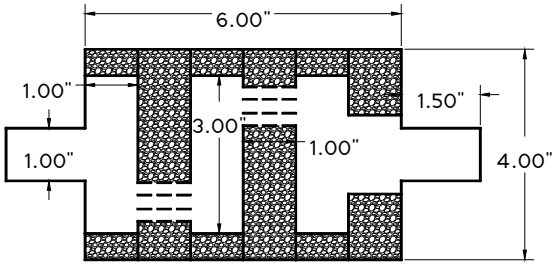

Figure 3.12: *Bend flow half* drawing.

Figure 3.13: *Bend flow half* picture.

3.2 – Silencers designed for the twin-cylinder engine

After preliminary tests were run on the single-cylinder ZDZ 40-RE engine, the 3W-150iB2 twin-cylinder engine was selected as the engine for powering the UAV. As shown in Figure 2.4, the 3W-150iB2 engine has one exhaust port for each of the two simultaneously firing cylinders. These two exhaust exits place different design constraints on a silencer than the single-cylinder engine. In some cases, separate silencers were used to silence each exhaust exit. In other cases, a single silencer was designed to silence the pressure pulses from both exhaust ports. Nine silencer designs were selected for testing on this engine. From these nine silencers, three are commercially available designs and five designs take advantage of the refractory foam absorbent. Modifications are also made to incorporate refractory foam into two of the commercially available silencers to explore the improvement of existing silencers using this new technology. To aid in visualizing the size and orientation of these different silencers, the pictures in this section will show the silencers mounted to the engine. Some of these silencers require the use of eight inch headers to connect the exhaust exits to the silencer inlets. Additional pictures are included to more clearly describe the silencers using advanced shell materials. For the designs fabricated in-house, drawings are supplied that show the inner dimensions of the silencers.

Single exit twins:

The *single exit twins* were designed specifically for the twin cylinder engine, and they are commercially available with part number 3W-106B2 [24]. This design incorporates two identical silencers, one for each exhaust port. The dimensions of one of these silencers can be seen in Figure 3.14 while Figure 3.15 shows the pair mounted to the twin cylinder engine. The *single exit twins* are made of aluminum, and their internal volume is 61.1 in^3 combined. The exit-to-inlet area ratio of the *single exit twins* is 3.54, which is the largest tested on this engine. Together these silencers weigh 479.8g.

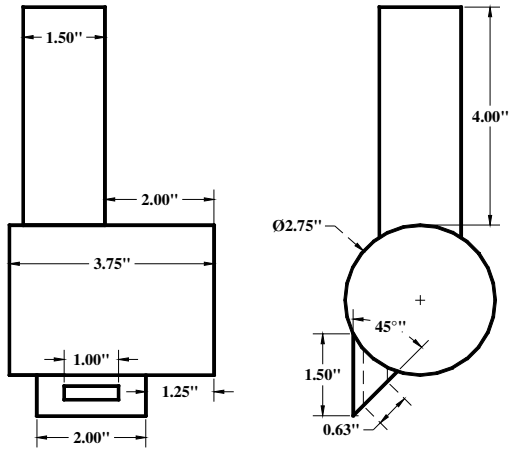

Figure 3.14: Drawing of the *single exit twins.*

Figure 3.15: Picture of *single exit twins* mounted on the twin cylinder engine.

Single exit twins w/ diffusers:

To decrease the exit area of the *single exit twins* and introduce absorptive material to the design, add-on diffusers were fabricated using refractory foam. The dimensions of these diffusers are shown in Figure 3.16. The design of these diffusers was based on an existing design which offers an adjustable exit area [26]. The aluminum plates shown in Figure 3.16 can be moved closer together by placing a smaller piece of refractory foam in the gap between the plates. This design adds minimal weight and provides noise absorption in addition to the noise reduction accomplished by the silencers alone. In Figure 3.17, these silencers are shown mounted to the engine. The addition of these diffusers adds $77.4\,in^3$ to the volume of *single exit twins,* and increases the weight to 1131.6g. The exit-to-inlet area ratio using refractory foam diffusers is reduced to 1.18,

but exit-to-inlet area ratio is calculated using only open space, so including the pores of the refractory foam would yield a higher ratio.

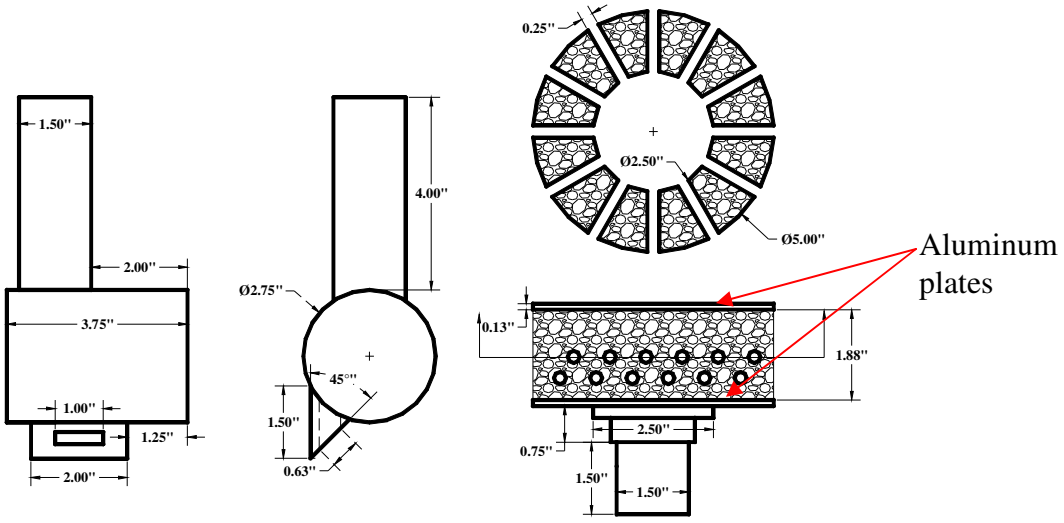

Figure 3.16: Drawing of the *single exit twins w/ diffusers.*

Figure 3.17: Picture of *single exit twins w/ diffusers* mounted on the twin cylinder engine.

Long twins:

The *long twins* are commercial designs available as the Art.-Nr. 95 V-4 [27]. These silencers use two identical $68.2\,in^3$ cylindrical silencers, resulting in a $136.4\,in^3$ total volume. The outer dimensions of one of these silencers are illustrated in Figure 3.18, and all that is known of their inner geometry is that each silencer houses 4 chambers. Together these silencers weigh 814.0g. Figure 3.19 shows a picture of this design mounted on the engine using eight inch headers. The *long twins* are fabricated from aluminum, and together they are the bulkiest silencer designs tested on the twin cylinder engine. The exit-to-inlet area ratio for this design is 0.62.

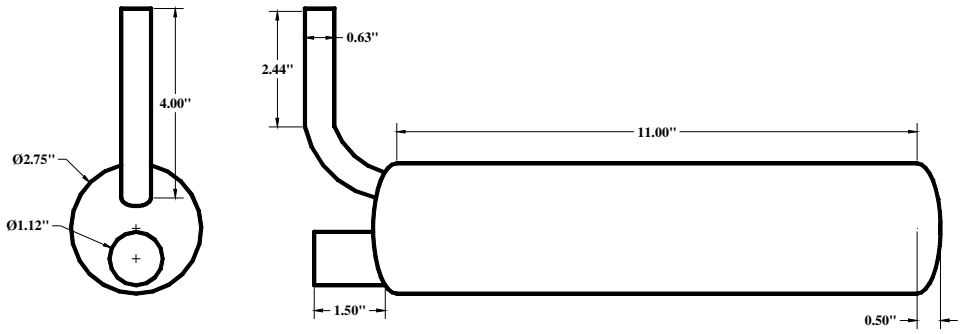

Figure 3.18: Drawing of the *long twins.*

Figure 3.19: Picture of the *long twins* mounted on the twin cylinder engine.

2 – 1 silencer:

This commercial silencer has one canister designed to silence exhaust gases from both exhaust ports. An illustration showing the outer dimensions of the *2-1 silencer* is given in Figure 3.20. It is available as the 3W-150 [24], and it is the only commercial design tested that mixes the exhaust flows from both exhaust ports inside the silencer. This configuration allows minimal bulk for the volume used. The *2-1 silencer* has two inlets and a single exit, and it requires the use of eight inch headers for attachment to the engine exhaust. A picture of this configuration is shown in Figure 3.21. This aluminum silencer has an internal volume of $129.7\,in^3$. The exit-to-inlet area ratio is 0.79, and it weighs 567.7g.

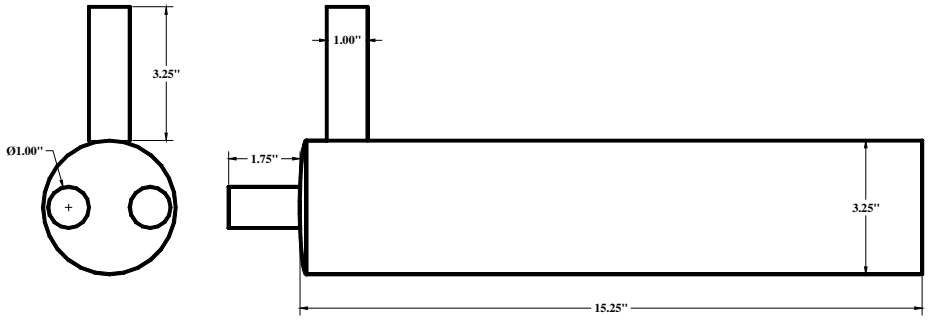

Figure 3.20: Drawing of the *2-1 silencer*.

Figure 3.21: Picture of the *2-1 silencer* mounted on the twin cylinder engine.

2 – 1 silencer w/ foam:

The *2-1 silencer w/ foam* uses the *2-1 silencer* described above, and adds a cylindrical refractory foam liner to its largest chamber. The dimensions of this liner are illustrated in Figure 3.22, and a picture of this silencer is shown in Figure 3.23. Refractory foam is added to test its effect in a commercially available design. The internal volume and exit-to-inlet area ratio of this design are equal to the *2-1 silencer*. The added foam increased the weight of this design by 34.0g.

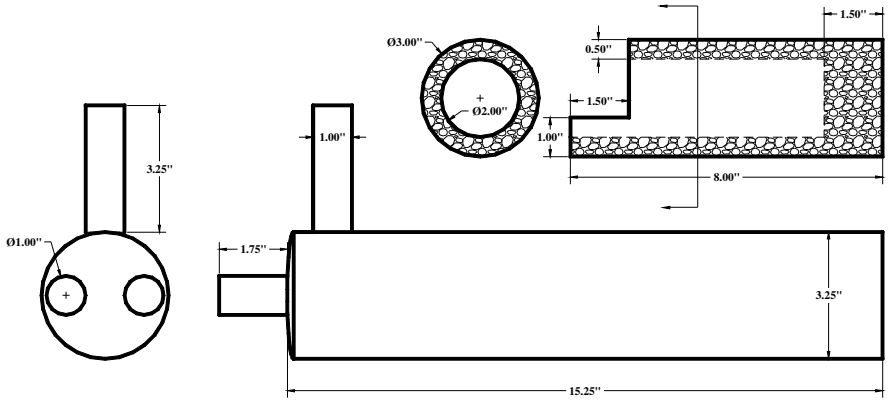

Figure 3.22: Drawing of the *2-1 silencer w/ foam.*

Figure 3.23: Picture of the *2-1 silencer w/ foam* mounted on the twin cylinder engine.

Expansion box:

The *expansion box* is a 10” x 4” x 2.5” aluminum box fabricated as a simple shell for the addition of different refractory foam designs. The dimensions of the *expansion box* are illustrated in Figure 3.24, and a picture of this simple silencer mounted to the engine is shown in Figure 3.25. This silencer was tested to quantify the effect of the refractory foam that will be later added to this simple box. It was not meant to be a competing design. The *expansion box* has two inlets and a single offset exit. It occupies $103.2\,in^3$, and has an exit-to-inlet area ratio of 0.79. It weighs 1465.0g.

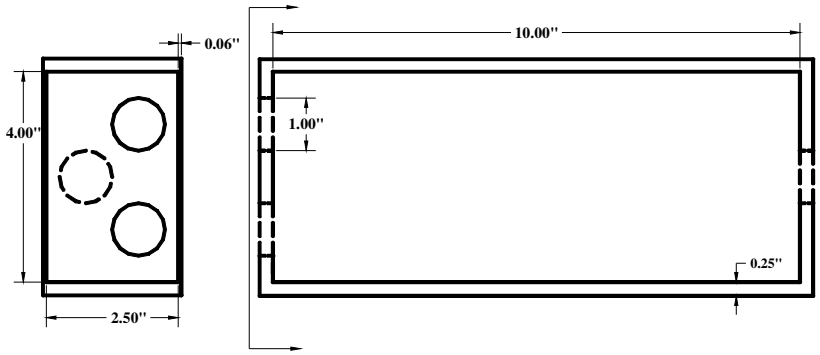

Figure 3.24: Drawing of the *expansion box* silencer design.

Figure 3.25: Picture of the *expansion box* mounted on the twin cylinder engine.

Box w/ 3-hole foam:

The *box w/ 3-hole foam* silencer takes the *expansion box* shell and adds a machined refractory foam block. The dimensions of this design are illustrated in Figure 3.26. Its internal volume and exit-to-inlet-area ratio are equal to the *expansion box*. The foam block added 47.0g to the *expansion box* silencer. This design can be seen attached to the engine in Figure 3.27. The design of the foam block incorporates two terminating inlet holes, and one separate outlet hole. The idea behind this design is to break up pressure pulses and maximize contact with the refractory foam by terminating the two inlet holes and forcing the flow through a small amount of refractory foam to reach a single exit hole.

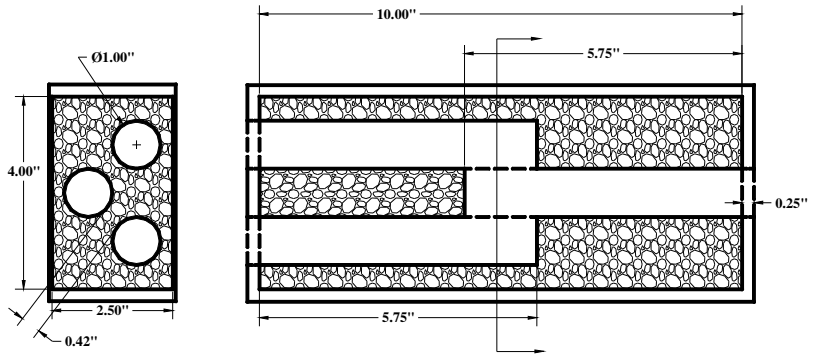

Figure 3.26: Drawing of the *box with 3-hole foam* silencer design.

Figure 3.27: Picture of the *box w/ 3-hole foam* mounted on the twin cylinder engine.

Nylon cylinder w/ 3-hole foam:

The focus of the *nylon cylinder w/ 3-hole foam* silencer was to explore the use of more advanced materials to reduce the weight of the *box w/ 3-hole foam* design. The dimensions of this silencer are shown in Figure 3.28. Because the shell of these silencers is the heaviest component, a more lightweight method of effectively covering the refractory foam was explored. MDS-Filled Nylon 6/6 was selected as the shell material for this silencer. Developing a silencer design that uses a nonmetallic shell material is attractive because it can later be modified to an injection mold capable of producing complex shell designs conformable with the UAV. MDS-Filled Nylon 6/6 has a max usable temperature of 210˚F, and a melting point of 490˚F, so isolation of the silencer shell from the exhaust gases was required. This protection was achieved using a quarter inch of an insulating material called Aerogel [28]. Aerogel is a flexible nanoporous insulation blanket designed for applications up to 1200˚F. The Aerogel blanket was placed between the shell and refractory foam, as illustrated in Figure 3.29, to reduce shell temperature. A picture of this silencer mounted on the engine is shown in Figure 3.30. This design has a 109.6 in^3 volume and an exit-to-inlet ratio of 0.79. It weighs 995.5g.

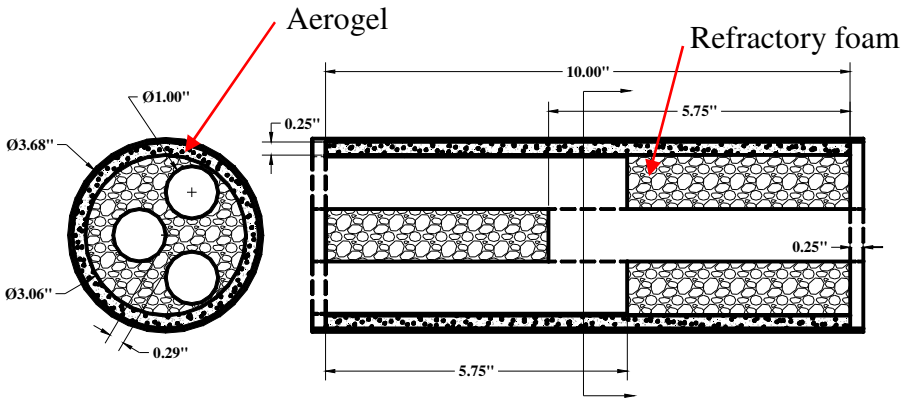

Figure 3.28: Drawing for *nylon cylinder w/ 3-hole foam* silencer design.

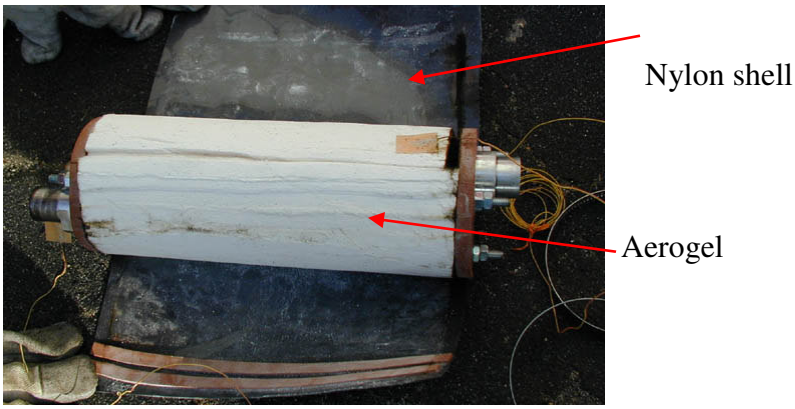

Figure 3.29: Inside of the n*ylon cylinder w/ 3 hole-foam* silencer showing the Aerogel layer.

Figure 3.30: Picture of the *nylon cylinder w/ 3-hole foam* mounted on the twin cylinder engine.

Aerodynamic shell w/ 3-hole foam:

The *aerodynamic shell w/ 3-hole foam* was the final design fabricated and tested on the twin cylinder engine. Using the acoustic knowledge gained from the use of refractory foam in previous designs and the material knowledge gained by testing of the *nylon cylinder w/ 3-hole foam* silencer, a design was fabricated to aerodynamically conform to the profile of the UAV pod. The dimensions of the aerodynamic shell and the refractory foam inside are illustrated in Figure 3.31. The aerodynamic shell was fabricated using selective laser sintering (SLS) technology [29]. This technology uses a thermoplastic material called DuraForm GF [29] that was designed for extreme testing conditions. It has a density of 0.84 g/cm^3 and a melting point of 365˚F. A picture of the SLS shell is shown in Figure 3.32 before the addition of refractory foam. Inside the aerodynamic shell, a quarter inch of Aerogel was used to insulate the shell from the exhaust gases. The refractory foam configuration uses the same 3-hole concept as the *box with 3-hole*

foam design, but it was modified to conform to the shape of the shell. A picture of this design mounted to the engine, but not yet integrated to the pod, is shown in Figure 3.33. Exhaust gases exit the 103.0 in^3 silencer by way of three half inch holes drilled near the nose of the shell. The exit-to-inlet area ratio for this silencer is 0.59, and it weighs 551.1g. Since this design was fabricated after the other silencers had already been tested, speaker testing was not performed on this silencer.

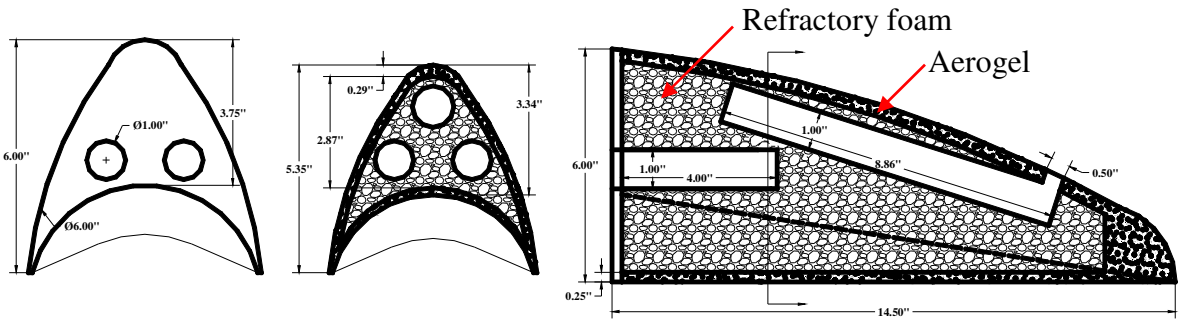

Figure 3.31: Drawing of the *aerodynamic shell w/ 3-hole foam.*

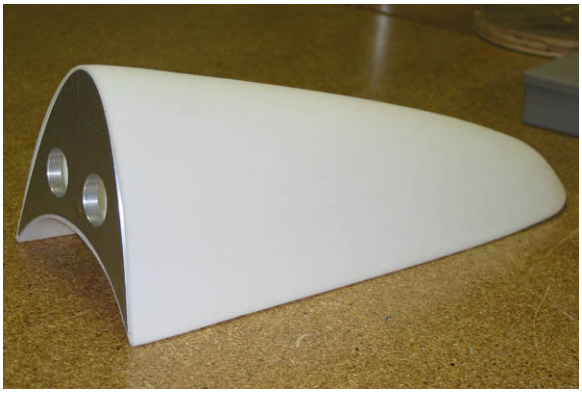

Figure 3.32: Picture of the SLS shell before refractory foam was added.

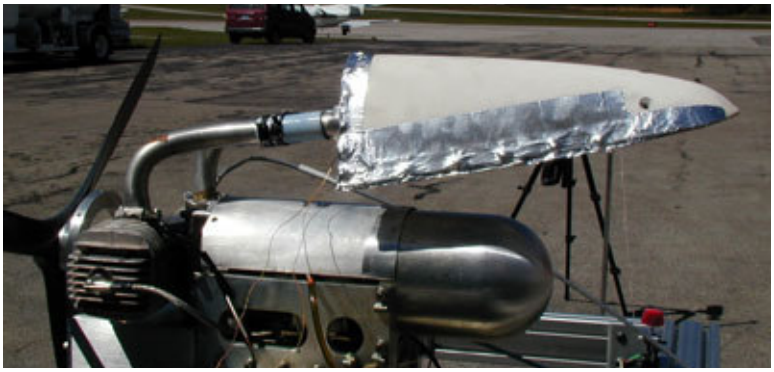

Figure 3.33: Picture of the *aerodynamic shell w/ 3-hole foam* mounted on the twin cylinder engine.

3.3 Summary

Through the course of this research, the above silencer designs were tested in anechoic and outdoor environments with the goal of developing an effective silencer for the UAV. Table 3.1 provides a summary of the characteristics found in each of these silencers.

Table 3.1: A summary of the characteristics found in each of the tested silencers.

Silencer name	Weight (g)	Volume (in^3)	Exit-to-inlet area ratio	Fabrication materials	Engine designed for	Key objective
Double exhaust exit	186.6	6.9	0.79	Aluminum	single cylinder engine	Learn about existing silencers
Black single exit	218.3	15.5	0.39	Aluminum	single cylinder engine	Learn about existing silencers
Airplane silencer	1969.0	165.2	9.82	Steel Refractory foam	single cylinder engine	Retest a previous refractory foam silencer
Airplane silencer w/ plug	2020.0	165.2	0.3	Steel Refractory foam	single cylinder engine	Improve a previous refractory foam silencer
Chevron liner	2356.0	178.3	1.57	Aluminum Refractory foam	single cylinder engine	Improve a previous refractory foam silencer
Bend flow	2238.7	165.7	1.57	Aluminum Refractory foam	single cylinder engine	Fabricate an effective refractory foam silencer
Bend flow half	1942.4	77.8	1.57	Aluminum Refractory foam	single cylinder engine	Fabricate a small refractory foam silencer
Single exit twins	479.8	61.1	3.53	Aluminum	twin cylinder engine	Learn about existing silencers
Single exit twins w/ diffusers	1131.6	138.5	1.18	Aluminum Refractory foam	twin cylinder engine	Improve an existing silencer
Long twins	814.0	136.4	0.62	Aluminum	twin cylinder engine	Learn about existing silencers
2-1 silencer	567.7	129.7	0.79	Aluminum	Twin cylinder engine	Learn about existing silencers
2-1 silencer w/ foam	601.7	129.7	0.79	Aluminum Refractory foam	Twin cylinder engine	Improve an existing silencer
Expansion box	1465.0	103.2	0.79	Aluminum	Twin cylinder engine	Baseline to show refractory foam improvement
Box w/ 3-hole foam	1512.0	103.2	0.79	Aluminum Refractory foam	Twin cylinder engine	Show refractory foam improvement over baseline
Nylon cylinder w/ 3-hole foam	995.5	109.6	0.79	Aluminum Refractory foam Aerogel Nylon shell	Twin cylinder engine	Design of a more lightweight silencer through the use of advanced materials
Aerodynamic shell w/ 3-hole foam	551.1	103.0	0.59	Aluminum Refractory foam Aerogel SLS shell	Twin cylinder engine	Design of a lightweight and aerodynamic silencer through the use of advanced materials

Chapter 4 Preliminary Speaker Test Results

In this chapter, the results for the speaker input tests are presented. Using the procedure outlined in chapter 2.1, speaker tests were performed in an anechoic environment to attain preliminary acoustic data on the silencer designs described in chapter 3. Since these speaker tests do not take all engine effects into account, the results in this chapter can not be directly correlated to the engine test results presented in chapter 5. The results in this chapter provide accurate attenuation information for a silencer across the frequency range of interest using a consistent noise source. This information is used to predict how effective a silencer will be across the broadband of frequencies the engine is radiating.

Chapter 4 is divided into four sections. First, speaker testing was performed to evaluate the contribution of inlet and exit tube geometries. For the UAV project, it is desirable to achieve a silencer design that fits into a confined space. To accurately achieve this, it is important to know how the inlet and exit tube geometries affect the silencers acoustic performance. Next, the results for the speaker tests modeling the single cylinder engine are laid out. Then, the results are shown for the speaker tests modeling the twin cylinder engine. Finally, a chapter summary is presented.

4.1 Acoustic contribution of inlet and exit pipe geometry

The length and diameter of inlet and exit pipes can have a profound effect on both noise reduction and engine performance [11]. To quantify these inlet and exit pipe effects, different inlet and exit pipe geometries have been tested using the *expansion box* silencer, as shown in Figure 4.1. In order to fabricate a single inlet and single outlet configuration, an aluminum inner wall was installed to divide the volume of the *expansion box* in half. The inlet and exit pipes used for this testing were made of PVC.

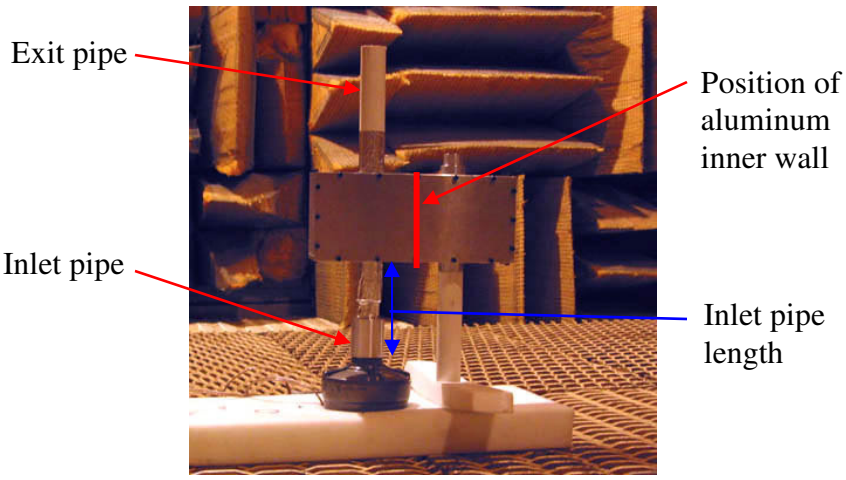

Figure 4.1: Picture of the expansion box configuration used to determine the effects of inlet and exit pipe geometries.

Speaker test results for different inlet pipe lengths:

Inlet pipe lengths were defined in this test as the distance between the silencer inlet and the source. Using an exit pipe 2" in length, 2", 4", and 6" long inlet pipes were tested with a single source. According to the IL results seen in Figure 4.2, entrance tube length does not greatly impact the acoustic results. The absorption peaks and valleys vary, but overall, using an entrance tube length in the tested 2" - 6" range will not have a large impact on acoustic results. These results were expected because the acoustic affects introduced by inlet tube length are often masked because they are small and upstream of the silencer element.

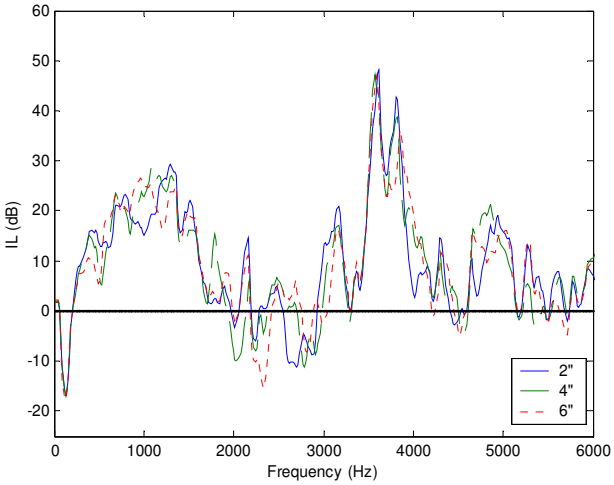

Figure 4.2: Insertion loss measurements for 3 different inlet pipe lengths.

Speaker test results for different exit pipe lengths:

In a silencer system, exit pipe lengths can have a large impact on acoustic results. An exit pipe terminates into the atmosphere causing sound wave reflections back toward the silencer body. These reflections cause some frequencies to resonate in the exit pipe and others to be further reduced. 2", 4", and 6" exit tube lengths were tested to asses the effect of exit pipe lengths on acoustic signature. The IL results for these tests are shown in Figure 4.3. These results reveal varying IL valleys in the 900-2000 Hz range. These valleys correspond to the resonance frequencies of the exit pipes. The resonant frequencies of an open ended unflanged pipe are

$$f_n = \frac{n}{2}\frac{c}{L+0.6a} \qquad (4.1)$$

where c is the speed of sound, L is the length of the pipe, and a is the radius of the pipe. This equation holds in the frequency range $\lambda_n >> a$, where λ_n is wavelength. For the tested tube geometries, 2600 Hz is the highest frequency for which Equation 4.1 can be applied. This corresponds to a wavelength one order of magnitude greater than the 0.5" radius pipe used in these tests. Using Equation 4.1 the first resonant frequencies of these exit pipes were calculated, and the valleys they correspond to are noted in Figure 4.3. The IL results shown in Figure 4.3 reveal that the 2" exit pipe has a higher first natural frequency and thus performs better at low frequencies. Above 2500 Hz, exit pipe lengths in this range do not have a substantial effect on the attenuation. The first resonance in the 2" pipe occurs at 2000 Hz which is above the 0-1500 Hz frequency range where the majority of small IC engine noise occurs. Using a shorter exit pipe is preferable for this silencer design because of the limited space available to integrate a silencer into the UAV. Therefore, exit tubes of roughly 2" were selected for the silencer designs fabricated for testing.

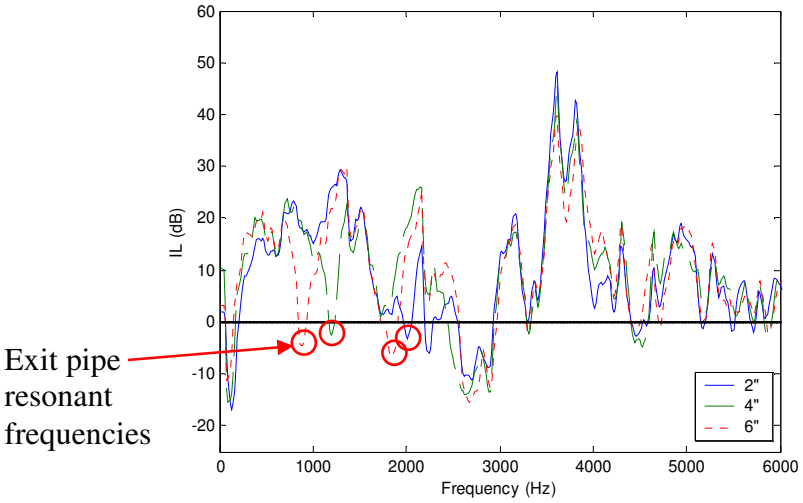

Figure 4.3: Insertion loss measurements for 3 different exit tube lengths.

Speaker test results for different exit pipe diameters:

Exit pipe diameter in a silencer is very important not only to noise reduction, but also to backpressure. Unfortunately, noise reduction and backpressure are indirectly proportional in relation to exit pipe diameter. A reduction in exit pipe diameter increases the amount of acoustic energy reflected in the silencer, but that reflected energy causes an increase in backpressure. Therefore, the ideal exit pipe diameter for a particular application provides a usable compromise between increasing reflections in the silencer and increasing load on the engine. To quantify the effect of the exit pipe diameter on acoustic results, diameters of 1" and ¾" were tested for 2", 4", and 6" exit pipe lengths. The acoustic results of these pipe diameters tested on the 2" exit pipe are shown in Figure 4.4. The results for all 3 pipe lengths revealed similar trends. The 2" exit pipe results are shown here because they most accurately model the exit pipes used in the fabricated silencers. In Figure 4.4, noise reduction is seen to increase slightly using the ¾" diameter exit pipe, as expected. This trend was observed in all cases tested, but it was decided that since backpressure could not be tested during preliminary speaker testing, that an exit area approximately equal to a 1" diameter would be used for the fabricated silencer designs. So that a better understanding of the backpressure variable could be attained during engine testing, some of the silencer designs allow for easy adjustment of the exit area.

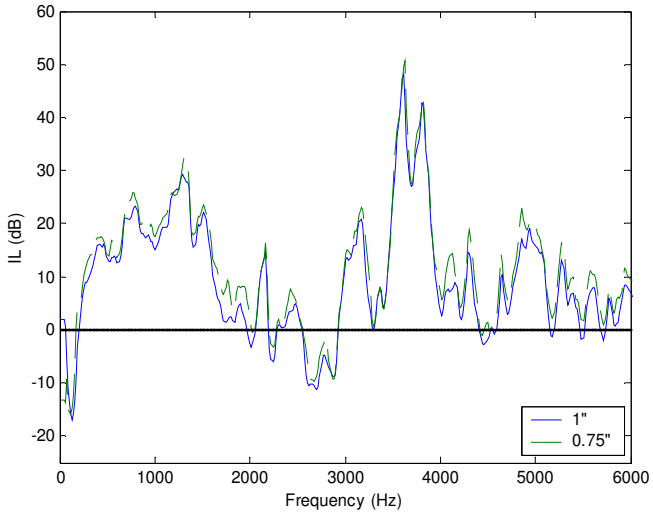

Figure 4.4: Insertion loss plot for 2" long exit tubes with 1" and 0.75" diameters.

4.2 Speaker input test results

The speaker test results for the silencer designs introduced in Chapter 3 are presented here in the form of insertion loss plots. Many of the silencers that take advantage of refractory foam were first tested without it to reveal the effect of the added absorbent. For these cases, the IL with and without refractory foam are shown on the same graph. For comparisons to experimental data, theoretical IL predictions were also performed for the silencer designs that could most accurately be modeled using an expansion chamber approach. SilencerApp [30], a software program designed to predict the attenuation of simple reactive silencer geometries, was used to compute the theoretical expansion chamber results. The predicted attenuation data is then plotted in the 0-2 kHz frequency range on the IL plots. According to Blair [7], there is little useful correlation between diffusing silencer theory and experimental results after 1.5 kHz. However, in these tests, the predictions agree well with experimental data up to 2 kHz. Exhaust pipe resonances were computed for the commercial silencers using Equation 4.1, and identified in IL plots with a red circle similar to Figure 4.3. To provide a simple metric to quantify IL results, average IL quantities were calculated over two frequency ranges. Since the majority of the noise present in small IC engines occurs over the 0-1500 Hz frequency range, an average low frequency IL was calculated for this range. An average high frequency IL calculation was also computed for the remaining 1501-6000 Hz frequency band.

4.2.1 Test results modeling the single cylinder engine input

Double exhaust exit:

The IL results for the *double exhaust exit* silencer (see Figures 3.1 and 3.2) are shown in Figure 4.5. These results reveal poor reduction in the low frequency range, which leads to an average low frequency IL of 17.1 dB. At frequencies above 1300 Hz the overall IL increases, but its frequency spectrum shows many pass-band frequencies caused by silencer resonances. The average IL of the *double exhaust exit* silencer in the high frequency range is 32.2 dB. The first exhaust pipe resonance is identified in Figure 4.5 as a drop in the IL at 2200 Hz. With a volume of $6.9 in^3$, this is the smallest silencer tested. Because of the low volume present in the *double exhaust exit* silencer, low frequencies are not effectively reduced.

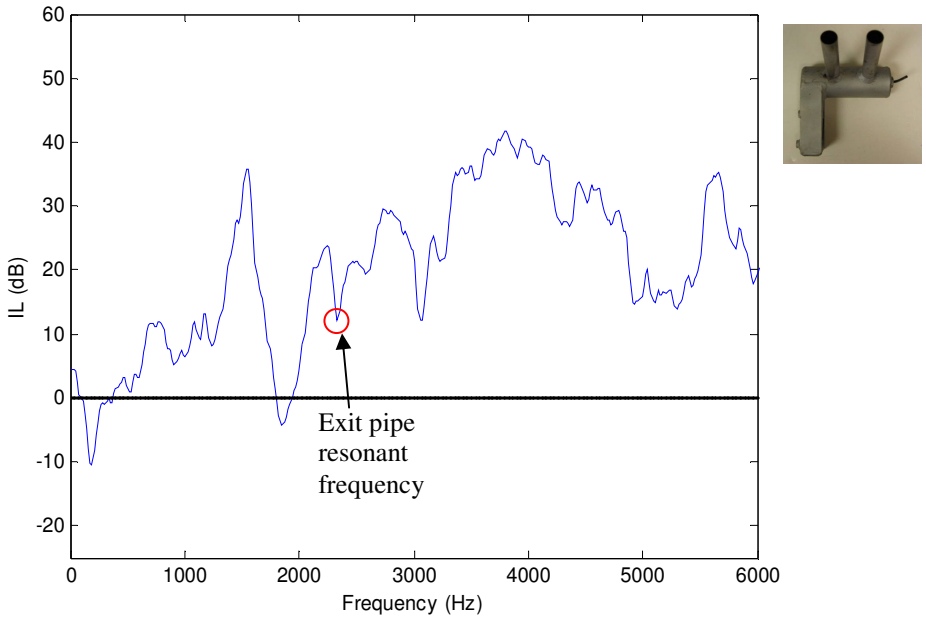

Figure 4.5: Insertion loss plot for the *double exhaust exit* silencer.

Black single exit:

Figure 4.6 shows the IL results for the *black single exit* silencer (see Figures 3.3 and 3.4). The *black single exit* silencer shows considerable acoustic improvements over the *double exhaust exit* design. Using a small $15.5 in^3$ volume, the *black single exit* silencer provides an average low frequency IL of 34.5 dB, and an average high frequency IL of 42.0 dB. It must be reemphasized that with an exit-to-inlet area ratio of 0.39, this is the most constrictive silencer tested. This constriction plays a part in the improved acoustic performance. A small resonance at approximately 3100 Hz is identified in Figure 4.6 as the first resonance of the exit pipe.

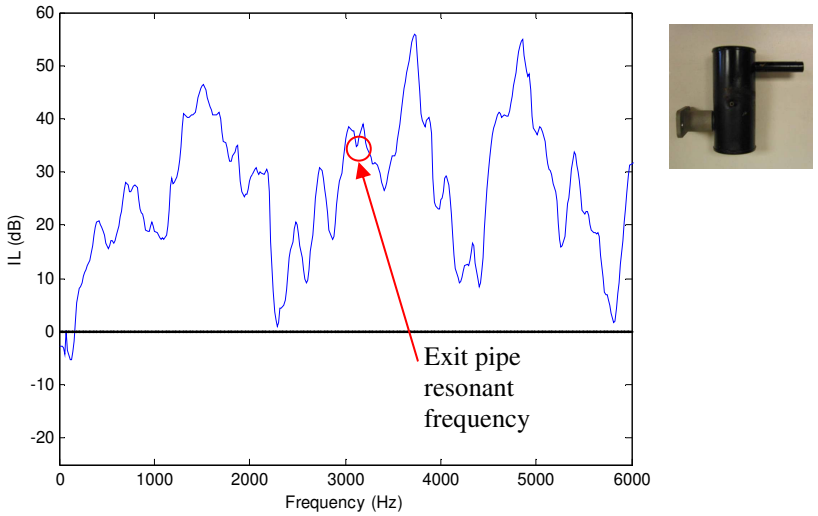

Figure 4.6: Insertion loss plot for the *black single exit* silencer.

Airplane silencer & airplane silencer with plug:

Figure 4.7 compares the IL results of the *airplane silencer* (see Figures 3.5 and 3.6) and the *airplane silencer with plug* (see Figures 3.6 and 3.7), along with the theoretical predictions for this geometry without using refractory foam. The large inlet and exit diameters of the *airplane silencer* design allow a great percentage of the noise to pass straight through a large path of little resistance. This results in an average low frequency IL of 13.6 dB. Due to the presence of a refractory foam liner, the high frequency average IL is an impressive 45.1 dB. The predicted results shown in Figure 4.7 reveal the large impact that refractory foam has on the absorption characteristics of this silencer. Above

1000 Hz the refractory foam starts eliminating the pass-band frequencies shown in the theoretical results.

With the addition of an exhaust tube plug, consisting of three quarter inch holes, the IL was further increased by approximately 10 dB over all frequencies except those at which the *airplane silencer* results were already considerable. The addition of this plug increased the average low frequency IL by 13 dB, and the average high frequency IL was slightly reduced to 44.5 dB. This outcome speaks strongly to the noise reduction that can be achieved by reducing the exit area and allowing more exhaust noise to be absorbed before exiting the silencer. However, it is important not to reduce the exit area to the point of causing a large increase in backpressure.

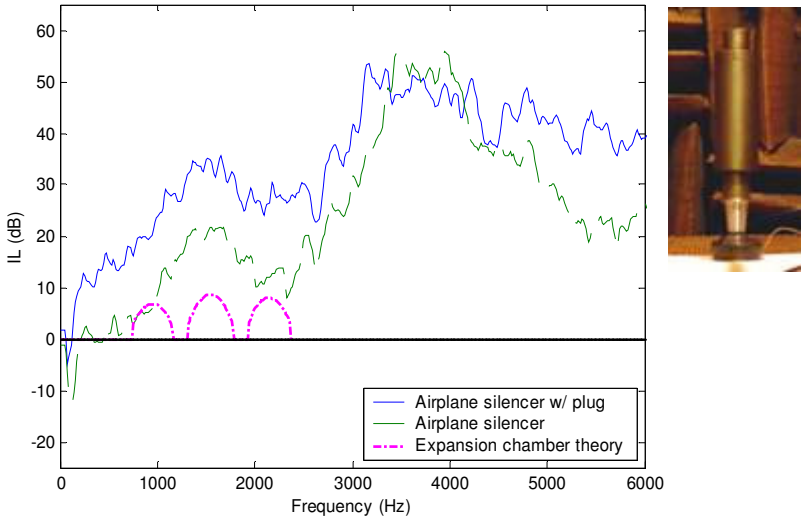

Figure 4.7: Insertion loss plot comparing the *airplane silencer w/ plug, airplane silencer*, and theoretical expansion chamber results.

Chevron liner

The IL results for a 14" expansion chamber with and without a *chevron liner* (see Figures 3.8 and 3.9) are plotted in Figure 4.8 along with the theoretical results for the no foam case. The experimental results shown for the 14" expansion chamber correlate well with the theoretical results up to 2 kHz. Beyond 2 kHz, the expansion chamber is full of pass-bands caused by the silencer resonances.

With the addition of the chevron-shaped liner, the low frequency resonances were eliminated, and at higher frequencies, the IL showed an increase of up to 30 dB beyond the simple expansion chamber results. The *chevron liner* has an average low frequency IL of 31.9 dB and an average high frequency IL of 50.2 dB. These are the highest IL results found using a single inlet configuration. These results can be attributed to both the large $178.3 in^3$ volume and the effective refractory foam liner.

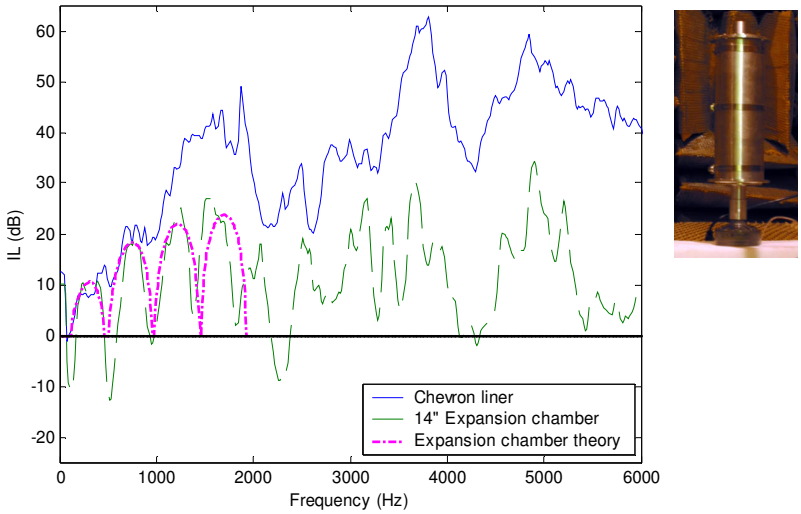

Figure 4.8: Insertion loss plots comparing the *chevron liner*, 14" expansion chamber, and theoretical expansion chamber results.

Bend flow

The IL results for the *bend flow* silencer (see Figures 3.10 and 3.11) and 13" expansion chamber are shown in Figure 4.9 along with the theoretical expansion chamber results. Figure 4.9 shows that the experimental 13" expansion chamber results correlate well with expansion chamber theory up to 2 kHz. Beyond 2 kHz, the silencer resonances cause pass-bands throughout the remaining frequency spectrum.

By placing the *bend flow* refractory foam design inside the 13" expansion chamber, the low frequency resonances were reduced. Above 2 kHz the refractory foam made a great impact on the IL seen at all but two frequencies which already demonstrated high IL in

the expansion chamber results. The average low frequency IL for the *bend flow* silencer is 20.5 dB, and the average high frequency IL is 36.2 dB.

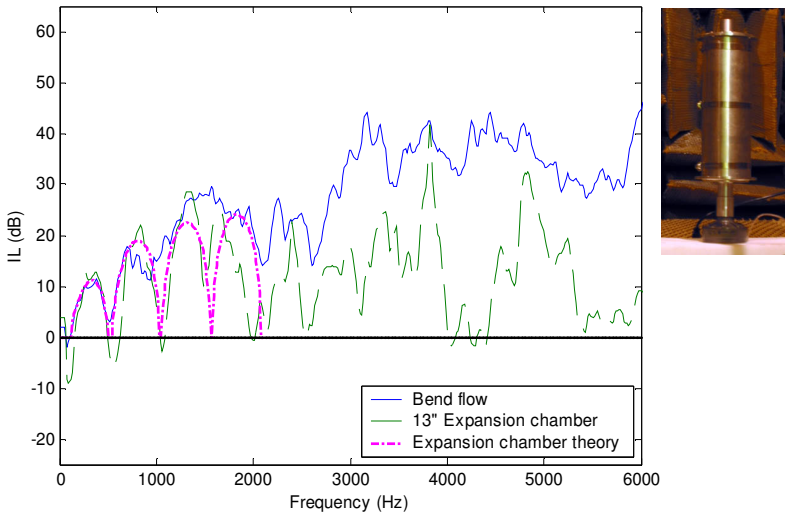

Figure 4.9: Insertion loss plots comparing the *bend flow*, 13" expansion chamber, and theoretical expansion chamber results.

Bend flow half

The IL results for the *bend flow half* (see Figures 3.12 and 3.13) and 6" expansion chamber silencers are shown in Figure 4.10, along with the expansion chamber theoretical results. The experimental 6" expansion chamber results correlate well with the expansion chamber theory for the first two resonant frequencies. After 2 kHz, the resonant frequencies of the expansion chamber theory were evident in the 6" expansion chamber, but they were no longer the most prominent factor in the acoustics of the silencer.

The addition of refractory foam in the *bend flow half* had a similar effect as in previous silencers, but the acoustic reduction was decreased because less absorbent was used. Here the refractory foam of the *bend flow half* silencer damps out many of the resonant frequencies seen in the expansion chamber, but at high frequencies it does not show the high IL typical of the silencers using refractory foam absorption. The average low frequency IL for the *bend flow half* is 20.4 dB and the average high frequency IL is 25.1

dB. For a silencer with a volume of only $77.8\ in^3$, these results are impressive, but a reduction in exhaust tube diameter might provide the extra contact time with the absorbent needed to further improve acoustic results.

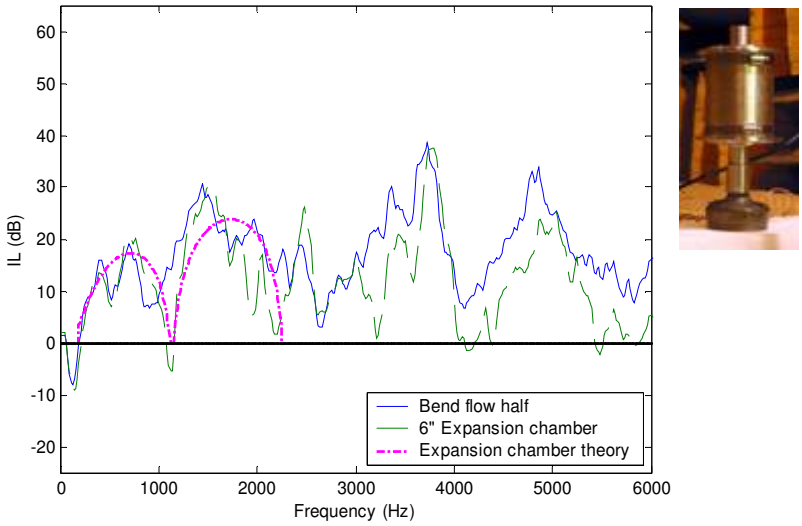

Figure 4.10: Insertion loss plots comparing the *bend flow half*, 6" expansion chamber, and theoretical expansion chamber results.

4.2.2 Test results modeling the twin cylinder engine input

Single exit twins & Single exit twins with diffusers:

The IL results for the *single exit twins* (see Figures 3.14 and 3.15) with and without the added diffusers (see Figures 3.16 and 3.17) are plotted in Figure 4.11. The *single exit twins* achieved an average low frequency IL of 8.5 dB and an average high frequency IL of 18.4 dB. These results make the *single exit twins* the poorest acoustic performers in the speaker test. Calculation of the exit pipe resonant frequency reveals an explanation for the valley seen in Figure 4.11 at 1330 Hz.

Add-on diffusers were fabricated as a potential improvement of the silencer. In this case, the use of a refractory foam external diffuser did not dramatically impact the IL results. The add-on diffusers improved the average IL by close to 5 dB resulting in a low frequency average IL of 13.8 dB and an average high frequency IL of 23.5 dB. The porosity of the refractory foam coupled with the exposed two inch foam thickness used in

the diffusers resulted in very little friction between the exhaust gasses and the absorbent. It is this friction turning acoustic energy to heat that provides absorption of sound in absorptive layers. [13, 14].

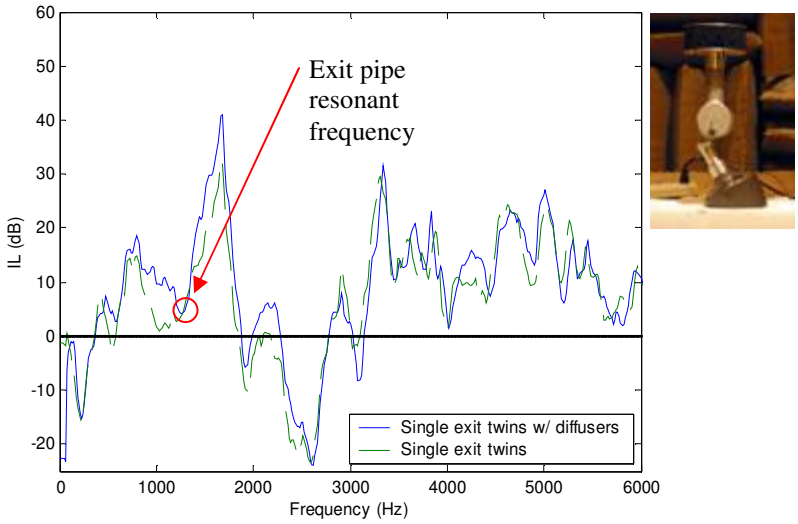

Figure 4.11: Insertion loss plots comparing *single exit twins w/ diffusers* and *single exit twins.*

Long twins:

The *long twins* (see Figures 3.18 and 3.19) are a commercially available set of two identical silencers whose IL results are plotted in Figure 4.12. All that is known about the internal geometry of *long twins* is that each silencer contains four internal chambers. This design demonstrates impressive IL across most of the frequency spectrum, even though many narrow pass-bands are caused by chamber resonances. The average low frequency IL for the *long twins* is 39.2 dB, which is the highest low frequency IL average of the silencers tested. The average high frequency IL calculated for the *long twins* is 37.3 dB. The small resonance at 1300 Hz corresponds to the first resonance of the exit pipe. These results were among the most impressive seen from a commercial design during speaker testing.

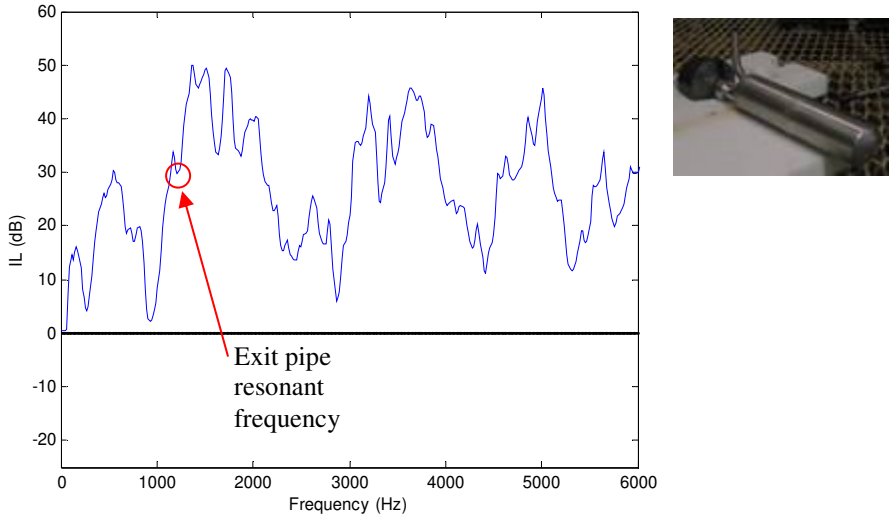

Figure 4.12: Insertion loss plot for the *long twins.*

2-1 silencer & 2-1 silencer w/ foam:

Figure 4.13 compares the IL results for the *2-1 silencer* (see Figures 3.20 and 3.21) and the *2-1 silencer w/ foam* (see Figures 3.22 and 3.23) designs. At all frequencies above 300 Hz, an IL of over 10 dB was consistently achieved through the whole spectrum of the *2-1 silencer* design. An exit pipe resonance is shown in Figure 4.13 to contribute to the large resonance at 1750 Hz. This silencer achieved an average low frequency IL of 34.5 dB and an average high frequency IL of 29.6 dB.

The *2-1 silencer w/ foam* is a commercially available design which was modified to incorporate refractory foam technology. With the addition of the refractory foam cylinder, one major valley at approximately 900 Hz was eliminated while the two IL peaks at approximately 600 Hz and 1400 Hz were slightly decreased. The average low frequency IL for the *2-1 silencer w/ foam* is 35.5 dB. In the high frequency range, the IL of the *2-1 silencer with foam* produces consistently better results than those shown for the *2-1 silencer*. These results provide an average high frequency IL of 39.0 dB. The *2-1 silencer* provided the most consistent broadband reduction seen in a commercial silencer during speaker testing, and the addition of refractory foam further improved these results.

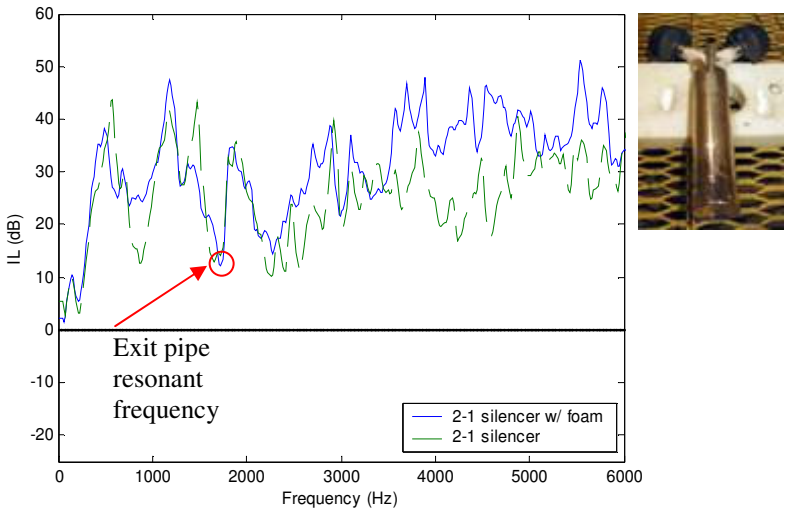

Figure 4.13: Insertion loss plots comparing the *2-1 silencer w/ foam* and the *2-1 silencer.*

Box with 3-hole foam & Expansion box:

The IL plots for the *box w/ 3-hole foam* (see Figures 3.26 and 3.27) and the *expansion box* (see Figures 3.24 and 3.25) are shown in Figure 4.14 along with the theoretical predictions. The expansion chamber theory modeling the *expansion box* reveals close correlation with the resonant frequencies seen in the experimental results. On the other hand, the experimental results yield much higher IL peaks than the theory around 1000 Hz and 1700 Hz. The average low frequency IL for the *expansion box* is 15.7 dB and the average high frequency IL is 23.7 dB.

After adding the 3-hole refractory foam block to the expansion box, many of the resonances that were present in the expansion box were eliminated. Above 3800 Hz, the foam causes a large increase in IL. The average low frequency IL for the *box w/ 3-hole foam* is 20.6 dB and the average high frequency IL is 31.4 dB.

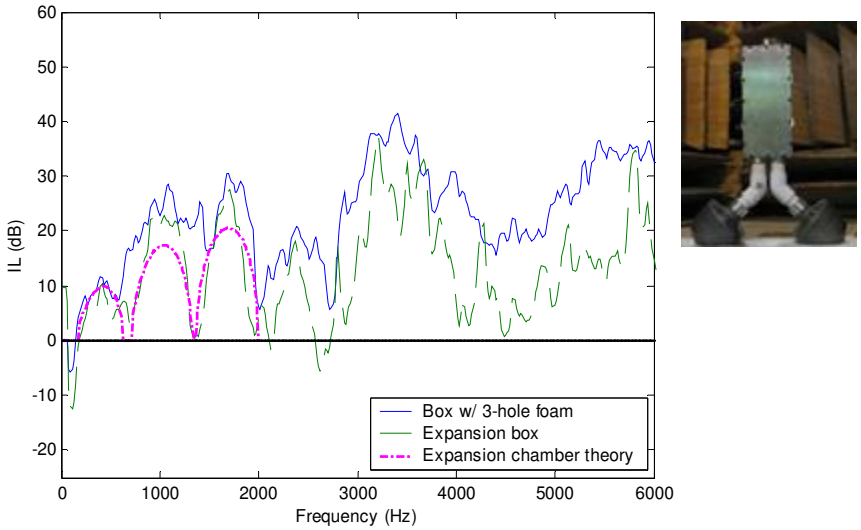

Figure 4.14: Insertion loss plots comparing the *box w/ 3-hole foam*, *expansion box,* and theoretical expansion chamber results.

Nylon cylinder with 3-hole foam:

Figure 4.15 contains the IL results for the *nylon cylinder w/ 3-hole foam* (see Figures 3.28, 3.29, and 3.30), and the theoretical results for an expansion chamber of these dimensions. It can be seen in Figure 4.15 that the *nylon cylinder w/ 3-hole foam* follows expansion chamber theory for the first 500 Hz. Then, when an empty expansion chamber would resonate, the IL of the *nylon cylinder w/ 3-hole foam* continues to increase. This silencer yielded the most consistent broadband acoustic absorption seen in silencers using a dual inlet configuration. At frequencies greater than 800 Hz, the IL remains above 15 dB. The average low frequency IL of the *nylon cylinder w/ 3-hole foam* is 22.3 dB, and the average high frequency IL is 32.8 dB. These are impressive results for a silencer using a volume of $109.6 in^3$. These results can be attributed to the lack of a metal shell, along with the use of refractory foam and the aerogel insulator. By using a nylon shell and aerogel in place of aluminum, acoustic radiation that would be present in a metallic shell is significantly damped out.

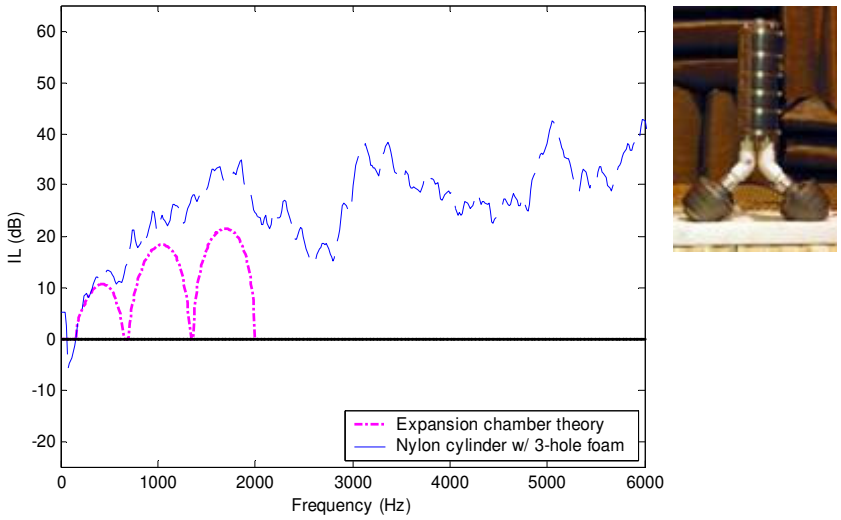

Figure 4.15: Insertion loss plot for the *nylon cylinder w/ 3-hole foam* silencer.

4.3 Summary

For easy numerical comparison, Table 4.1 includes average IL values for low frequency, high frequency, and overall frequency in the 0-6000 Hz range for each silencer tested. In addition, internal volume and Exit-to-inlet area ratio for each silencer are also included from Table 3.1. In Figure 4.16, an overall average IL vs. volume plot is presented for all speaker tested silencers. This plot reveals the basic trend of increasing average IL with increasing volume which works against the goal of designing a small and effective silencer design. On the other hand, this figure also reveals how refractory foam can make a large impact on IL without the addition of extra volume.

Table 4.1: Average IL values along with silencer volume and Exit-to-inlet area ratio values for each silencer design.

Silencer name	Average IL (dB) 0-1500 Hz	Average IL (dB) 1501-6000 Hz	Average IL (dB) 0-6000 Hz	Volume (in^3)	Exit-to-inlet area ratio	Engine designed for
Double exhaust exit	17.1	32.2	31.2	6.9	0.79	Single cylinder engine
Black single exit	34.6	42.0	40.9	15.5	0.39	Single cylinder engine
Airplane silencer	13.6	45.1	43.6	165.2	9.82	Single cylinder engine
Airplane silencer w/ plug	26.6	44.5	43.0	165.2	0.30*	Single cylinder engine
Chevron liner	31.9	50.2	48.8	178.3	1.57	Single cylinder engine
Bend flow	20.5	36.2	36.1	165.7	1.57	Single cylinder engine
Bend flow half	20.4	25.1	24.1	77.8	1.57	Single cylinder engine
Single exit twins	8.5	18.4	17.9	61.1	3.53	twin cylinder engine
Single exit twins w/ diffusers	13.8	23.5	22.3	138.5	1.18*	twin cylinder engine
Long twins	39.2	37.3	37.6	136.4	0.62	twin cylinder engine
2-1 silencer	34.5	29.6	31.9	129.7	0.79	twin cylinder engine
2-1 silencer w/ foam	35.5	39.0	38.4	129.7	0.79	twin cylinder engine
Expansion box	15.7	23.7	22.5	103.2	0.79	twin cylinder engine
Box w/ 3-hole foam	20.6	31.4	34.4	103.2	0.79	twin cylinder engine
Nylon cylinder w/ 3-hole foam	22.3	32.8	33.1	109.6	0.79	twin cylinder engine

* The effective exit area is larger due to the porosity of refractory foam used in the exit pipe

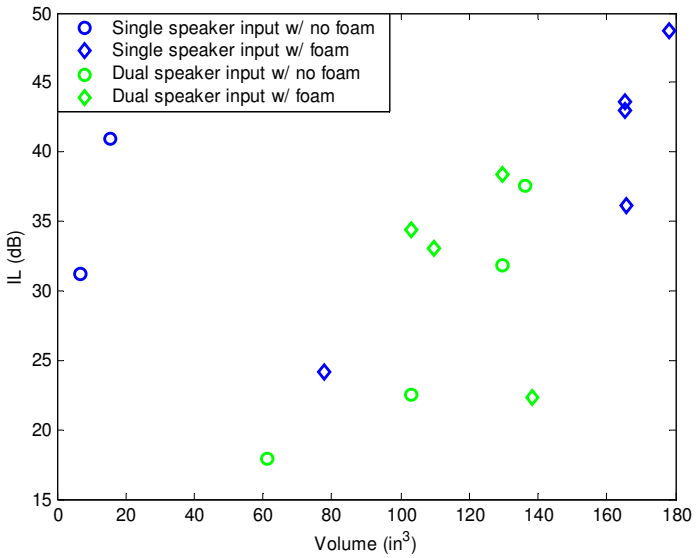

Figure 4.16: Overall average insertion loss vs. volume plot for all speaker tested silencers.

Based on IL plots and the average IL values, the best silencers were the larger volume designs using refractory foam. Speaking strictly in terms of IL, the top 5 silencers all

used refractory foam except *black single exit* silencer which, because of its flow constriction, would not operate at the required engine rpm during engine testing. A better method of determining the most effective silencer based on speaker input tests is to compare ratios of the internal volume and overall average IL. Achieving maximum noise reduction in the smallest package possible is the goal of the UAV effort, and this ratio provides a way to quantify it. Using these ratios, the top three twin cylinder engine silencers are the *2-1 silencer with foam, the box with three-hole foam*, and the *nylon cylinder with 3-hole foam*. For the silencers with the highest IL, the key effect of the refractory foam was to attenuate the silencer acoustic resonances, and thus greatly increase attenuation. This conclusion is especially evident at high frequencies. According to the results in this chapter, refractory foam does not significantly affect the acoustic results below 700 Hz, but above 700 Hz refractory foam substantially impacts the acoustic potential of a silencer.

Chapter 5 Engine Test Results

Using the procedure outlined in Chapter 2.2, acoustic testing was performed on the silencers introduced in Chapter 3. Engine test data was recorded at 6500 rpm for the ZDZ 40-RE 40 2-stroke single cylinder engine, and 5000 rpm for the 3W-150iB2 2-stroke twin cylinder engine. This chapter is divided into four sections. First, preliminary engine tests results are presented. During preliminary testing, the contribution of propeller noise to engine test results is explored as well as the relationship between engine speed and sound pressure level. Next, tests results are presented for the single cylinder engine followed by the results for the twin cylinder engine. The results from these two sections are graphically represented in the form of average frequency spectrums and directivity plots. The average frequency spectrums and directivity plots for each silencer were generated using the procedure explained in Chapter 2.3. The results for the baseline case are also plotted in these figures for easy evaluation of the silencer performance. The additional information provided in these sections includes overall A-weighted SPL (OASPL) values, temperature measurements, and engine speed measurements. Backpressure measurements are also provided for selected silencers. Finally, a summary of these results is laid out. This summary includes a table consisting of important silencer values from the last three chapters, and envelope and directivity plots to expose trends and compare results for the best silencers.

5.1 Preliminary engine tests

Propeller noise isolation tests:

Engine tests were performed to isolate propeller noise from the acoustic data. Since propeller noise is present in the noise signal recorded by the microphone array, it is important to know what impact this noise source has on overall measurements. Propeller noise occurs at harmonics of a fundamental blade pass frequency (BPF). The fundamental BPF is defined as

$$Fundamental\ BPF = fundamental\ engine\ base\ frequency \times \#\ of\ propeller\ blades \quad (5.1)$$

Harmonics of the fundamental will occur at multiples of the engine base frequency that correspond to the number of propeller blades. Therefore, performing acoustic tests with different propeller blade numbers provides a method of isolating the contribution of the propeller noise. With this in mind, acoustic data was recorded for 5 distinct engine speeds using two-blade and three-blade propellers. A zoomed-in result from one these tests is shown in Figure 5.1. Contribution of the propeller noise is revealed by analyzing the change in magnitude at corresponding frequency peaks. Comparing 2-bladed and 3-bladed frequency data revealed that the fundamental BPF is the only one that contributes to the overall engine noise levels. As shown in Figure 5.1, the contribution of the fundamental BPF can be up to 5 dB. Higher harmonics of the BPF are found to have little or no effect on the acoustic frequency spectrum. Therefore, when viewing the engine input test results, it should be noted that for the single cylinder engine results, the 2nd engine base frequency will contain propeller noise. For the twin cylinder engine test results, the 3rd engine base frequency multiple will contain engine noise, because a 3-bladed propeller was used for this engine.

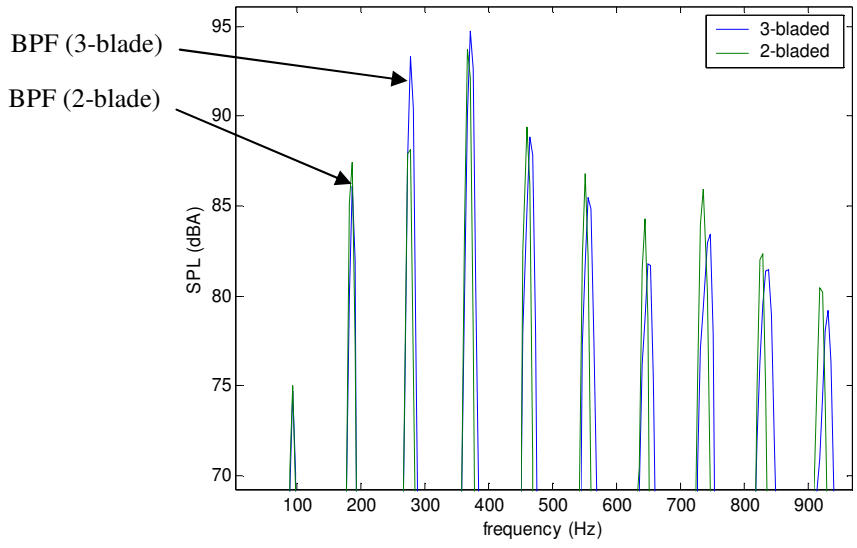

Figure 5.1: Zoomed in view of the first 10 engine base frequency multiples for the *single exit twins* at 5500 RPM.

Engine speed vs. OASPL tests:

Noise measurements were performed at different engine speeds to develop a relationship between engine speed and OASPL. For these tests, the engine testing procedure laid out in Chapter 2.2 is performed at 5 discrete engine speeds between 3000 rpm and 5500 rpm. The experimental results for the twin cylinder engine baseline case and the *single exit twins* silencers are shown in Figure 5.2, along with curve fits to the data. The expressions for the curve fits are given as

$$OASPL(dBA) = {}^{4}\!/_{1000}\,[Engine\ rpm] + 85 \qquad \text{(no silencer)} \qquad (5.3a)$$

$$OASPL(dBA) = {}^{4.4}\!/_{1000}\,[Engine\ rpm] + 79 \qquad (single\ exit\ twins) \qquad (5.3b)$$

These curve fits show that the slope remains relatively constant. This means a 1000 rpm rise in engine speed will result in an approximate noise level increase of 4 dB.

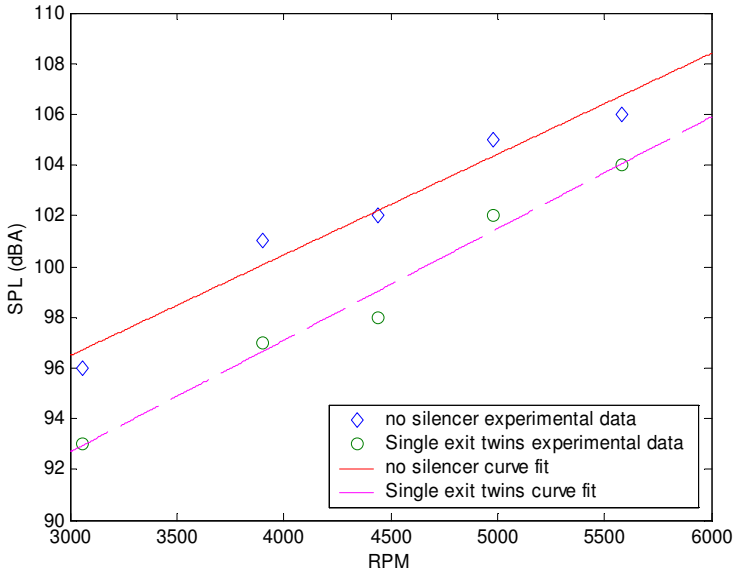

Figure 5.2: SPL vs. RPM plot for the baseline and *single exit twins* with their curve fits.

The difference in the slopes represented in Equation 5.3 provide insight into the possible measurement error in these tests. Many errors are present whenever an acoustic measurement is taken. Fortunately, most of them are small. The largest error present in these engine tests is related to the accuracy of the engine speed measurements. As shown

in Figure 5.2, SPL is dependent on engine speed. During testing, it is difficult to operate the engines at exactly the same rpm. Therefore, the possible error present due to engine speed measurement can be approximated using Equation 5.3b. This is the steeper of the two slopes, and will yield the worst case scenario. According to the engine speeds recorded during testing, 70% of the test data was taken within ± 100 rpm of the target value, which yields a possible 0.44 Db error according to Equation 5.3b. The remaining 30% of the testing was within ± 300 RPM, which yields a possible 1.32 dB error.

5.2 Engine test results for single cylinder engine designs

Baseline case:

The baseline case is defined in this chapter as the engine without a silencer attached. The average frequency spectrum of the baseline case for the single cylinder engine is plotted in Figure 5.3, followed by its directivity plot in Figure 5.4. The temperature measured at the engine exhaust outlet for the baseline case was 375 ˚F, and the OASPL calculated for this test was 102.9 dBA.

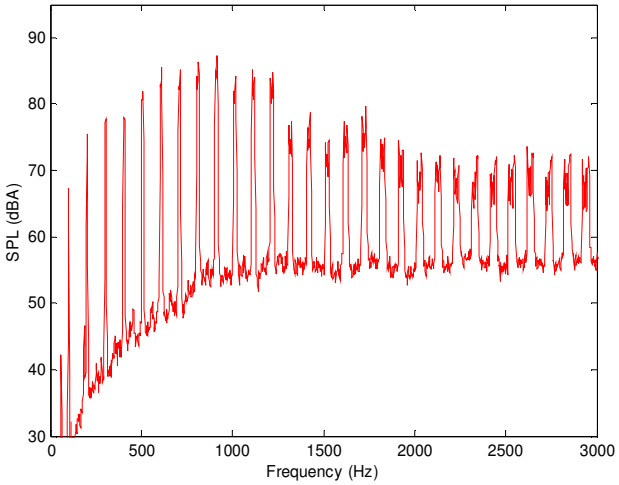

Figure 5.3: Average sound pressure level frequency spectrum for the baseline case of the single cylinder engine.

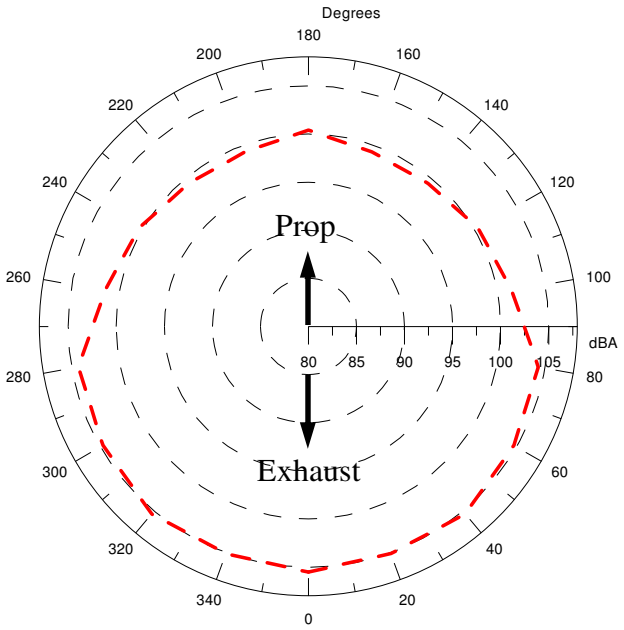

Figure 5.4: Directivity plot for the baseline case of the single cylinder engine.

Double exhaust exit:

The average frequency spectrum for the *double exhaust exit* silencer is shown in Figure 5.5. According to this plot, the *double exhaust exit* design is not effective until after the 3rd engine base frequency multiple, and at higher frequencies, reduction is minimal. These results correlate well with the IL results shown in Figure 4.5. It is difficult to make correlations between IL and engine test results because of a shift toward higher frequencies that occurs in acoustic noise levels as exhaust temperatures are increased. The directivity plot in Figure 5.6 shows how the *double exhaust exit* silencer reduces noise radiation behind the engine better than it does in front of the propeller. This trend is common for the testing performed using the single cylinder engine because the exhaust exit is located directly behind the engine. Therefore, the noise levels of the baseline case are heavily weighted to the rear of the engine. The *double exhaust exit* was tested at 6350 rpm, and had an inlet temperature of 419 ˚F. The OASPL for this silencer was 96.2 dBA.

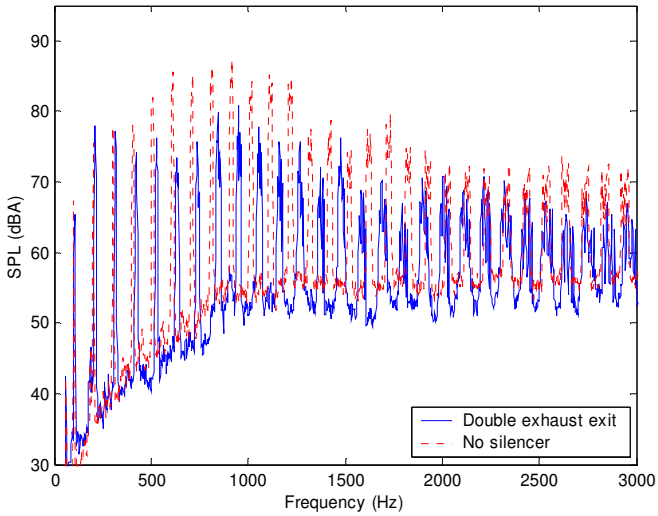

Figure 5.5: Average frequency spectrums for the *double exhaust exit* and no silencer cases.

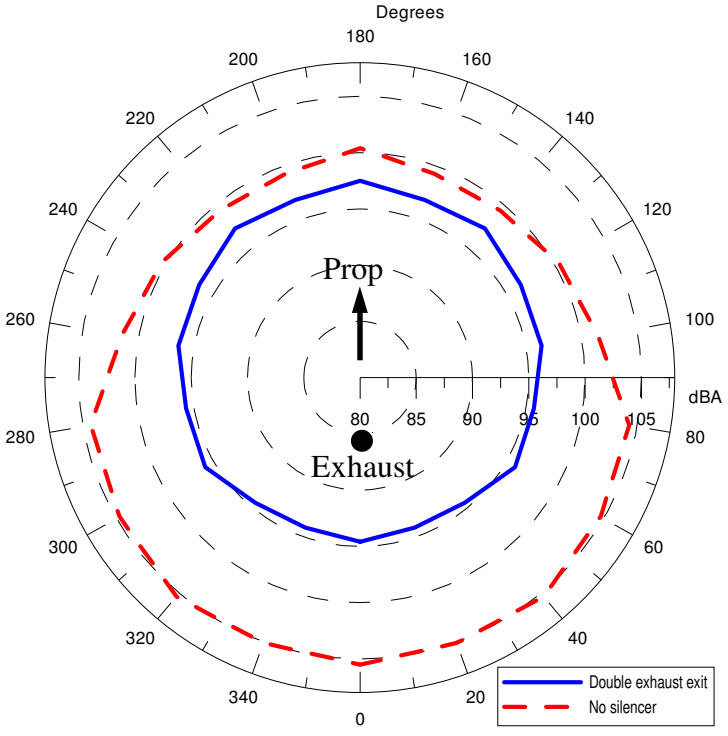

Figure 5.6: Directivity plots for the *double exhaust exit* and no silencer cases.

Black single exit:

The average frequency spectrum results shown for the *black single exit* silencer in Figure 5.7 are impressive for a design of this size. The problem with this silencer is that it greatly constricts exhaust gas flow. The data shown in Figure 5.7 was recorded at 5850 rpm, 650 rpm below the target engine speed, because the engine could not operate above this rpm with the constriction placed on it by this silencer. This constriction also led to an inlet temperature of 478 ˚F, the highest temperature recorded for the single cylinder engine. The OASPL calculated for the *black single exit* was 92.9 dBA. The directivity plot shown in Figure 5.8 reveals good reduction, but getting these results out of such a small design requires placing too much restriction on the exhaust gas flow. This constriction causes a backpressure that makes the *black single exit* silencer unusable for the UAV application.

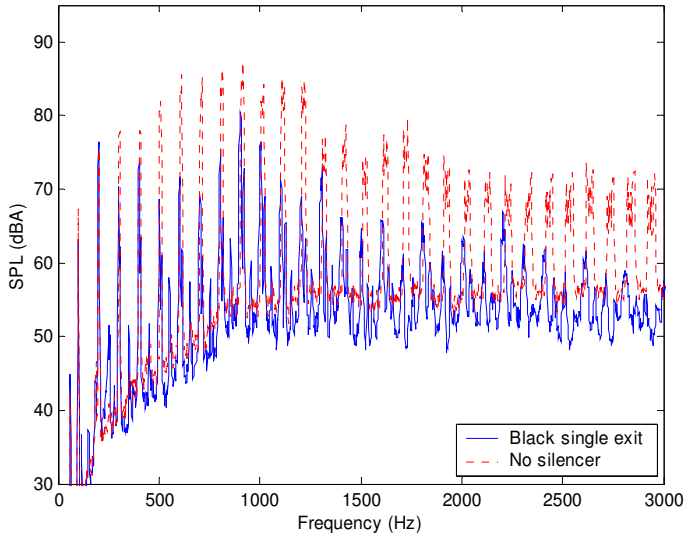

Figure 5.7: Average frequency spectrums for the *black single exit* and no silencer cases.

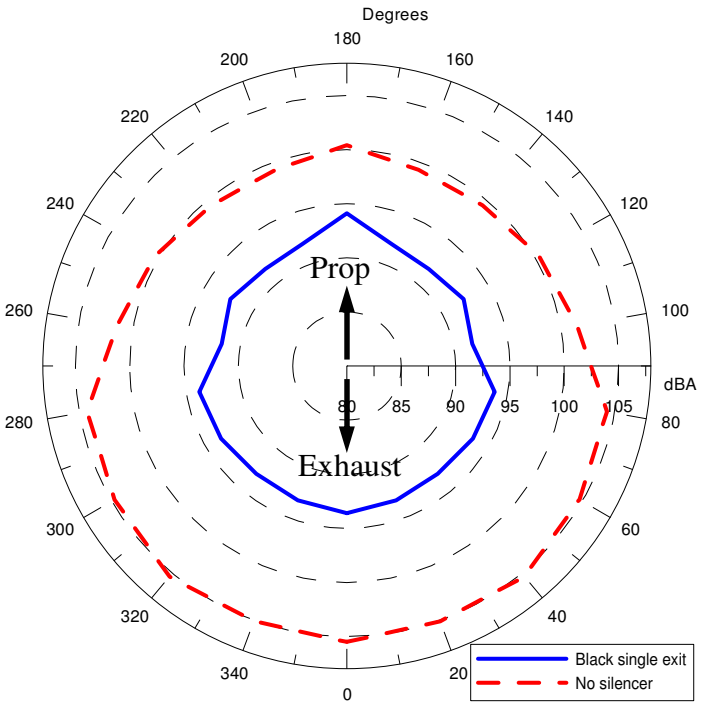

Figure 5.8: Directivity plots for the *black single exit* and no silencer cases.

Airplane silencer:

According to the average frequency spectrum shown in Figure 5.9, the *airplane silencer* caused noise levels higher than the baseline case in 4 out the first 5 engine base frequencies. This can be explained by the small and often negative IL found in the first 500 Hz of the *airplane silencer* results shown in Figure 4.7. The refractory foam liner starts to provide adequate mid-high frequency reduction, i.e. above 1100 Hz. The directivity plot for the *airplane silencer* is shown in Figure 5.10 to provide adequate reduction weighted to the rear of the engine. This test was run at 6400 rpm, which led to an inlet temperature of 394 ˚F. The OASPL calculated for the *airplane silencer* was 97.0 dBA.

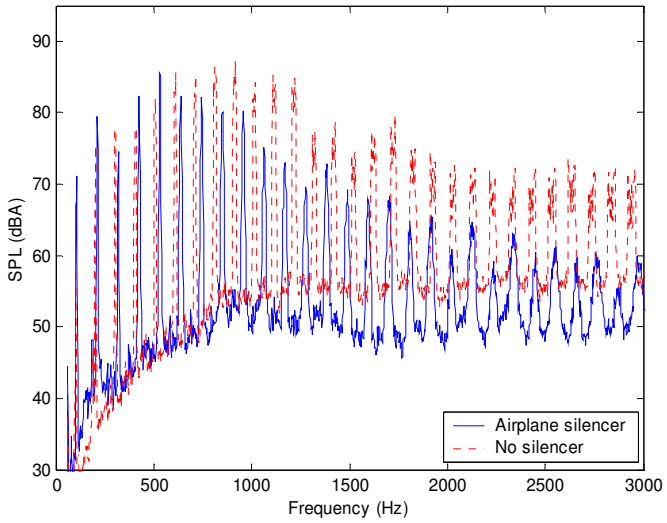

Figure 5.9: Average frequency spectrums for the *airplane silencer* and no silencer cases.

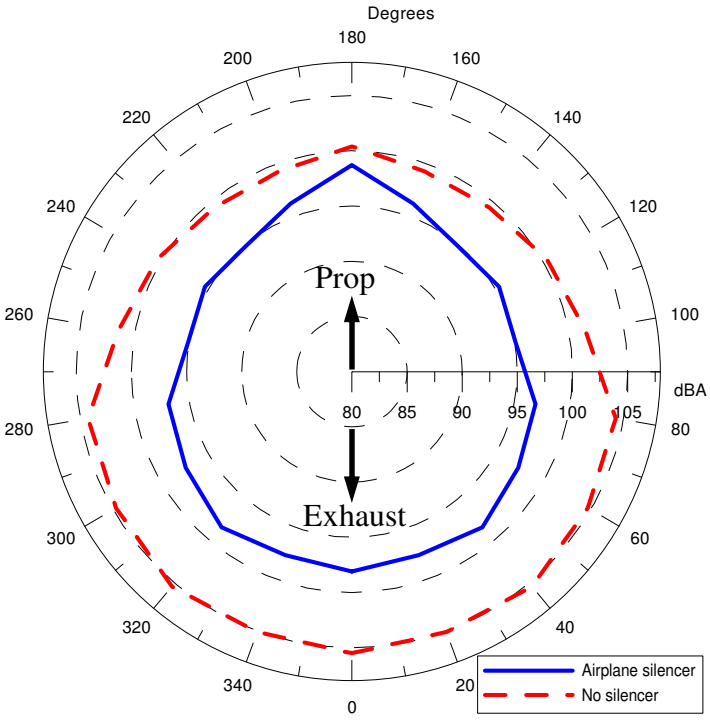

Figure 5.10: Directivity plots for the *airplane silencer* and no silencer cases.

Airplane silencer with plug:

With the simple addition of a plug to the *airplane silencer* design, the acoustic attenuation is drastically increased. The frequency spectrum in Figure 5.11 reveals acoustic absorption over all frequencies but the 2nd engine base frequency multiple. This is because propeller noise is contributing to that engine base frequency. The addition of this plug reduced the OASPL to 91.7 dBA, but increased the inlet temperature to 415 ˚F. This temperature increase is an indication of the backpressure increase caused by this plug. This silencer was tested at an engine speed of 6200 rpm. The directivity plot in Figure 5.12 reveals that the *airplane silencer w/ plug* consistently reduces the radial propagation of noise around engine. This silencer represents a baseline in design technique for following refractory foam designs.

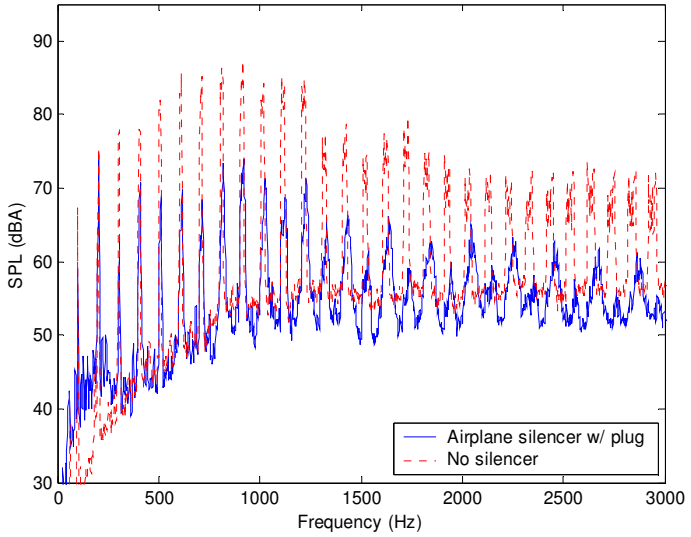

Figure 5.11: Average frequency spectrums for the *airplane silencer w/ plug* and no silencer cases.

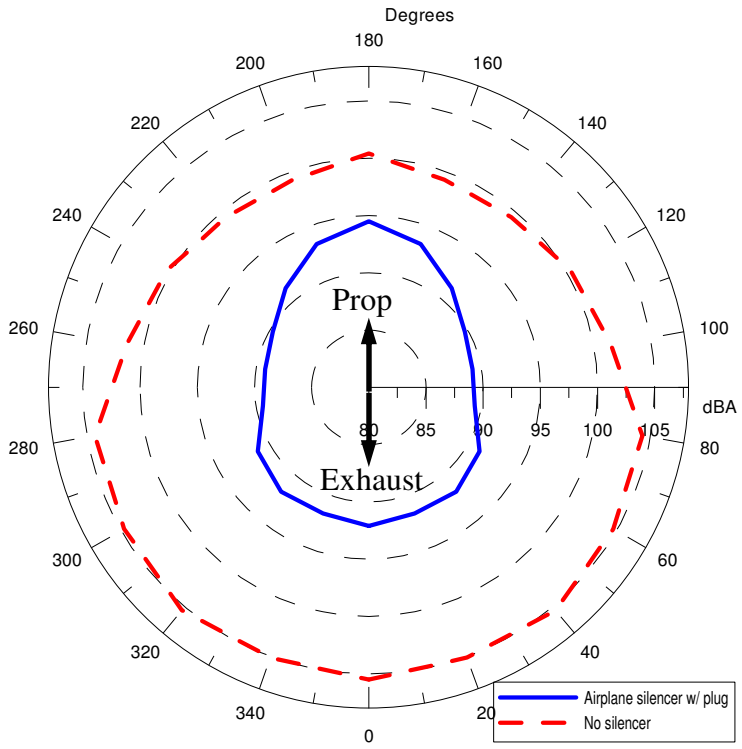

Figure 5.12: Directivity plots for the *airplane silencer w/ plug* and no silencer cases.

Chevron liner:

The results seen in Figure 5.13 prove the *chevron liner* to be acoustically the most effective silencer tested on the single cylinder engine. The two prominent peaks near 1000 Hz in the frequency spectrum are caused by the first resonance of this expansion chamber shown in Figure 4.8. This was found by using SilencerApp [30] to predict what frequencies the expansion chamber resonances would translate too in the high exhaust temperature environment present during engine testing. This design provides great broadband attenuation which yields an OASPL of 90.5 dBA. These results are somewhat explained by its large $178.3 in^3$ volume, but they are greatly attributed to the chevron shape of the refractory foam liner. This liner effectively breaks up exhaust pressure pulses without greatly constricting the exhaust gas flow. An inlet temperature of 350 ˚F provides an indication of the low backpressure placed on the engine by the *chevron liner.* The directivity results in Figure 5.14 show that this design consistently reduces the noise radiation in all directions. In the exhaust exit direction, the *chevron liner* reduces the OASPL by 15 dBA. This silencer was tested at the target engine speed of 6500 rpm.

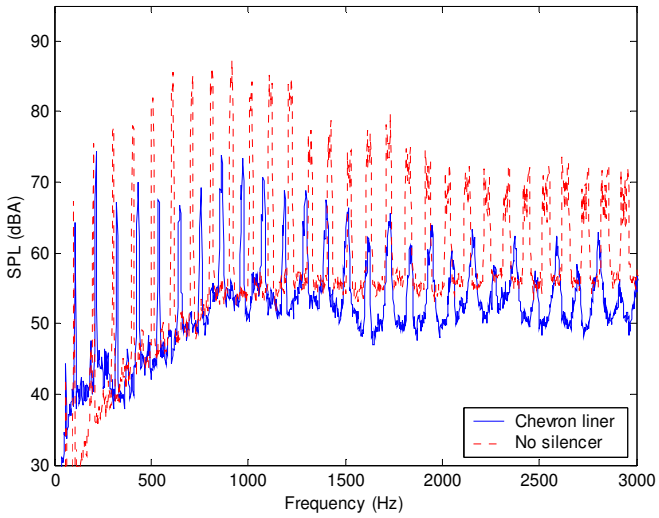

Figure 5.13: Average frequency spectrums for the *chevron liner* and no silencer cases.

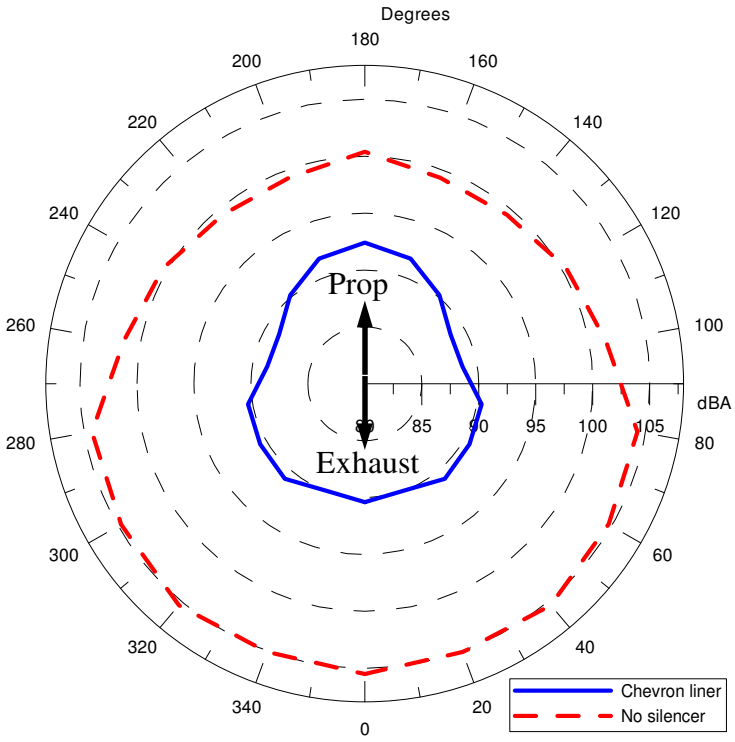

Figure 5.14: Directivity plots for the *chevron liner* and no silencer cases.

Bend flow:

Engine testing of the *bend flow* refractory foam design yielded similar acoustic results to the *chevron liner* using a smaller 165.7 in^3 volume. The average frequency spectrum for the *bend flow* silencer is shown in Figure 5.15. Using SilencerApp [30], it is predicted that the three prominent peaks around 1000 Hz are caused by the first resonant frequency of the expansion chamber shown in Figure 4.9. The directivity plot for this test is shown in Figure 5.16. The *bend flow* silencer was tested at 6400 rpm, and the inlet temperature was measured at 360 ˚F. The OASPL calculated for this silencer was 91.3 dBA.

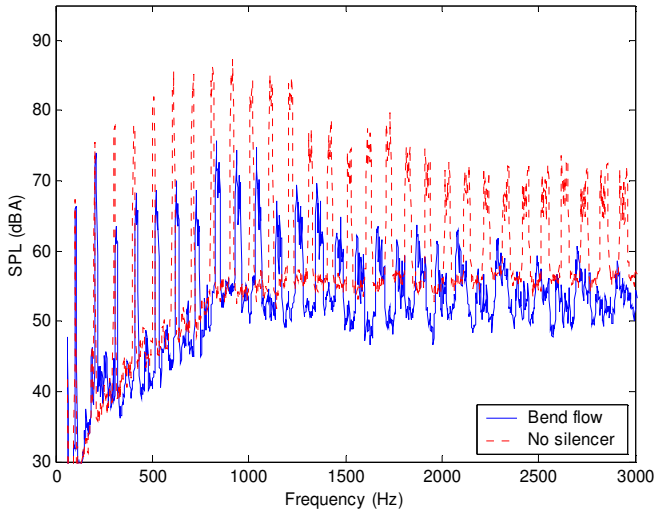

Figure 5.15: Average frequency spectrums for the *bend flow* and no silencer cases.

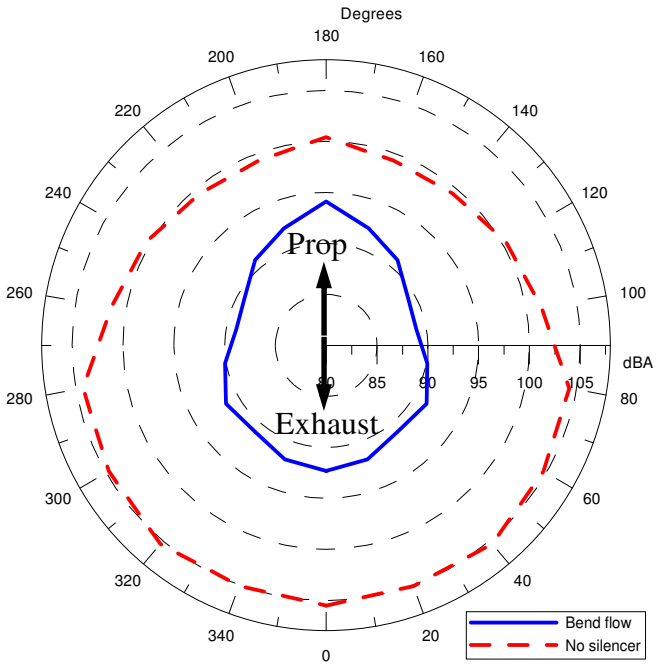

Figure 5.16: Directivity plots for the *bend flow* and no silencer cases.

Bend flow half:

Given the layered nature of the *bend flow* silencer, it was easy to fabricate a silencer using this concept in a much smaller package. According to Figure 5.17, the *bend flow half* achieves good attenuation after the 2^{nd} engine base frequency multiple. These results are impressive considering that its $77.8 in^3$ volume is less than half the volume used by the *bend flow* silencer. The OASPL calculated for this silencer was 93.0 dBA. The directivity plot shown in Figure 5.18 confirms that a considerable reduction is attained over the whole radial range using the *bend flow half* silencer. This silencer was tested at an engine speed of 6590 rpm. For its combination of performance and size, the *bend flow half* is the most promising silencer tested on the single cylinder engine.

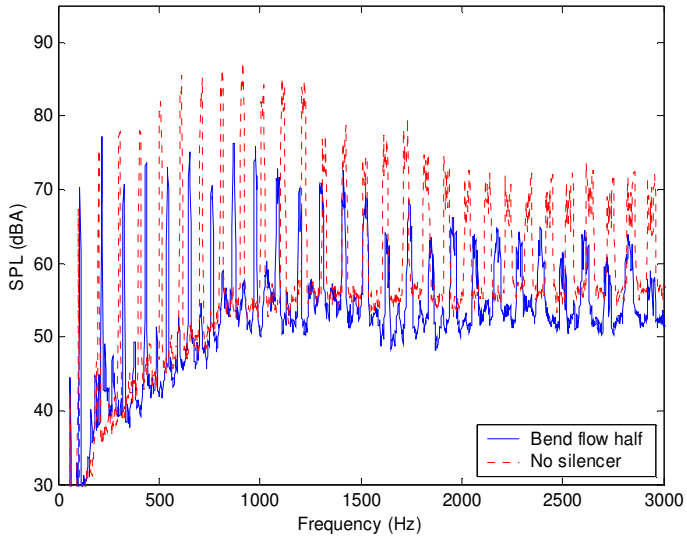

Figure 5.17: Average frequency spectrums for the *bend flow half* and no silencer cases.

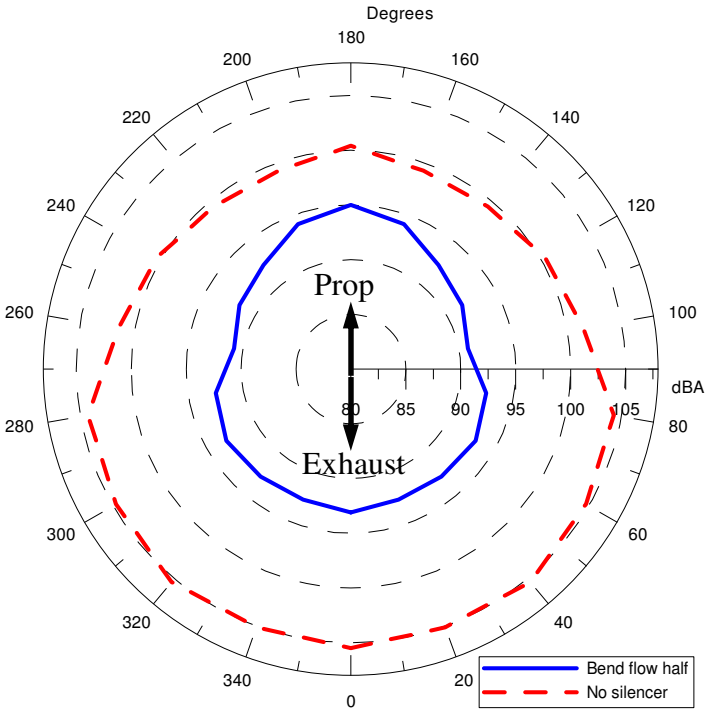

Figure 5.18: Directivity plots for the *bend flow half* and no silencer cases.

5.3 Engine test results for twin cylinder engine designs

Baseline case:

The average frequency spectrum for the baseline case of the twin cylinder engine is shown in Figure 5.19 followed by its directivity plot in Figure 5.20. This test was run at an engine speed of 5020 rpm, which led to an exhaust gas outlet temperature of 750 ˚F. An OASPL of 105.9 dBA was calculated for the baseline case.

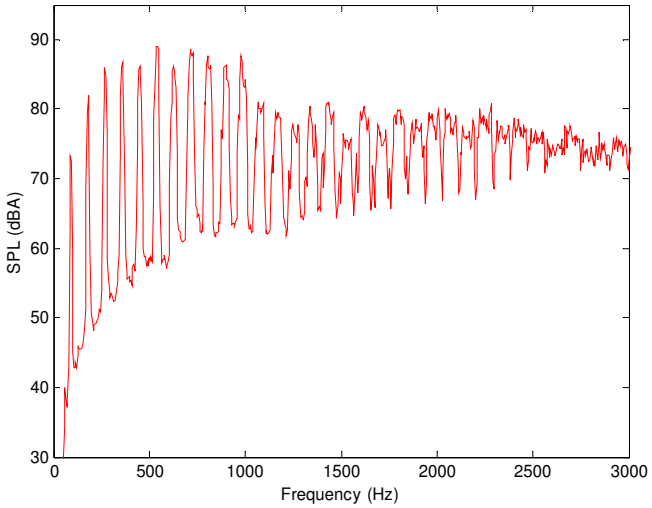

Figure 5.19: Average frequency spectrum for the baseline case of the twin cylinder engine.

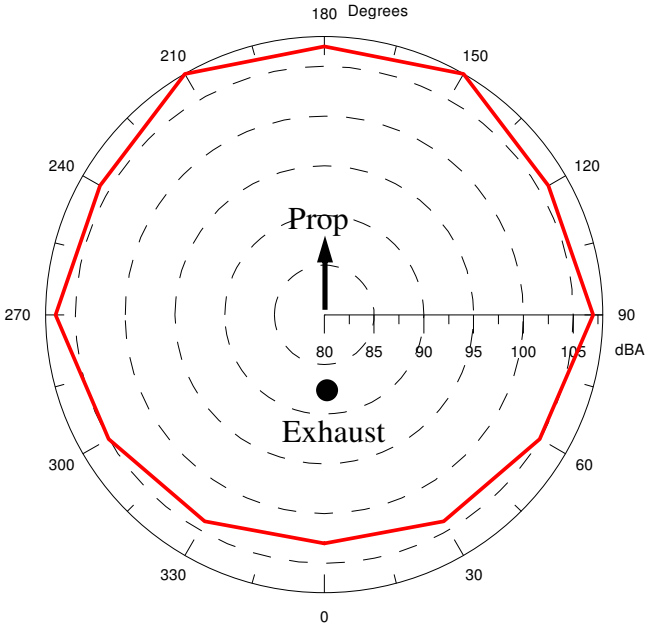

Figure 5.20: Directivity plot for the baseline case of the single cylinder engine.

Single exit twins:

According to the average frequency spectrums seen in Figure 5.21, the *single exit twins* are not effective until after the 5th engine base frequency multiple. This poor low frequency attenuation can be explained by the negative IL results from 0-300 Hz shown in the Figure 4.11. According to Figure 5.21, this silencer is effective over the 600-1500 Hz frequency range, but from 1500-2000 Hz reduction is minimal. The directivity plot shown in Figure 5.22 reveals how failure to attenuate low frequency peaks can make it difficult to reduce OASPL values. The *single exit twins* were tested at 5230 rpm, and had an inlet temperature of 832 ˚F. The OASPL for this silencer was 102.9 dBA.

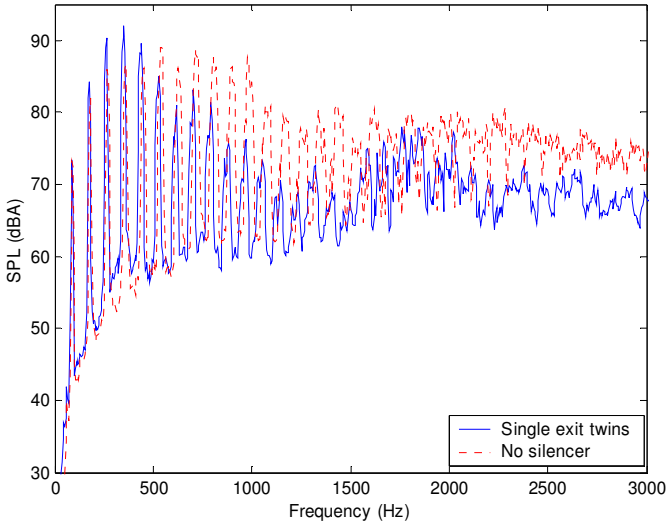

Figure 5.21: Average frequency spectrums for the *single exit twins* and no silencer cases.

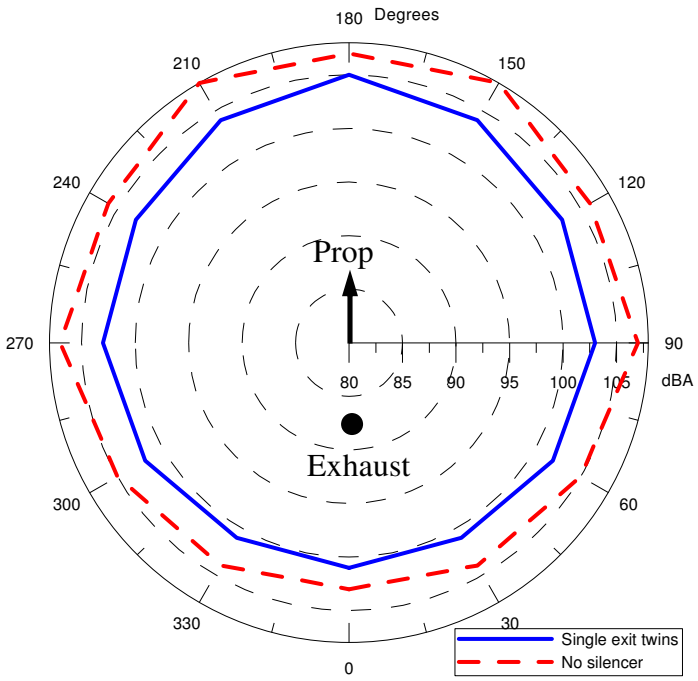

Figure 5.22: Directivity plots for the *single exit twins* and no silencer cases.

Single exit twins w/ diffuser:

To attempt further acoustic reduction with the *single exit twins*, diffusers were fabricated to take advantage of refractory foam technology. As seen in Figure 5.23, these diffusers made little acoustic impact at low frequencies, but they did eliminate the performance issues seen in the *single exit twins* over the 1500-2000 Hz range. These diffusers also improved the overall high frequency performance above 2000 Hz. The design of these diffusers left a large radial exit area for the flow, resulting in very little contact with the absorbent. This lack of absorption resulted in an OASPL of 101.5 dBA, which improved only 1.4 dBA over the *single exit twins.* According to the directivity plot in Figure 5.24, these diffusers made the most impact on the radiated noise levels behind the engine. The *single exit twins w/ diffusers* were tested at 5270 rpm.

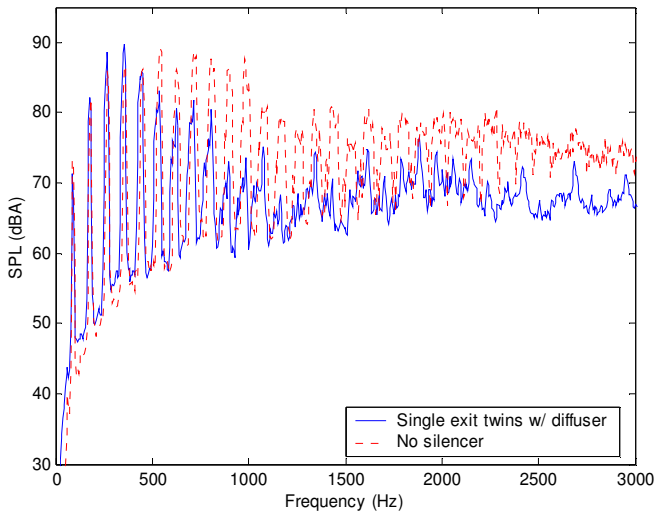

Figure 5.23: Average frequency spectrums for the *single exit twins w/ diffuser* and no silencer cases.

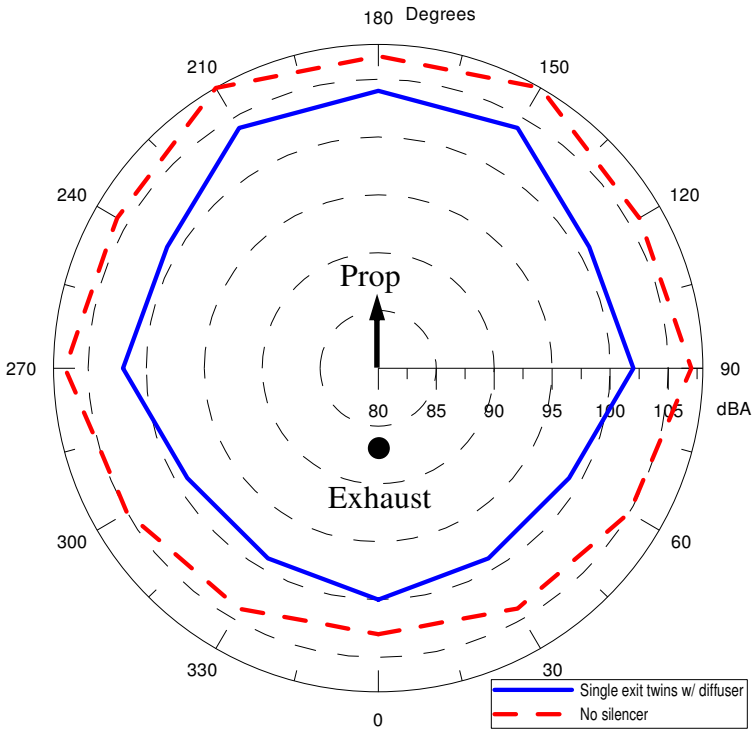

Figure 5.24: Directivity plots for the *single exit twins w/ diffuser* and no silencer cases.

Long twins:

The average frequency spectrum shown in Figure 5.25 for the *long twins* reveals great noise reduction across a broad band of frequencies. This broadband attenuation yielded an OASPL of 95.1 dBA. The *long twins* were the best acoustic performers among all the commercial silencers tested. The directivity plot in Figure 5.26 reveals consistent noise

reduction in all directions. The *long twins* were tested at the target speed of 5000 rpm, which led to an inlet temperature of 920˚F. A relatively low backpressure measurement of 6.5 inH_2O was recorded for these silencers, but the down side is that the *long twins* were the bulkiest designs tested.

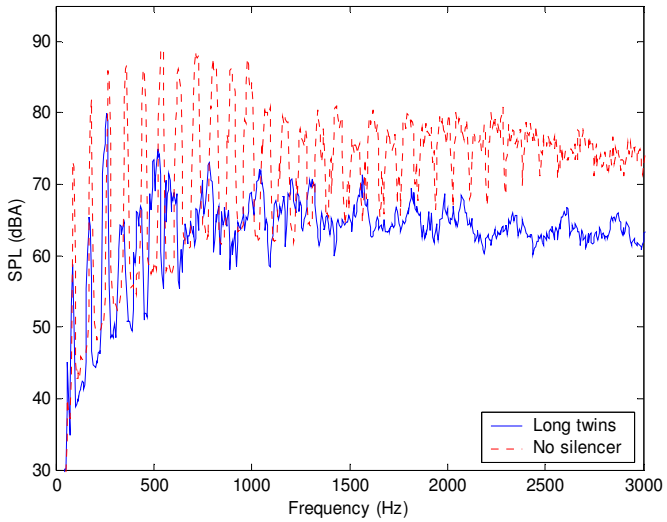

Figure 5.25: Average frequency spectrums for the *long twins* and no silencer cases.

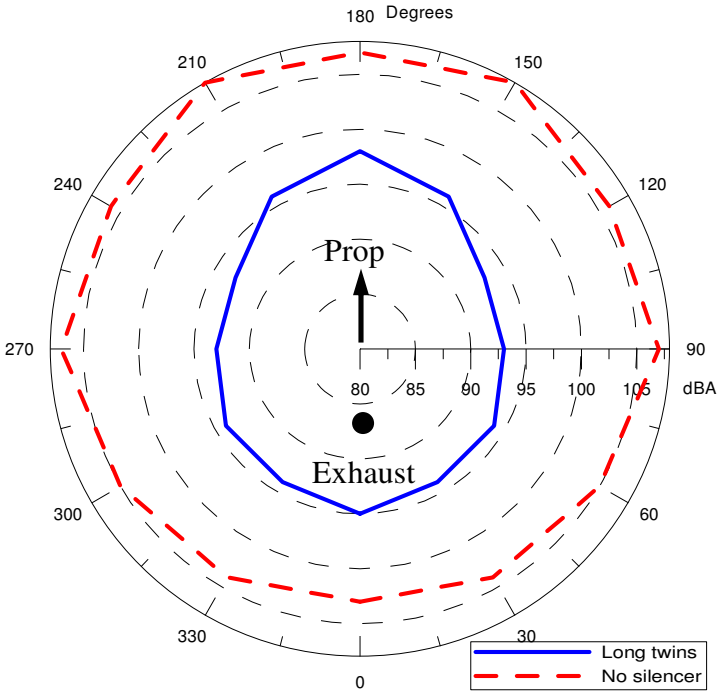

Figure 5.26: Directivity plots for the *long twins* and no silencer cases.

2-1 silencer:

As seen in Figure 5.27, the *2-1 silencer* does a great job of reducing low frequency noise, but two resonances occur at approximately 1200 Hz and 2300 Hz which negatively affect the acoustic results. Because this silencer was cut open after testing, the internal geometries were known, so expansion chamber resonance approximations could be predicted using SilencerApp [30]. Using this program to compensate for exhaust temperature change, these resonances were correlated to the large 800 Hz and 1700 Hz pass-bands in the IL results seen in Figure 4.13. If these two resonances could be reduced, this silencer would be one of the best performers. These results lead to an OASPL of 97.0 dBA. The directivity plot in Figure 5.28 reveals radial noise propagation for the *2-1 silencer* that is weighted toward the rear of the engine. This design was tested at 4970 rpm, and the inlet temperature was recorded at 832 ˚F.

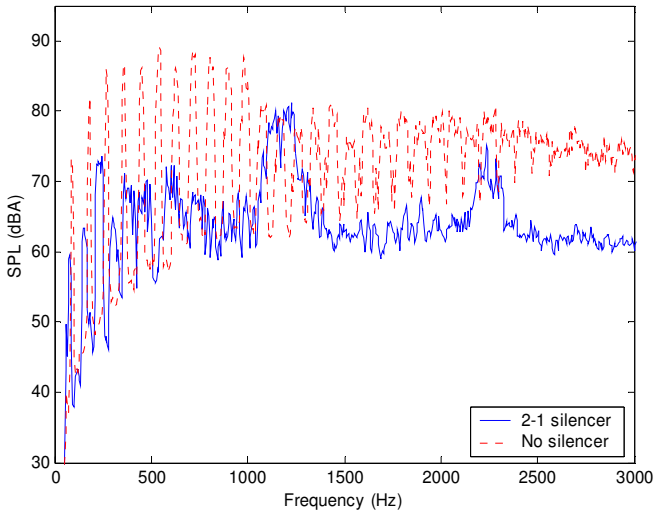

Figure 5.27: Average frequency spectrums for the *2-1 silencer* and no silencer cases.

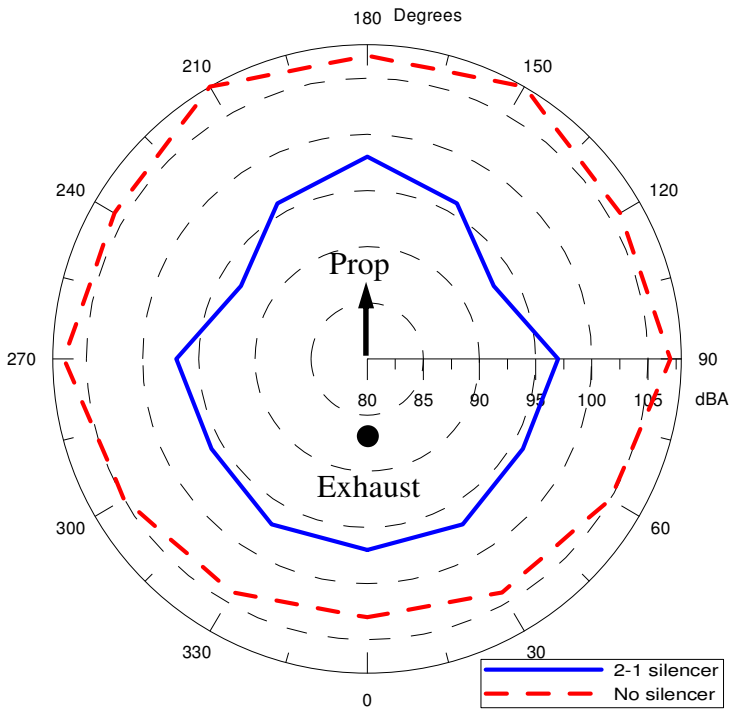

Figure 5.28: Directivity plots for the *2-1 silencer* and no silencer cases.

2-1 silencer w/ foam:

The addition of a refractory foam cylinder to the *2-1 silencer* resulted in an uncharacteristic trend. Inspection of Figure 5.29 reveals a prominent resonance at every 3rd engine base frequency multiple. This led to an OASPL of 93.6 dBA, which was the lowest OASPL recorded for the twin cylinder engine. Most of the remaining silencers in this test provide a more consistent broadband reduction than this design, but because the *2-1 silencer w/ foam* virtually eliminates two thirds of the engine base frequency multiples, its AOSPL is lower. The directivity plot in Figure 5.30 illustrates radial noise levels that remain below 95 dBA at all but one microphone location. The microphone located directly in front of the propeller has an OASPL of 97 dBA. This silencer demonstrated as acoustic trend that is not yet fully understood, but overall it yielded great attenuation. This silencer was tested at an engine speed of 5050 rpm. With an inlet temperature of 975 ˚F that was the highest recorded during engine testing, it was no surprise that the $12.2\,inH_2O$ backpressure was the highest measured in the tested silencers.

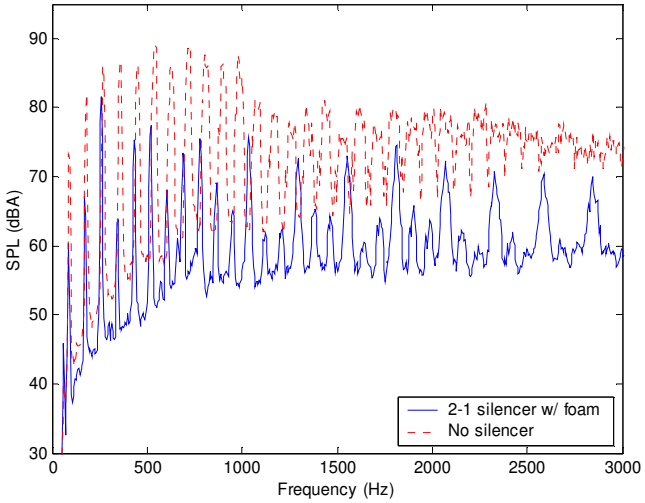

Figure 5.29: Average frequency spectrums for the *2-1 silencer w/ foam* and no silencer cases.

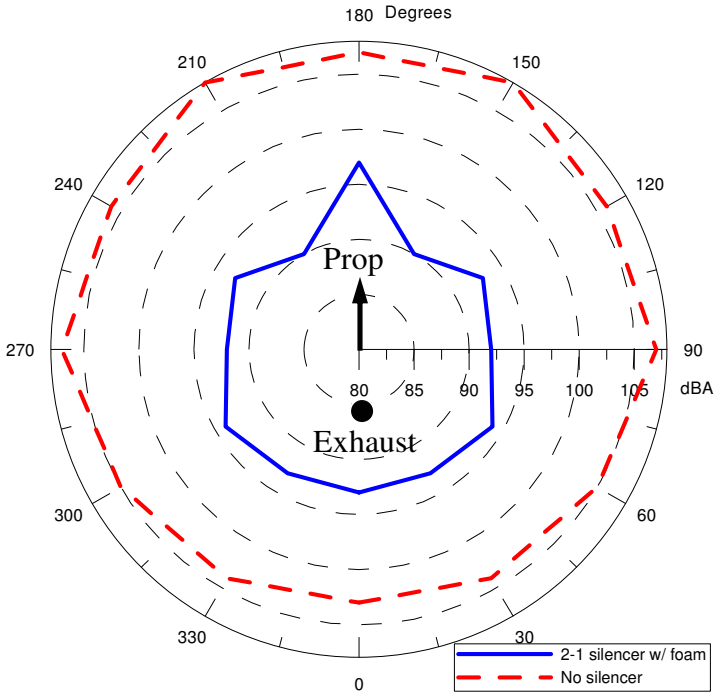

Figure 5.30: Directivity plots for the *2-1 silencer w/ foam* and no silencer cases.

Expansion box:

The *expansion box* was not very effective at attenuating engine noise. In Figure 5.31, the average frequency spectrum shows acceptable attenuation from 1300-1700 Hz and 2200-2700 Hz. The prominent acoustic peaks in the frequency spectrum at approximately 1000 Hz, 1900 Hz, and 2800 Hz were traced using SilenerApp [30] to the first three resonances of the *expansion box* seen in the IL results shown in Figure 4.14. The directivity plot in Figure 5.32 shows noise levels behind the engine to be louder than the baseline case. This silencer was tested at an engine speed of 5000 rpm, which led to an inlet temperature of 870 ˚F. Engine testing revealed a backpressure of $7.2\,inH_2O$. The OASPL of the *expansion box* was 104.6 dBA, making it the loudest silencer tested. This design was tested for comparison with the *box w/ 3-hole foam* silencer, and was not intended to be a competing silencer.

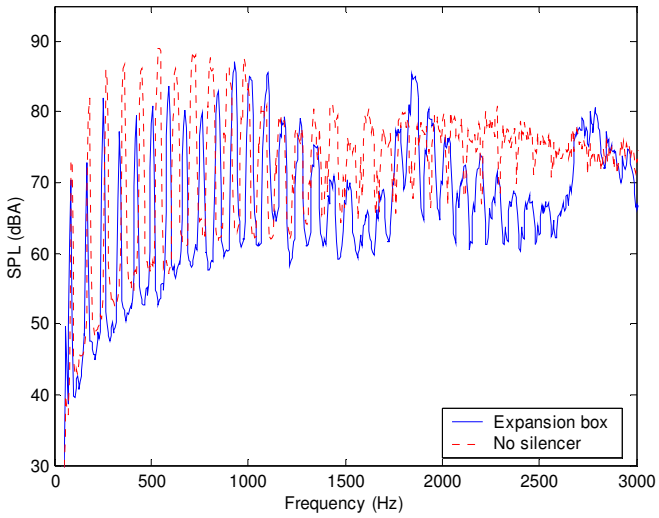

Figure 5.31: Average frequency spectrums for the *expansion box* and no silencer cases.

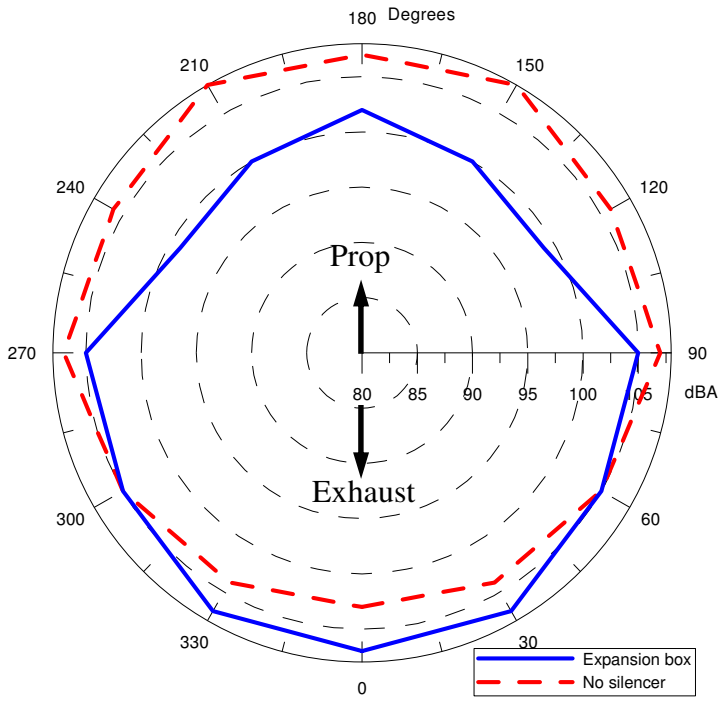

Figure 5.32: Directivity plots for the *expansion box* and no silencer cases.

Box w/ 3-hole foam:

By adding refractory foam to the *expansion box,* acoustic results were significantly improved. The average frequency spectrum in Figure 5.33 shows impressive broadband attenuation, which led to an OASPL of 96.4 dBA. Noise levels remain below 70 dBA after 1100 Hz, and drop below 65 dBA at frequencies above 2200 Hz. The directivity plot in Figure 5.34 reveals a relatively consistent radial propagation from the engine. This *box w/ 3-hole foam* silencer was tested at 5030 rpm, and had an inlet temperature of 914 $^{\circ}$F. These acoustic results, coupled with a volume just over $100\,in^3$, and a backpressure of only $5.2\,inH_2O$, make this silencer one of the most promising designs tested.

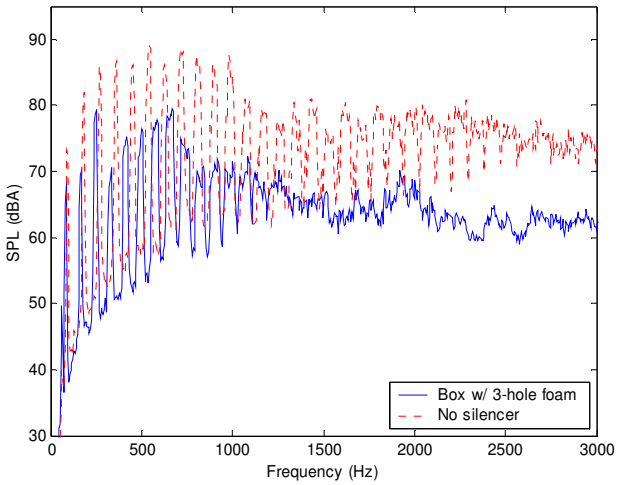

Figure 5.33: Average frequency spectrums for the *box w/ 3-hole foam* and no silencer cases.

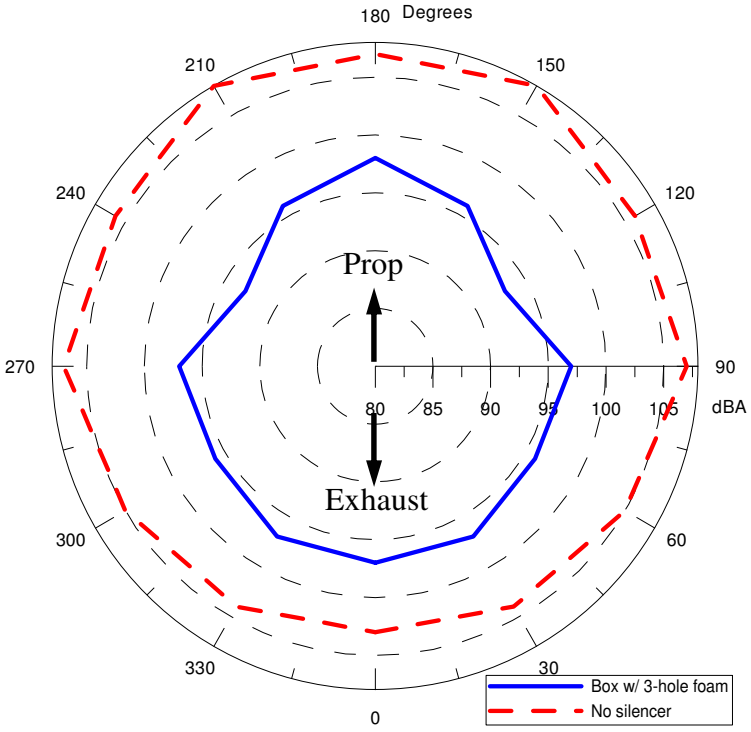

Figure 5.34: Directivity plots for the *box w/ 3-hole foam* and no silencer cases.

Nylon cylinder w/ 3-hole foam:

To reduce the weight of the *box w/ 3-hole foam* silencer, nylon was explored as a silencer shell. The average frequency spectrum for this design is shown in Figure 5.35. Its acoustic results are similar, but slightly better than the *box w/ 3-hole foam* silencer. The OASPL for the *nylon cylinder w/ 3-hole foam* silencer was 94.4 dBA, which provided a

reduction of 2.0 dBA over the *box w/ 3-hole foam* design. The directivity plot shown in Figure 5.36 depicts relatively consistent radial noise propagation. This silencer was tested at 4870 rpm, and had an inlet temperature of 940 ˚F. The backpressure recorded for this design was $6.8\,inH_2O$, which was slightly higher than the *box w/ 3-hole foam* silencer. Overall, this is the best performing design tested on the twin cylinder engine.

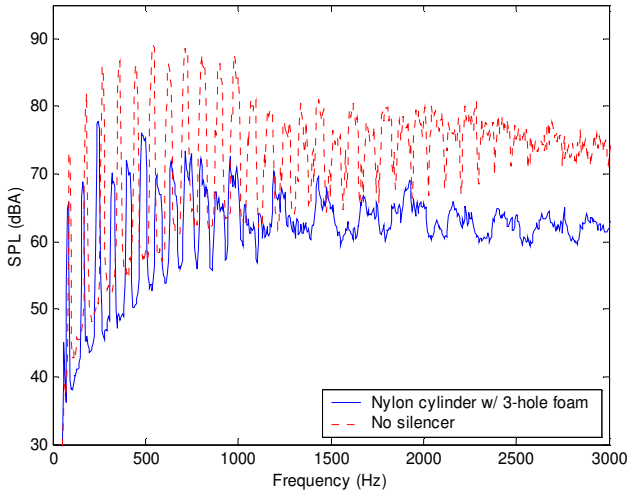

Figure 5.35: Average frequency spectrums for the *nylon cylinder w/ 3-hole foam* and no silencer cases.

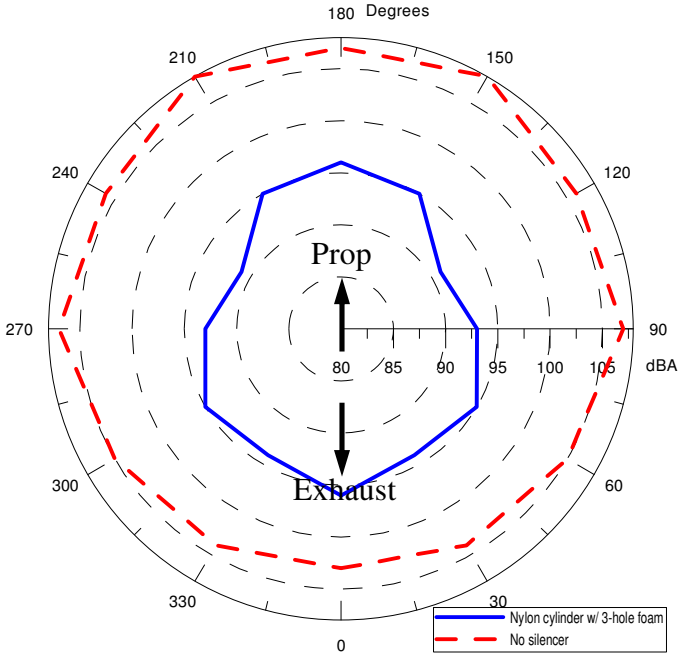

Figure 5.36: Directivity plots for the *nylon cylinder w/ 3-hole foam* and no silencer cases.

Due to the 490 ˚F melting point of the nylon shell, a temperature insulator called Aerogel [28] was required to protect the shell from the exhaust gas. To test the effectiveness of this insulation material, the shell and silencer inlet temperatures were recorded over time for different engine speeds using the *nylon cylinder w/ 3-hole foam* silencer. The temperature results as a function of time are plotted in Figure 5.37. This plot proves the effectiveness of the Aerogel insulator. During this test, 500-900 ˚F inlet temperatures yield shell temperatures less than 200 ˚F with the use of the Aerogel insulator. By inspection of the engine speed versus time plot in Figure 5.38, a direct correlation can be drawn between engine speed and inlet temperature. This test proves the Aerogel insulators effectiveness at keeping the nylon shell temperature well within its normal operating temperatures.

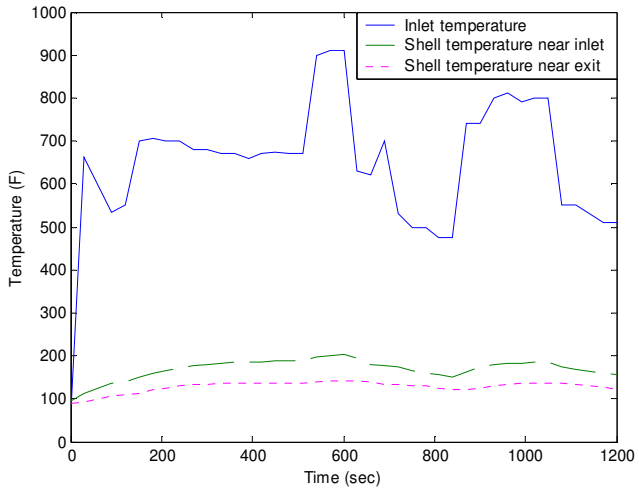

Figure 5.37: Temperature as a function of time for the *nylon cylinder w/ 3-hole foam* silencer.

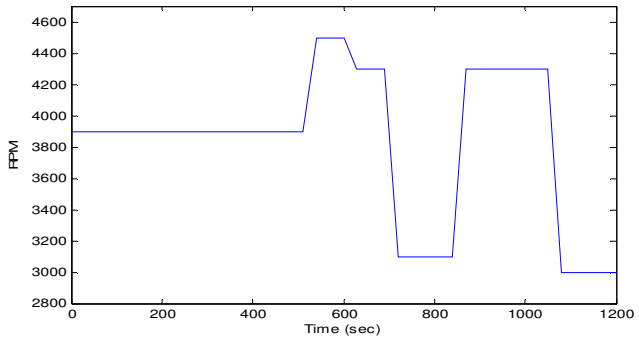

Figure 5.38: Engine speed as a function of time for the *nylon cylinder w/ 3-hole foam* silencer.

Aerodynamic shell w/ 3-hole foam:

To show how this technology can be conformed to the UAV, an aerodynamic outer shell was fabricated along with an inner refractory foam block using the same concept as the *nylon cylinder w/ 3-hole foam* silencer. Due to the complex shape of this shell, providing a consistent Aerogel barrier between the exhaust gasses and the shell was difficult. Therefore, gaps in the Aerogel insulation allowed the shell to reach its melting temperature. This melting led to leaks, which adversely affected the acoustic results shown in Figures 5.39 and 5.40. This silencer was tested at 4900 rpm, and its OASPL was measured at 100.9 dBA. This test proved that with more careful shell insulation, an effective and lightweight silencer can be conformed to the UAV using refractory foam technology.

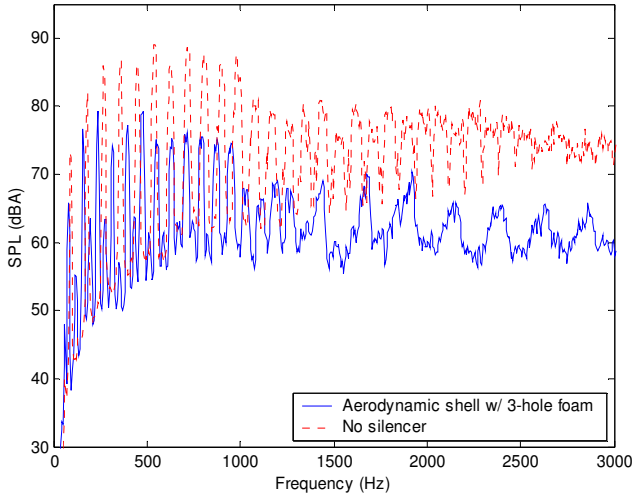

Figure 5.39: Average frequency spectrums for the *aerodynamic shell w/ 3-hole foam* and no silencer cases.

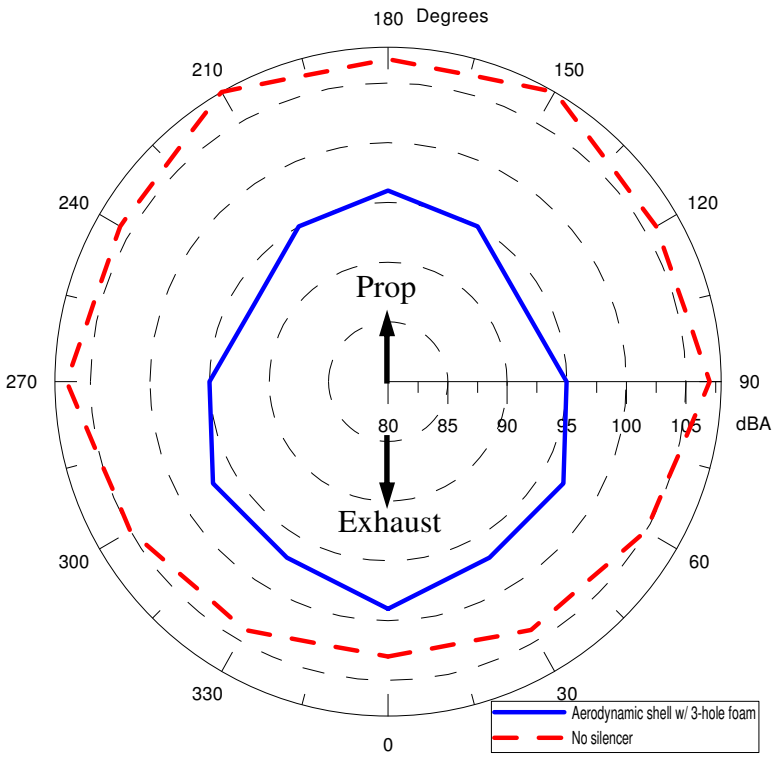

Figure 5.40: Directivity plots for the *aerodynamic shell w/ 3-hole foam* and no silencer cases.

5.4 Summary

This chapter has presented the engine test results for the silencer designs tested on single cylinder and twin cylinder engines. Table 5.1 provides an overview of the test results along with other important parameters for comparing these silencers. A plot of OASPL versus volume for each of these silencer designs is shown in Figure 5.41. Not only can a trend be drawn here between the general decrease in OASPL as volume increases, but a stronger trend can be extracted showing the decrease in OASPL seen when refractory foam is added to silencers of similar volume. It is interesting to note that Figure 5.41 is nearly a mirror image of Figure 4.16. This is because high IL results yield low OASPL results. This similarity provides a strong link between the IL results presented in chapter 4 and the engine test results in this chapter.

Table 5.1: Test values calculated for each silencer design.

Silencer name	Overall A-weighted SPL	RPM	Temp. (°F)	Backpressure (inH_2O)	Volume (in^3)	Exit-to-inlet area ratio	Engine
Baseline case	102.9		375		n/a	n/a	single cylinder engine
Double exhaust exit	96.2	6350	419		6.9	0.79	single cylinder engine
Black single exit	92.9	5860	478		15.5	0.39*	single cylinder engine
Airplane silencer	97.0	6400	394		165.2	9.82	single cylinder engine
Airplane silencer w/ plug	91.7	6200	415		165.2	0.3	single cylinder engine
Chevron liner	90.5	6500	350		178.3	1.57	single cylinder engine
Bend flow	91.3	6400	360		165.7	1.57	single cylinder engine
Bend flow half	93.0	6590			77.8	1.57	single cylinder engine
Baseline case	105.9	5020	750		n/a	n/a	twin cylinder engine
Single exit twins	102.9	5230	832		61.1	3.53	twin cylinder engine
Single exit twins w/ diffusers	101.5	5270	837		138.5	1.18*	twin cylinder engine
Long twins	95.1	5000	920	6.5	136.4	0.62	twin cylinder engine
2-1 silencer	97.0	4970	832		129.7	0.79	twin cylinder engine
2-1 silencer w/ foam	93.6	5050	975	12.2	129.7	0.79	twin cylinder engine
Expansion box	104.6	5000	870	7.2	103.2	0.79	twin cylinder engine
Box w/ 3-hole foam	96.4	5030	914	5.2	103.2	0.79	twin cylinder engine
Nylon cylinder w/ 3-hole foam	94.4	4870	940	6.8	109.6	0.79	twin cylinder engine
Aerodynamic shell w/ 3-hole foam	100.9	4900			103.0	0.59	Twin cylinder engine

* The effective exit area is larger due to the porosity of refractory foam used in the exit pipe

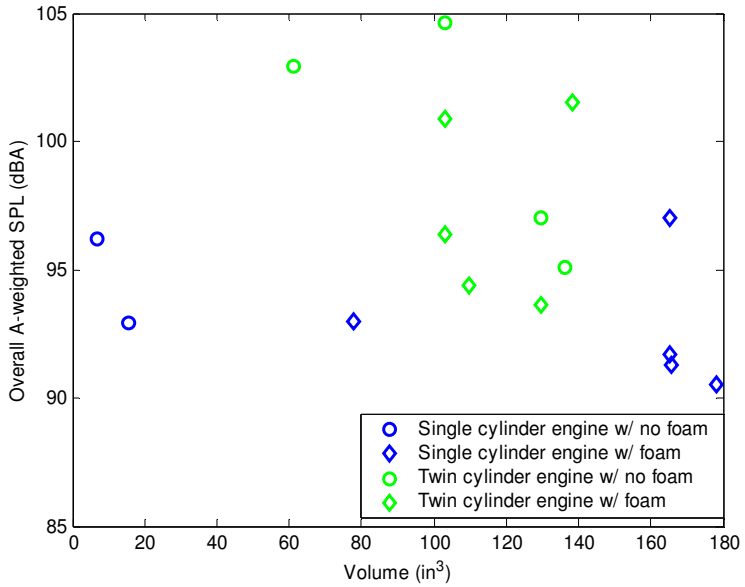

Figure 5.41: Overall A-weighted SPL vs. volume plot for all engine tested silencers.

Based on average frequency spectrums, directivity plots, OASPL, volume, temperature, and backpressure results, the 3 best silencer designs were selected for each engine tested. To assist in visualizing the best engine test results, envelope plots and directivity plots are shown to compare the 3 best silencers for the single cylinder and twin cylinder engines. The envelope plots were made according to the procedure explained in Chapter 2.3. The envelope plot showing the results for the 3 best silencers tested on the single cylinder engine can be seen in Figure 5.42, and the corresponding directivity plot is in Figure 5.43. Acoustically, the *chevron liner* is the best performer tested on the single cylinder engine, but it was also the largest in the test. Overall, the *bend flow half* was selected as the best silencer tested on the single cylinder engine. Even though its attenuation is not as high as other silencers tested, the *bend flow half* possesses the best balance between size and acoustic attenuation.

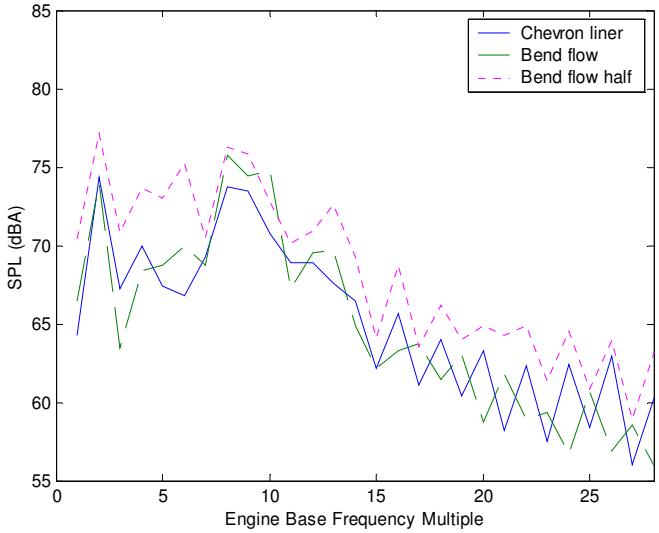

Figure 5.42: Envelope plots for the 3 best single cylinder engine designs.

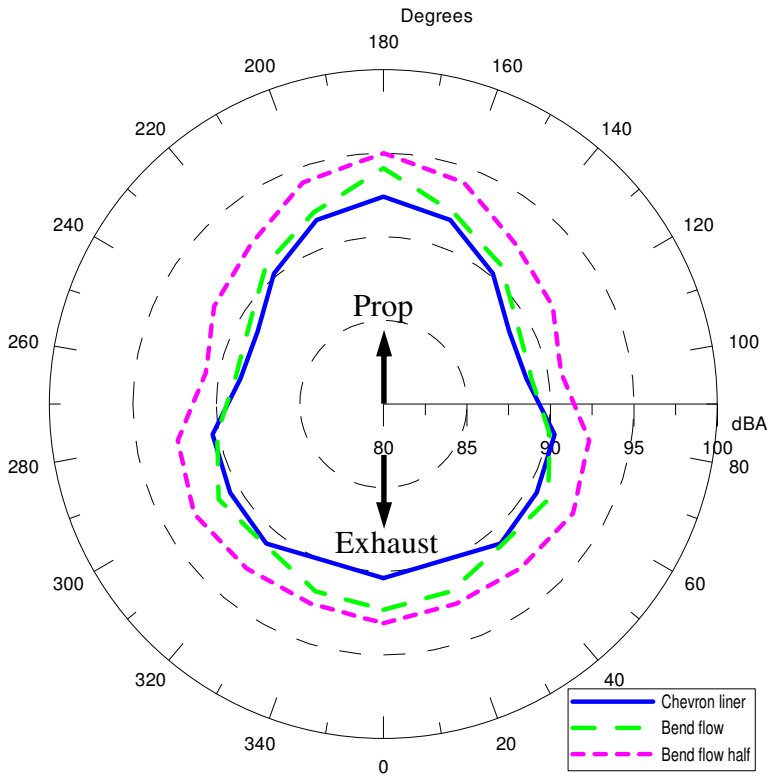

Figure 5.43: Directivity plots for the 3 best single cylinder engine designs.

For a comparison of the 3 best silencers tested on the twin cylinder engine, an envelope plot is shown in Figure 5.44, and a directivity plot can be observed in Figure 5.45. The *long twins* represent the best that could be found in the world of commercial silencers for this application. The *long twins* are bulky, but they provide good broadband attenuation and their backpressure measurements are very similar to the *nylon cylinder w/ 3-hole foam* silencer. The *box w/ 3-hole foam* design boasts the lowest volume and lowest backpressure of these 3 designs, but its acoustic attenuation is not as high as the other 2 silencers. The envelope and directivity plots show the *nylon cylinder w/ 3-hole foam* outperforming the other 2 designs acoustically, and it places a small load on the engine. This silencer only weighs 2.2 lbs, with potential for weight savings. It is important to note the temperature performance achieved with the combination of the Aerogel insulation and the nylon shell used in this design. Immediately after a 20 minute test, the *nylon cylinder w/ 3-hole foam* silencer was cool enough to handle without gloves. The simple fabrication of this silencer also lends itself to easy volume modification for size scaling. Easy scalability is an important benefit for this UAV since the end goal is to

produce a family of different sized vehicles. All these advantages work to make the *nylon cylinder w/ 3-hole foam* the most promising silencer tested on the twin cylinder design, and the most advanced silencer fabricated in the course of this research project.

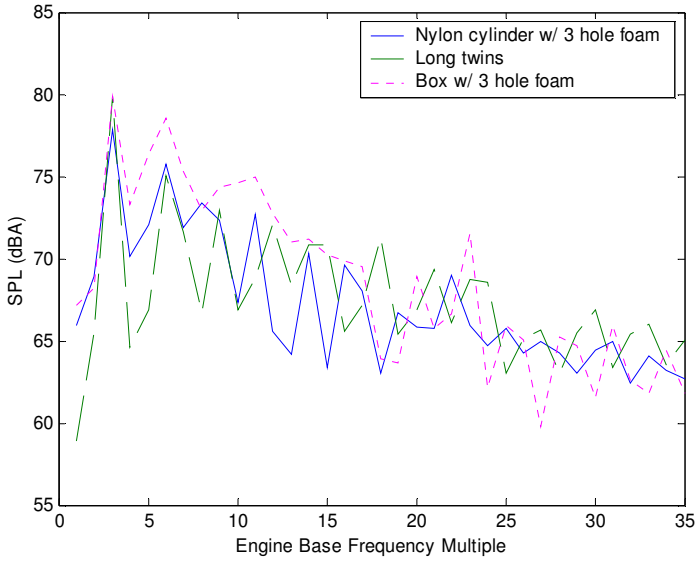

Figure 5.44: Envelope plots for the 3 best twin cylinder engine designs.

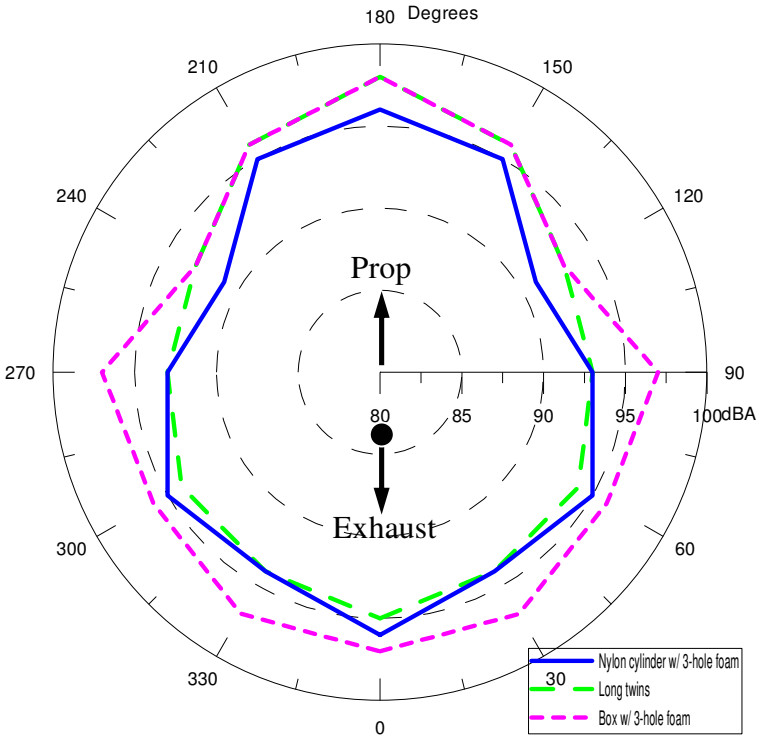

Figure 5.45: Directivity plots for the 3 best twin cylinder engine designs.

Chapter 6 Conclusions

6.1 Refractory foam conclusions

The objective of this research was to design a small, lightweight, and effective silencer for use in a UAV application. This was achieved with the use of refractory foam technology. Refractory foam silencers proved to provide ample acoustic reduction over a broad frequency band, while meeting the UAV requirements. All this was done without imposing a large backpressure to the engine. It was also proven that an aerodynamic silencer could be fabricated with refractory foam capable of being integrated to the UAV. As these silencer designs evolved through a series of tests that refined the design process to take full advantage of refractory foam technology, the *nylon cylinder w/ 3 hole foam* emerged as the height of this evolution. This design met the goals of this project in the following ways:

- The average overall SPL was reduced by 12.1 dBA compared to the baseline case.
- These results were achieved using a volume of only $109.6\,in^3$.
- This design placed a small $6.8\,inH_2O$ of backpressure on the engine.
- By using a thermal insulator in conjunction with a nylon shell, this design weighed in at only 2.2 lbs, with potential for added weight savings.
- This design was tested multiple times, and no sign of wear could be seen in the refractory foam or the nylon shell.

Over the course of this research, many refractory foam advantages were exploited to achieve the results desired for the UAV application. The properties of this acoustic absorbent which proved most important in meeting the objectives of this research were:

- Extreme lightweight of refractory foam. Its densities lie in the $0.01 - 1.45\,g/cm^3$ range.

- Ability to handle temperatures up to 1700˚C in air.
- Ease of machining, which made complex flow patterns possible that were unheard of in high temperature acoustic absorbers previous to this research.
- Can be made in different pores per square inch (ppi) configurations.
- The SiC version of this material has an extremely high strength to weight ratio graphed in Figure 1.3.
- Ability to greatly impact acoustic reduction above 1000 Hz.
- Effectively damps out many of the chamber resonances common in silencer designs.

Overall, this material proved to be an effective acoustic absorber capable of yielding passive silencer designs for extreme environments that can contend with, or improve, any stock design in present production.

6.2 Recommendations for future research

This research merely shed a light on this new absorbent. Designs were fabricated, tested, and refined, but there is still work to be done before silencers using refractory foam can make it into production. Currently, testing is being done on refractory foam to determine its absorptive coefficient. This will allow the material to be compared to other absorbers strictly in its ability to absorb sound. Other issues that must be addressed before these designs can be fully understood include:

- Long term durability testing under simulated temperature and vibration conditions.
- Most aeronautical applications require minimal fluid absorption, therefore testing must be done to determine how well fluid escapes from the material.
- Learning to model exhaust gas flow through the absorbent to assist in making acoustic predictions.
- If a nonmetal shell is to be used, this shell must be tested against the elements common in an aeronautical environment.

The End

References

[1] Bone, Elizabeth, Unmanned Aerial Vehicles: Background and Issues for Congress*, Congressional Research Service – The Library of Congress*, April 25 2003.

[2] Information: http://uav.wff.nasa.gov/uavs.cfm?Available=Yes.

[3] Information: http://www.alliedaerospace.com/UAVs.htm

[4] Wilson, J.R., "Carrying your Aircraft into Battle"*, Aerospace America,* July 2003.

[5] Munjal, M.L., *Acoustics of Ducts and Mufflers,* A Wiley-Interscience publication, John Wiley & Sons, Inc., 1987.

[6] Ultramet, 12173 Montague St. Pacoima, CA 91331, e-mail - mail@ultramet.com available: www.ultramet.com.

[7] Blair, Gordon P., *Design and Simulation of Two-Stroke Engines,* Society of Automotive Engineers, Inc., 1996.

[8] Venkanna, B. K. Wadawadagi, Swati B., "Experimental Investigations on Noise Attenuation of a Twin Cylinder Stationary Diesel Engine with Different Types of Mufflers", *Journal of Vibration & Acoustics*-Transactions of the ASME, v 121 n 3, 1999, p 351-354.

[9] Shenoda, F. B., "Exhaust Silencers with Minimum Power Loss", *Archives of Acoustics,* v 11 n 2, 1986, p 137-150.

[10] El-Sharkawy, A. I. El-Chazly, N. M., "A Critical Survey of Basic Theories used in Muffler Design and Analysis", *Applied Acoustics,* v 20 n 3, 1987, p 195-218.

[11] Bies, David A., *Engineering Noise Control*, E & FN Spon, Taylor & Francis Group, 1999.

[12] Blackstock David T., *Fundamentals of Physical Acoustics,* A Wiley-Interscience publication, John Wiley & Sons, Inc., 2000.

[13] Clark, Raymond C., "Gas turbine engine noise control using fiber metal lined ducts", *Proceedings - National Conference on Noise Control Engineering,* Inst of Noise Control Engineering, Poughkeepsie, NY, v 1, 1996, p 121-126.

[14] Selamet, A. Lee, I. J. Huff, N. T., "Acoustic attenuation of hybrid silencers", *Journal of Sound and Vibration,* v 262 n 3, May 1 2003, p 509-527.

[15] Paun, F. Gasser, S. Leylekian, L., "Design of materials for noise reduction in aircraft engines", *Aerospace Science and Technology,* v 7, 2003, p 63-72.

[16] Cummings, A. Chang, I. -J., "Sound attenuation of a finite length dissipative flow duct silencer with internal mean flow in the absorbent", *Journal of Sound & Vibration,* v 127 n 1, Nov 22 1988, p 1-17.

[17] Ishikawa, Ryousuke, "Performance Analysis of Motorcycle Mufflers", *Small Engine Technol Conf Proc.,* Publ by Soc of Automotive Engineers of Japan, Tokyo, Jpn, *91,* p 187-193.

[18] Rittmueller, Stephen P. Mann, J Adin III. Holger, David K., "Iterative design method to reduce the exhaust and venting noise of a vacuum cleaner motor with minimum use of absorptive foam", *Noise Control Engineering Journal,* v 45 n 2, Mar-Apr 1997, p 63-68.

[19] Cvjeticanin, N. Wolf, A. Spitznagel, F., "Quiet boost", *Kunststoffe Plast Europe,* v 87 n 6, June 1997, p 18-20.

[20] Heng, Sangvavann Stankiewicz, Edwin P. Sherman, Andrew J., "Noise Reduction System for General Aviation Aircraft, Phase II", *Lewis Research Center.*

[21] Lewis Research Center, "Improved Mufflers for General Aviation", *NASA Tech Briefs,* LEW-16324.

[22] Sherman, Andrew J. Tuffias, Robert H. Kaplan, Richard B., "Refractory Ceramic Foams: A Novel New High Temperature Structure", *Ultramet website,* available: www.ultramet.com.

[23] Available: www.rcshowcase.com.

[24] Available: www.aircraftinternational.com.

[25] Available: www.davisdieseldevelopment.com.

[26] Information: www.supertrapp.com/disc_technology/disc_technology.htm.

[27] Available: www.krumscheid-metallwaren.de.

[28] Aspen Aerogels, Inc., 184 Cedar Hill Street Marlborough, MA 01752
e-mail- info@aerogel.com, available: www.aerogel.com.

[29] 3D Systems, 26081 Avenue Hall Valencia, CA 91355,
e-mail- moreinfo@3dsystems.com, available: www.3Dsystems.com.

[30] Martin Hepperle, SilencerApp, Version 1.1, Rev. 27, © 1998-1999
e-mail- Martin.Hepperle@dlr.de

Appendix A

Sound Propagation in an Expansion Chamber

Equation A.1 lays out the equations for the pressure waves present in each of the three silencer sections seen in Figure 1.5:

$$P_I = \underbrace{A_1 e^{-jkx}}_{p_1^{in}} + \underbrace{B_1 e^{jkx}}_{p_1^{r}} \tag{A.1a}$$

$$P_{II} = A_2 e^{-jkx} + B_2 e^{jkx} \tag{A.1b}$$

$$P_{III} = \underbrace{A_3 e^{-jk(x-l)}}_{p_3^{tr}} \tag{A.1c}$$

Using conservation of pressure and volume velocity, equations can be written to represent each change in cross sectional area. Equation A.2 illustrates the first change in cross sectional area, and Equation A.3 shows the equations derived for the second change in cross sectional area.

$$A_1 + B_1 = A_2 + B_2 \tag{A.2a}$$

$$A_1 - B_1 = \frac{S_2}{S_1}\left(A_2 - B_2\right) \tag{A.2b}$$

$$A_2 e^{-jkl} + B_2 e^{jkl} = A_3 \tag{A.3a}$$

$$A_2 e^{-jkl} - B_2 e^{jkl} = \frac{S_3}{S_2} A_3 \tag{A.3b}$$

Solving the previous four equations for A_1/A_3 yields the transmission coefficient (T) seen in Equation A.4.

$$T = \frac{2}{\left(1 + \frac{S_3}{S_1}\right)\cos(kl) + j\left(\frac{S_3}{S_2} + \frac{S_2}{S_1}\right)\sin(kl)} \tag{A.4}$$

Assuming $S_1 = S_3$, and substituting into the transmission loss equation (TL), yields Equation A.5.

$$TL = 10\log_{10}\left[1+\frac{1}{4}\left(\frac{S_2}{S_1}-\frac{S_1}{S_2}\right)^2 \sin^2(kl)\right] \qquad \text{(A.5)}$$

Vita

Josh Sesler was born in Panama City, FL. After a few moves, he settled in Cleveland, TN from the 5th grade through high school. From high school he began undergraduate studies in Mechanical Engineering at Tennessee Technological University. After completing his first vibrations course, he selected an acoustic and vibrations specialty path within the Mechanical Engineering curriculum. As a result of some interesting talks given by Virginia Tech faculty at the ASME National Symposium, he began to research Virginia Tech for graduate studies. In the Spring of 02' he began studies at Virginia Tech with a research assistantship working in the VAL lab under Dr. Ricardo Burdisso's advisement. In the spring of 05', he began work at DSM in Franklin, TN. DSM specializes in custom piezoelectric actuators and amplifier systems for micro positioning applications. He graduated with his master's degree from Virginia Tech in the Fall of 05'.